

## ABSTRACT

Title of Dissertation: PROGRAMMABLE BIOMOLECULE  
ASSEMBLY AND ACTIVITY IN  
PREPACKAGED BIOMEMS

Xiaolong Luo, Doctor of Philosophy, 2008

Directed By: Professor Gary W. Rubloff  
Department of Materials Science and Engineering  
and the Institute for Systems Research

Antibiotic resistance is an increasing public health concern and few new drugs for bacterial pathogenesis have been obtained without addressing this resistance. Quorum sensing (QS) is a newly-discovered system mediated by extracellular chemical signals known as “autoinducers”, which can coordinate population-scale changes in gene regulation when the number of cells reaches a “quorum” level. The capability to intercept and rewire the biosynthesis pathway of autoinducer-2 (AI-2), a universal chemical signaling molecule, opens the door to discover novel antimicrobial drugs that are able to bypass the antibiotic resistance.

In this research, chitosan-mediated *in situ* biomolecule assembly has been demonstrated as a facile approach to direct the assembly of biological components into a prefabricated, systematically controlled bio-microelectromechanical system (bioMEMS). Our bioMEMS device enables post-fabricated, signal-guided assembly of labile biomolecules such as proteins and DNA onto localized inorganic surfaces inside microfluidic channels with spatial and temporal programmability. Particularly, the

programmable assembly and enzymatic activity of the metabolic pathway enzyme Pfs, one of the two AI-2 synthases, have been demonstrated as an important step to reconstruct and interrogate the AI-2 synthesis pathway in the bioMEMS environment. Additionally, the bioMEMS has been optimized for studies of metabolic pathway enzymes by implementing a novel packaging technique and an experimental strategy to improve the signal-to-background ratio of the site-specific enzymatic reactions in the bioMEMS device. I envision that the demonstrated technologies represent a key step in progress toward a bioMEMS technology suitable to support metabolic engineering research and development.

PROGRAMMABLE BIOMOLECULE ASSEMBLY AND ACTIVITY IN  
PREPACKAGED BIOMEMS

By

Xiaolong Luo

Dissertation submitted to the Faculty of the Graduate School of the  
University of Maryland, College Park, in partial fulfillment  
of the requirements for the degree of  
Doctor of Philosophy  
2008

Advisory Committee:  
Professor Gary W. Rubloff, Chair  
Professor Williams E. Bentley  
Professor Reza Ghodssi  
Professor Gregory F. Payne  
Professor Raymond A. Adomaitis  
Professor Joonil Seog

© Copyright by  
Xiaolong Luo  
2008

## Acknowledgements

I am especially grateful to my advisor Prof. Gary W. Rubloff for all his guidance and encouragement. He has not only provided me with wise supervision and a great working environment, but has also given me support and consideration in the time of difficulties. I would also like to sincerely thank Professors Bentley, Ghodssi and Payne for all of your guidance and support in this research project.

I would also like to especially thank Angela Lewandowski for her friendship while working together in the initial experiments of enzyme assembly in microfluidics and her support in preparing the biological materials. I would like to thank Jung Jin Park and Dr. Hyunmin Yi for their guidance and support, especially when I was new to the group. Of course, I would like to thank to all the current and past Rubloff Group members including Susan Buckout-White, Israel Perez, Dean Larios Berlin, Laurent Henn Lecordier, Parag Benerjee, Erin Robinson and Wei Lei for all the friendships, encouragement, and helpful discussion of results. Finally, I want to thank Stephan Koev in MSAL and the Nanocenter staff for their help and discussions in microfabrication.

This work was supported in part by the Deutsch Foundation, the NSF EFRI program, and the FabLab facilities in the Maryland NanoCenter.

## Dedication

This dissertation is dedicated to my dear wife Holly Hong, who has supported me throughout the entire venture. It is also dedicated to my lovely son Jabez Junyi Luo, who has never stopped entertaining me since his fetation.

This dissertation is further dedicated to the memory of my dear father Guangshi Luo and my dear mother Juzhao Yang, who had given me being physically and mentally, and had never stopped supporting and encouraging me until they rested from their labors in this world. It is also dedicated to my kin brothers and sisters in the Luo family who have always been my guidance and supporters both spirituality and materially.

# Table of Content

|   |      |
|---|------|
| Acknowledgements.....   | ii   |
| Dedication.....   | iii  |
| Table of Content.....   | iv   |
| List of Figures.....  | viii |
| List of Tables.....   | xiii |
| Chapter 1. Introduction.....  | 1    |
| 1.1 Quorum sensing.....   | 1    |
| 1.2 Lab-on-a-chip technology and biopolymer-based bioMEMS.....                                  | 3    |
| 1.3 Enzyme assembly in bioMEMS.....   | 6    |
| 1.4 Metabolic pathway in bioMEMS.....   | 8    |
| 1.5 Research goal and outline.....  | 10   |
| Chapter 2. BioMEMS Devices, Control System and Chitosan as Soft-interconnect in<br>BioMEMS..... | 11   |
| 2.1 BioMEMS devices for biomolecule assembly.....   | 11   |
| 2.2 BioMEMS system control technology.....  | 14   |
| 2.3 Chitosan as soft interconnect in bioMEMS.....   | 17   |
| 2.4 Summary.....  | 19   |
| Chapter 3. Programmable Model Protein Assembly and DNA Hybridization in<br>BioMEMS.....         | 20   |
| 3.1 Programmable GFP assembly via glutaraldehyde activation.....                                | 21   |
| 3.1.1 Materials and methods.....  | 21   |
| 3.1.2 Results and discussion.....   | 23   |
| 3.2 Programmable GFP assembly via <i>in situ</i> enzymatic activation.....                      | 25   |
| 3.2.1 Materials and methods.....  | 25   |
| 3.2.2 Results and discussion.....   | 26   |

|   |    |
|---|----|
| 3.3 DNA hybridization in bioMEMS.....   | 31 |
| 3.3.1 Materials and Methods.....  | 31 |
| 3.3.2 Results and discussion .....  | 33 |
| 3.4 Conclusions.....  | 35 |
| Chapter 4. Programmable Enzyme Assembly in Prepackaged BioMEMS .....                                  | 37 |
| 4.1 Introduction.....   | 38 |
| 4.2 Materials and methods .....   | 41 |
| 4.2.1 Materials .....   | 41 |
| 4.2.2 Plasmid construction.....   | 41 |
| 4.2.3 Purification of (His) <sub>6</sub> -Pfs-(Tyr) <sub>5</sub> .....                                | 42 |
| 4.2.4 Chitosan and Pfs-chitosan conjugate preparation .....   | 43 |
| 4.2.5 BioMEMS device fabrication and packaging.....   | 43 |
| 4.2.6 One-step electrodeposition of enzyme-chitosan conjugate and sequential enzymatic reactions..... | 44 |
| 4.2.7 Negative controls .....   | 46 |
| 4.2.8 Analysis of enzymatic reaction products .....   | 46 |
| 4.3 Results.....  | 48 |
| 4.3.1 One-step electrodeposition of enzyme-chitosan conjugate and sequential enzymatic reactions..... | 48 |
| 4.3.2 Negative controls to examine non-specific binding and dead volume ...                           | 51 |
| 4.3.3 Performance of enzyme assembled on electrodes .....   | 54 |
| 4.3.4 Enzyme stability and activity.....  | 55 |
| 4.3.5 Transient response.....   | 58 |
| 4.4 Discussions .....   | 60 |
| 4.4.1 Enzyme assembly and activity in bioMEMS.....  | 60 |
| 4.4.2 Quantification .....  | 61 |
| 4.4.3 Optimization .....  | 62 |



|  |    |
|--|----|
| 4.5 Conclusions.....   | 63 |
| Chapter 5. BioMEMS Optimization for Enzyme Assembly and Activity.....        | 65 |
| 5.1 Introduction.....  | 66 |
| 5.1.1 Motivation: enzymatic reactions and metabolic pathways in bioMEMS..... | 66 |
| 5.1.2 Limitations and goals.....   | 68 |
| 5.1.3 Eliminating reservoir dead volume.....                                 | 69 |
| 5.1.4 Reducing impact of nonspecifically bound enzyme.....                   | 71 |
| 5.2 Detailed design, fabrication and packaging.....                          | 73 |
| 5.2.1 Packaging aligners to eliminate interconnection reservoirs.....        | 73 |
| 5.2.2 Cross-channel design to separate sequential flow directions.....       | 76 |
| 5.3 Experimental methods.....  | 77 |
| 5.3.1 Materials.....   | 77 |
| 5.3.2 Pfs-chitosan conjugate preparation.....                                | 78 |
| 5.3.3 Enzyme assembly and enzymatic reactions.....                           | 79 |
| 5.3.4 Analysis of enzymatic reaction products.....                           | 80 |
| 5.4 Quantification and simulation of interconnect dead volume.....           | 82 |
| 5.5 Quantification of parasitic reactions and overall analysis.....          | 85 |
| 5.5.1 Enzyme reaction and controls.....                                      | 85 |
| 5.5.2 Enzyme conversion signal/background.....                               | 87 |
| 5.6 Discussion.....  | 89 |
| 5.7 Conclusions.....   | 90 |
| Chapter 6. Conclusions and Future Work.....                                  | 92 |
| 6.1 Conclusions.....   | 92 |
| 6.2 Future work.....   | 96 |
| Appendices.....  | 99 |
| Appendix I Estimation of enzyme specific activity.....                       | 99 |
| Appendix II Calculation of the missing enzymatic conversion of               |    |

|                            |     |
|----------------------------|-----|
| intersection-channels..... | 102 |
| References.....            | 108 |

## List of Figures

|  |    |
|--|----|
| Figure 1-1: The metabolic pathway of autoinducer-2 (AI-2) synthesis.....   | 2  |
| Figure 1-2: Summary of bioMEMS and biopolymer-based bioMEMS that is<br>biofunctionalized on demand after microfabrication.....   | 5  |
| Figure 1-3: BioMEMS platform to study quorum sensing.....  | 8  |
| Figure 1-4: Outline of this research that integrates engineering with biology.....   | 10 |
| Figure 2-1: The bioMEMS device for biomolecule assembly. (a) Schematic of a 4”<br>Pyrex wafer with 6 SU-8 microchannels with two electrodes underneath each<br>microchannel. (b) 3-D drawing of a microchannel. (c) Non-permanent sealing of a<br>microchannel by a PDMS gasket with pressure. (d) Assembled microfluidic<br>device with electric and fluidic connections.....   | 12 |
| Figure 2-2: Improvements of the bioMEMS device by curving the microchannel<br>(A→A’, B→B’) and shrinking the interconnection reservoirs (C→C’, D→D’)......   | 13 |
| Figure 2-3: BioMEMS control system. The control system controls the selections<br>from multiple solution sources and the pumping flow rate into microfluidic<br>channels.....  | 14 |
| Figure 2-4: BioMEMS control system. The control system controls the selections<br>from multiple solution sources and the pumping flow rate into microfluidic<br>channels.....  | 15 |
| Figure 2-5: Chitosan as the biointerfacial material in microfluidics. (a) Solubility of the<br>polysaccharide chitosan is pH dependent. (b) Electrical signal-guided chitosan<br>deposition at cathode surface where pH gradient is created by negative electrical<br>potential. (c) Chitosan enables spatial/temporal biofunctionalization of bioMEMS<br>device and immobilization of biomolecules in microfluidic channel..... | 17 |
| Figure 3-1: Programmable assembly of green fluorescent protein (GFP) via<br>glutaraldehyde activation of chitosan scaffold. Left: Schematic of protein   |    |

|   |    |
|---|----|
| assembly procedure. Right: Fluorescent photographs and intensity contour of protein assembly.....   | 24 |
| Figure 3-2: Programmable assembly of green fluorescent protein (GFP) via <i>in situ</i> enzymatic activation. (a) A microfluidic device. (b) Schematic procedure. (c) Experiment: tyrosinase was added for <i>in situ</i> enzymatic activation thereby GFP was covalently assembled on chitosan scaffold. (d) Control: no tyrosinase was added for <i>in situ</i> enzymatic activation thereby no GFP was covalently assembled on chitosan scaffold. .... | 28 |
| Figure 3-3: DNA hybridization in bioMEMS. (a) Schematic procedure. (b) Fluorescent micrographs.....   | 32 |
| Figure 3-4: DNA hybridization in bioMEMS: Sequential micrographs during introduction of match target ssDNA.....   | 34 |
| Figure 4-1: Schematic flow of programmable enzyme assembly in a prepackaged reusable bioMEMS device. (a) Prefabricated device, (b) enzyme-chitosan conjugation, (c) electrically programmed assembly of Pfs-chitosan conjugate, (d) enzymatic small-molecule reaction, (e) mild acid wash to remove biofunctionalization and reuse bioMEMS device.....  | 39 |
| Figure 4-2: BioMEMS device for enzyme assembly. (a) Completely packaged bioMEMS system with electric connectors and fluidic inputs/outputs. (b) Color ink running through one microfluidic channel (left) and zoom-in view of one electrode at the bottom of the channel (right).....   | 44 |
| Figure 4-3: Programmable enzyme assembly, reproducibility after removal and robustness over time. (a) Schematic of programmable enzyme assembly, disassembly and reassembly and the corresponding enzymatic reactions. (b) Flow rates. (c) Reproducible catalytic activity after enzyme assembly, disassembly and re-assembly, and stability of assembled enzyme after 4 days.....  | 49 |
| Figure 4-4: Negative controls and corresponding experiments. (a) Preparation of   |    |

|  |    |
|--|----|
| assembly site surface. Green = pure chitosan, blue = Pfs-chitosan conjugate. (b) Enzymatic reactions. (c) Flow rates. (d) Enzymatic conversions. The * denotes a statistical difference ( $p < 0.01$ in all cases).....  | 52 |
| Figure 4-5: Simulation of the transient concentration response at sample collection point to the concentration change at reaction site. (a) At 3 $\mu\text{L}/\text{min}$ flow rate (blue). (b) At 22 $\mu\text{L}/\text{min}$ flow rate (purple).....   | 59 |
| Figure 5-1: Parasitic reactions in microfluidics due to enzyme trapped in interconnect reservoirs and non-specifically bound on microchannel walls. (a) Pfs enzyme converts SAH substrate into products SRH and adenine. (b) Assembly of Pfs-chitosan conjugate onto a localized assembly electrode in a microchannel. (c) Sequential enzymatic reaction in continuous flow. (d) Parasitic reactions in reservoirs and on microchannel wall as well as programmable reactions on enzyme assembly site..... | 67 |
| Figure 5-2: Eliminating interconnection reservoirs by aligners on prototype mold to guide microfluidic packaging. (a) Aligners on prototype mold. (b) Packaging way #1: punch holes via PDMS followed by coupler insertion. (c) Packaging way #2: punch holes via PDMS followed by tubing insertion. (d) Packaging way #3: align couplers for PDMS curing followed by coupler removal and tubing insertion.....  | 74 |
| Figure 5-3: Device and packaging. (a) Fabricated aligners on prototype mold. (b) Blue dye solution flowing through a packaged cross-channel without interconnection reservoirs. PE tubing was inserted. In experiment, enzyme solution flowed $A \rightarrow C$ , substrate solution flowed $B \rightarrow D$ . .....  | 75 |
| Figure 5-4: Minimize parasitic reactions by eliminating interconnection reservoirs and by separating sequential flow directions in cross channels. To test the background signal by parasitic reactions, Pfs enzyme solution was introduced without electro-assembly followed by buffer rinsing, then enzymatic substrate SAH was introduced and products were collected downstream to be analyzed by  |    |

|   |    |
|---|----|
| HPLC. (a) Single channel with interconnection reservoirs. (b) Single channel without interconnection reservoirs. (c) Cross-channel without interconnection reservoirs.....  | 80 |
| Figure 5-5: Quantification and simulation of dye intensity change from the interconnect point. Dye intensity was monitored over electrode patches 12mm downstream the microchannels. (a) Dye intensity change from interconnect with reservoir. (b) Dye intensity change from interconnect without reservoir. (c) Experimental quantification of dye intensity increasing from 10% to 90%: with reservoir, it takes 61 sec; without reservoir, it takes 32 sec. (d) Finite element simulation of dye intensity increasing from 10% to 90%: with reservoir, it takes 75 sec; without reservoir, it takes 25 sec. (e) The difference of intensity change from interconnects with and without reservoir..... | 83 |
| Figure 5-6: Background signals (parasitic enzymatic conversion) at different flow rates. Enzyme Pfs solution was introduced without electro-assembly followed by buffer rinsing, then enzymatic substrate SAH was introduced and products were collected downstream to be analyzed by HPLC. Legend: 1-ch_w/ res.: single channel with interconnection reservoirs (blue); 1-ch_No res.: single channel without interconnection reservoirs (pink); X-ch_No res.: cross-channel without interconnection reservoirs (red).....  | 86 |
| Figure 5-7: Conversions by non-specifically bound or trapped enzyme (blue) and conversions by site-specifically assembled enzymes (red) at 0.4 $\mu\text{L}/\text{min}$ flow rate. For the non-specific conversion, no electrical signal was applied to electrodeposit Pfs-chitosan conjugate. For the total conversion, a electrical signal of $3\text{A}/\text{m}^2$ current density was applied for 4 minutes to electrodeposit Pfs-chitosan conjugate onto the assembly electrodes.....   | 88 |
| Figure 6-1: Roadmap of this research and future work.....   | 96 |
| Figure S-1: Working electrodes (WE) were fabricated to match the exposed surface  |    |

|  |     |
|--|-----|
| area in both (a) single-channel and (b) cross-channel. ....  | 102 |
| Figure S-2: Factors that affect the enzymatic conversion in the cross-channel. (a)<br>Enzyme is only available within the diffusion distance for electrodeposition in the<br>horizontal side channel due to the low diffusivity of Pfs-chitosan conjugate. (b)<br>The enzymatic reaction in the vertical side channel, which mainly depends on the<br>diffusion of reaction substrate and products back and forth to the flow stream in<br>the horizontal channel, is not as efficient as that in the central cross area. (c)<br>Enlargement of the nominal active area including Pfs_diff area, SAH_diff area<br>and the central cross area. .... | 103 |
| Figure S-3: Simulation of SAH diffusion during enzymatic reaction. The vertical<br>channel is filled with buffer (turquoise blue). SAH (purple) in the horizontal<br>channel diffuses out of the flow stream into the vertical side channels and is<br>converted by assembled Pfs in side channels. Reaction products SRH and<br>adenine diffuse back to flow stream into the horizontal channel. Simulation<br>result shows that conversion in vertical side channels equals to 45% of conversion<br>in horizontal flow stream. ....  | 105 |
| Figure S-4: Normalization of enzymatic conversion. See the text for details. ....  | 106 |

## List of Tables

|   |    |
|---|----|
| Table 4-1: Experimental procedure to demonstrate programmable assembly of a catalytically active enzyme and its reproducibility.....  | 45 |
| Table 4-2: Estimated specific catalytic activities of assembled Pfs-chitosan conjugate in microchannel, Pfs-chitosan conjugate suspension, and free unconjugated Pfs enzyme solution on day 1 and on day 5 after 4 days in PBS buffer at room temperature. .... | 56 |



# Chapter 1. Introduction

## 1.1 Quorum sensing

Antibiotic resistance of bacterial pathogens is a fast emerging global crisis and an understanding of the underlying resistance mechanisms is paramount for design and development of new therapeutic strategies (Kumar and Schweizer 2005).

According to the Infectious Diseases Society of America (IDSA), 2 million people get bacterial infections each year, of which, 90,000 die. “More than 70 percent of the bacteria that cause hospital-acquired infections are resistant to at least one of the antibiotics most commonly used to treat them” (Leeb 2004). Traditional antibiotics target bacterial cell-wall synthesis, protein synthesis, DNA replication and repair, all of which ultimately lead to cell lysis, thus building up harsh selective pressure for bacteria to develop antibiotic-resistance and survive (Walsh 2000). As few new drugs have been developed through extensive screening campaigns, pharmaceutical companies are executing a disturbing exodus from the antimicrobial therapeutic area (Projan and Youngman 2002). Therefore, researchers have been directed to develop entirely new antibiotics based on novel bacterial targets so that less selective pressure is placed on the bacteria to develop antibiotic resistance.

Quorum sensing (QS) is one of such novel targets. Researchers have found that virulence genes are not expressed immediately upon infection when low bacteria numbers would be overwhelmed by the host’s immune system. Instead, the bacteria monitor their cell number and density, waiting until there is a critical mass before expressing virulence genes (Swift et al. 1996). This inter-cellular

bacterial signalling system is QS, which is mediated by extracellular chemical signals known as “autoinducers”. As bacterial cells accumulate in number and density, secreted autoinducers accumulate in their immediate surroundings, and these autoinducers can coordinate population-scale changes in gene regulation when the number of cell reaches a “quorum” level (March and Bentley 2004).

The capability to intercept and rewire this communication network may open a door to antimicrobial drug discovery. For this reason, we have targeted the synthesis and sensing of a bacterial autoinducer-2 (AI-2), a “universal signal” for interspecies communication among bacteria (Xavier and Bassler 2003). The metabolic pathway of AI-2 synthesis is schematically described in Figure 1-3. The precursor S-adenosylhomocysteine (SAH) is hydrolysed by enzyme Pfs (*S*-adenosylhomocysteine nucleosidase) into S-ribosylhomocysteine (SRH) and adenine, then SRH is converted by enzyme LuxS (*S*-ribosylhomocysteinase) into 4,5-dihydroxy-2,3-pentanedione (DPD) and homocysteine, and DPD finally stabilizes as AI-2 (Duerre 1962). We aim to reconstruct the AI-2 synthesis pathway in microsystems and interrogate this man-made platform for novel therapeutics discovery.

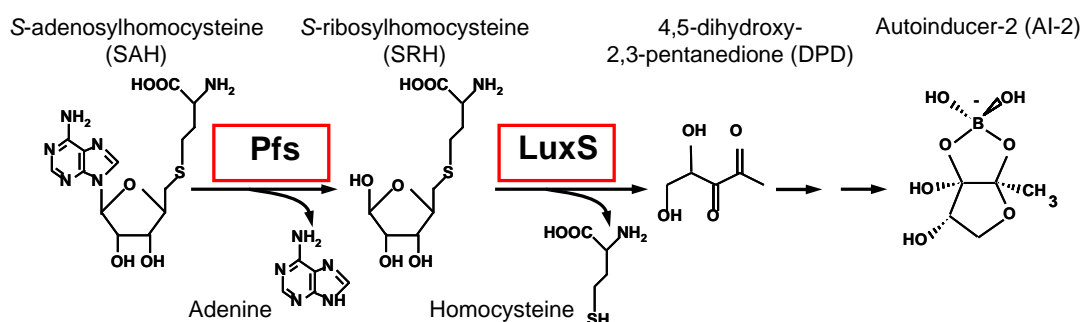


Figure 1-1: The metabolic pathway of autoinducer-2 (AI-2) synthesis.

## 1.2 Lab-on-a-chip technology and biopolymer-based bioMEMS

Microfluidics deals with a number of principles based on moving small quantities of liquids by gravity, pressure and electrokinetics through machined manifolds of channels with dimensions of 100  $\mu\text{m}$  or less. Since the first miniaturized gas chromatograph was realized on silicon wafer in 1979, incredible developments have emerged from this field, especially so during the last decade (Dittrich et al. 2006, Reyes et al. 2002). The now widely accepted lab-on-a-chip (LOC) or micro total analysis systems ( $\mu$ -TAS) go one step further and combine fluid movement with elements of processing, reacting, mixing, and fractionating of sample and reagents (Haber 2006). To explore the huge potential of different applications in the field, a component-based microfluidic approach is much too slow and the R&D effort much too expensive. Therefore, the community is now shifting from the “component-oriented solution” to an “integrated system approach” or in other words a “microfluidic platform approach” (Haeberle and Zengerle 2007). In this approach, microfluidic unit operations are combined to build application-specific microfluidic systems (Thorsen et al. 2002).

In my personal understanding, the term of microfluidics focuses more on the fluidic components and the manipulation of fluids, LOC and  $\mu$ -TAS are more commonly used by analytical chemists to stress the applications of microfluidic systems, while bio-microelectromechanical systems (bio-MEMS) emphasizes more on the functionality of such microsystems. MEMS devices built on

semiconductors convey electrical and optical signals and exhibit high throughput analysis. Biological components such as nucleic acids, enzymes and antibodies exhibit molecular recognition capabilities for biosensing functions. The integration of biology with MEMS (bioMEMS), especially with microfluidic systems, offers major advances in our ability to manipulate biomolecular systems (Andersson and van den Berg 2003, Andersson and van den Berg 2006, Atencia and Beebe 2005, Auroux et al. 2002, Beebe et al. 2002, Dittrich et al. 2006, Hong et al. 2006, Psaltis et al. 2006, Reyes, et al. 2002, Vilknær et al. 2004). Compared to traditional biochemical processing, the microfluidic environment of bioMEMS provides unprecedented advantages for biochemical analysis because of the ability to work with smaller reagent volumes, shorter reaction times and parallel operation (Beebe, et al. 2002, Bilitewski et al. 2003, Hong, et al. 2006, Shim et al. 2003).

Semiconductor-based devices are expensive due to the need of costly photolithographic equipments, the requirement of clean room access, and the time-consuming microfabrication processes. Therefore, much research has been directed to fabricate cheap disposable devices for biological applications by using alternative polymeric materials such as polydimethylsiloxane (PDMS) (Chang et al. 2003, Duffy et al. 1998, Jo et al. 2000, McDonald et al. 2000, Randall and Doyle 2005) and soft lithographic techniques such as microcontact printing (Duffy, et al. 1998, Jo, et al. 2000, McDonald, et al. 2000, Quist et al. 2005, Unger et al. 2000). However, this substitution of polymers for semiconductors poses new challenges in integrating multiple electrical and optical analysis capabilities with microfluidics, as

summarized in Figure 1-2.

Additionally, the traditional integration of biological components into microfabricated devices has been aimed at creating biosensors that meld the molecular recognition capabilities of biology with the high throughput analytical capabilities of microelectronics. The design flexibility of these devices is limited by the labile nature of these biological molecules that is incompatible with the lengthy and dry processing conditions often occurring in the device fabrication.

This research pursues a biopolymer-based bioMEMS with more design flexibility. The devices are first microfabricated, packaged and stored on the shelf. Biological elements are employed to programmably biofunctionalize the devices on demand for biological applications. Therefore, the biofunctionalization marries the signal transduction and processing capabilities of sustainable MEMS devices with the molecular recognition and self-assembly capabilities of labile biology as in Figure 1-2.

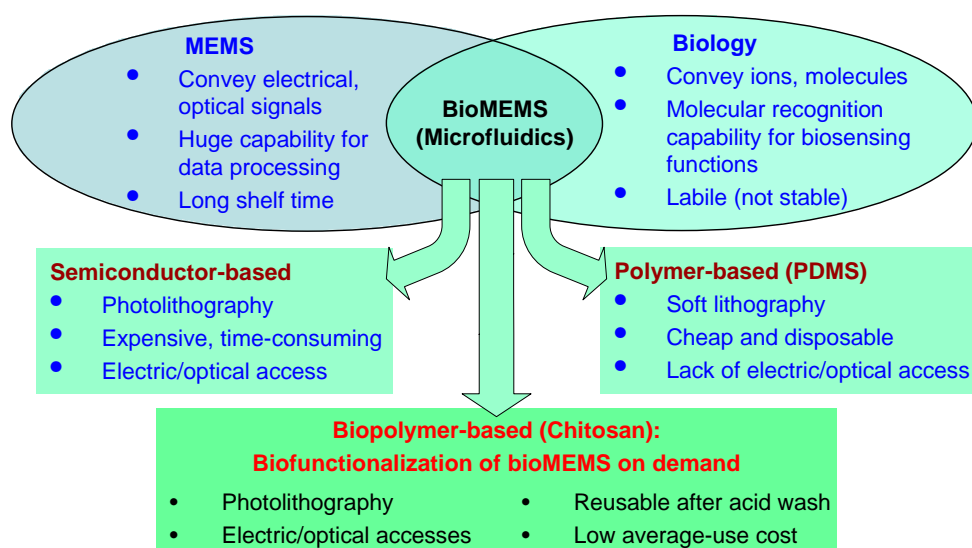


Figure 1-2: Summary of bioMEMS and biopolymer-based bioMEMS that is biofunctionalized on demand after microfabrication.

### 1.3 Enzyme assembly in bioMEMS

Miniaturized flow reactors used for enzyme assay offer a number of advantages over batch enzyme assay systems. First, only small quantities of enzyme, substrate and cofactor are needed in microfluidics, thus reducing the cost of laboratory-scale investigations. Second, in microreactors where the substrate and products flow out of the system, the problems of substrate inhibition and product inhibition encountered by some enzymes are avoided. Moreover, enzyme immobilization allows enzyme reuse and often helps to increase enzyme stability (Cao 2005, Hickey et al. 2007).

Conventional approaches of assembling enzymes in microreactors fall roughly into either the category of physical entrapment such as packed beads (Bilitewski, et al. 2003, Can Wang 2000, Ku et al. 2006, L'Hostis et al. 2000, Urban et al. 2006) or the broader category of surface immobilization (Bilitewski, et al. 2003, Chaki and Vijayamohanan 2002, Deng et al. 2006, Kisailus et al. 2006, Malpass et al. 2002, Niemeyer et al. 2003, Quist, et al. 2005). Many of the surface immobilization approaches require surface modification followed by adsorption or covalent attachment (Mao et al. 2002, Qu et al. 2004, Yakovleva et al. 2002). Standard chemistries such as formaldehyde or glutaraldehyde are used to crosslink enzymes to the modified surfaces (Hickey, et al. 2007, Honda et al. 2006, Li et al. 1999). Biotin-streptavidin chemistry is used to assemble streptavidin-linked enzymes onto biotinylated phospholipid bilayers coated inside PDMS microchannels and borosilicate microcapillary tubes (Mao, et al. 2002). Another common surface

assembly approach employs porous polymer monoliths fabricated in capillaries and microchannels by photopolymerization (Hickey, et al. 2007, Logan et al. 2007, Ma et al. 2007, Peterson et al. 2002), where the monoliths are normally modified with azlactone functionalities to react readily with the amine and thiol groups of enzymes. Layer-by-layer self-assembly of charged polysaccharides has also been implemented to incorporate enzymes on colloidal particles (Caruso and Schuler 2000) or onto the wall surfaces of a microfluidic channel (Liu et al. 2006).

Some researchers have investigated multiple steps enzymatic reactions in microdevices. Mao and co-workers performed coupled set of chemical reactions by connecting microchannels with a reversibly attachable U-shaped plastic tube (Mao, et al. 2002). Luckarift et al also connected individual microfluidic chips containing different types of enzymes in series to create a chemo-enzymatic synthesis system (Luckarift et al. 2007). Of particular interest is the work from Logan et al who used porous polymer monoliths within microfluidic devices to perform spatially separated multienzymatic reactions (Logan, et al. 2007).

In summary, microreactors provide the opportunity to reduce the cost of the investigation, only requiring microlitre amounts of substrate rather than the millilitre requirements of batch investigations and, in combination with enzyme immobilization, allow enzyme recycling, thereby further reducing the potential costs of the biocatalytic screening processes (Hickey, et al. 2007). In this research, we study the biomolecule assembly in bioMEMS device, with a particular interest in enzyme assembly and activity study in a continuous microreactor in a microchannel.

## 1.4 Metabolic pathway in bioMEMS

In this research, a unique biofunctionalization strategy has been implemented to assemble biomolecules at spatially selective sites in prepackaged bioMEMS devices. Specifically, the work focus on the programmable assembly and catalytic activity of the metabolic pathway enzyme, Pfs, in bioMEMS as an important step to reconstruct and interrogate the AI-2 synthesis pathway in the microfluidic environment. A bioMEMS was designed and fabricated that incorporates multiple microfluidic channels with optical access, two electrodes underneath each of the channels, non-permanent leak-tight sealing and systematic control of fluidic transport and electric transduction. The bioMEMS enables post-fabricated, signal-guided biofunctionalization of biomolecules such as model proteins, DNAs and metabolic pathway enzymes onto localized inorganic surface inside microfluidic channels.

The overall picture of reconstructing the metabolic pathway of AI-2 synthesis within a microfluidic channel is shown in Figure 1-3, which consists of the two AI-2 synthases, Pfs and LuxS, assembled onto the specific sites in a microfluidic channel. Precursor SAH introduced into the microchannel is enzymatically converted into

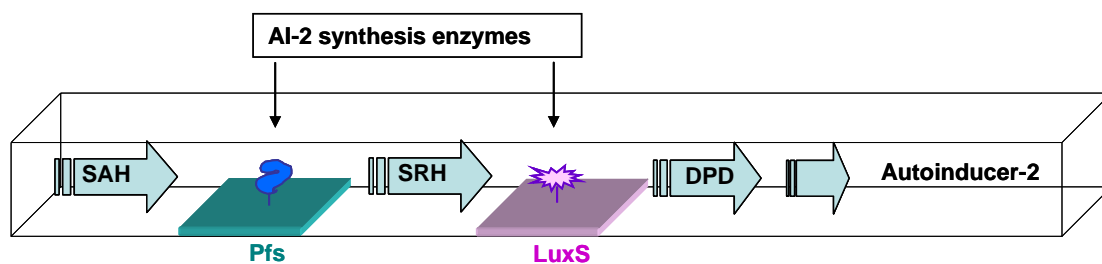


Figure 1-3: BioMEMS platform to study quorum sensing.



SRH and the byproduct adenine by the assembled enzyme Pfs, then SRH is converted into DPD and the byproduct homocysteine by the assembled enzyme LuxS. DPD stabilizes as AI-2. The biofunctionalization process is mediated by chitosan, a polysaccharide that enables electrodeposition onto spatially selective inorganic surface and covalent conjugation of biomolecules onto chitosan's primary amine groups. The enzymes with engineered pentatyrosine pro-tag are assembled onto readily addressable sites inside completely packaged microfluidic channels either by electrodepositing enzyme-chitosan conjugates or by enzymatic *in situ* activation and assembly onto electrodeposited chitosan scaffolds.

AI-2 is a small signal molecule that mediates interspecies bacterial cell-to-cell communication, or quorum sensing, which is involved in regulating many of the genes associated with bacterial pathogenesis (Balestrino et al. 2005, Barrios et al. 2006, Ren et al. 2001, Sperandio et al. 2001, Sperandio et al. 2002, Zhu et al. 2002). Inhibition or knock-down of enzymes in this pathway represent new opportunities for antimicrobial drugs that target population phenotype as opposed to essential biological functions (Rasmussen et al. 2005, Rasmussen et al. 2005). Therefore, the enzyme assembly strategy reported in this research provides a template toward rebuilding metabolic pathways in microfluidic environments for novel anti-microbial drug discovery.

## 1.5 Research goal and outline

The overall goal of this research is to demonstrate the programmable assembly and the biological activity of biomolecules in prepackaged bioMEMS devices.

This research represents an effort to integrate engineering principles and technologies with biological applications, as shown in the research outline in Figure 1-4. For this, Chapter 2 first discusses the bioMEMS devices for programmable biomolecule assembly and the unique, signal-guided biofunctionalization approach mediated with the polysaccharide chitosan. Next, the model protein assembly and DNA hybridization in bioMEMS devices are demonstrated in Chapter 3. In Chapter 4, the programmable assembly and activity of the metabolic pathway enzyme, Pfs, is demonstrated as an important step to reconstruct the AI-2 synthesis pathway in bioMEMS. The design and packaging optimization of bioMEMS devices are further discussed for programmable enzyme assembly and activity in Chapter 5. Finally, Chapter 6 summarizes conclusions and ongoing/future work.

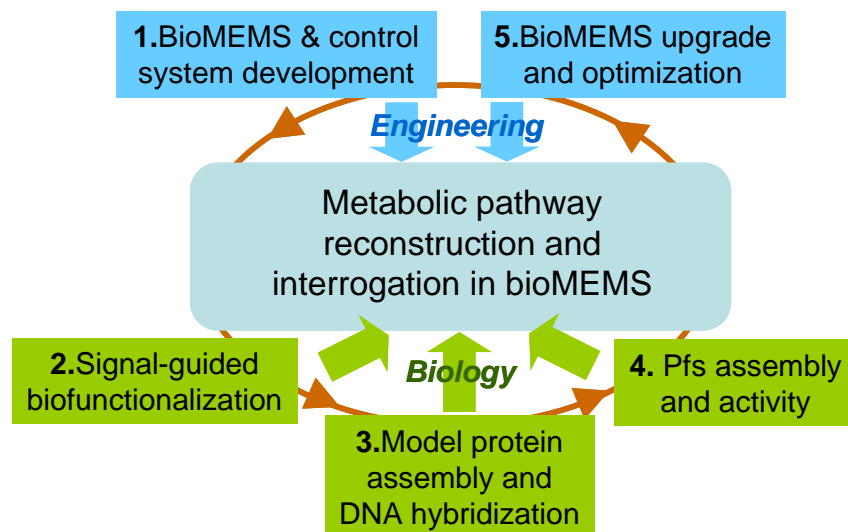


Figure 1-4: Outline of this research that integrates engineering with biology.

## **Chapter 2. BioMEMS Devices, Control System and Chitosan as Soft-interconnect in BioMEMS**

Integration of engineering principles and technologies with biological applications is exemplified throughout this research. This chapter first reviews the bioMEMS devices that have been developed for programmable biomolecule assembly and describes my contribution in the device development. Next is the discussion of a bioMEMS control system that I built to control the pumping and selection of fluidic sources for biochemical applications that require multiple process in microsystems. Finally, the chitosan-mediated, signal-guided biofunctionalization approach that was implemented in the following chapters is discussed for programmable assembly and activity of biomolecules in bioMEMS devices.

### **2.1 BioMEMS devices for biomolecule assembly**

The design and fabrication process of our bioMEMS device with packaging shown in Figure 2-1 was reported previously (Park et al. 2006). Briefly, the bioMEMS device features six identical microchannels evenly distributed on a 4" Pyrex wafer with two rectangular gold electrodes underneath each microchannel, one as working electrode and the other as counter electrode. A chromium adhesion layer (100 Å) and then a gold layer (2000 Å) were first deposited onto a 4" Pyrex wafer, and rectangular gold electrode patterns (1 mm × 0.5 mm) were created by

photolithography. SU-8 50 (MicroChem, Newton, MA) was patterned on the top of substrate and electrode surface to form structures which serve a dual function, namely (1) sidewalls for a microfluidic channel of 150  $\mu\text{m}$  high and 500  $\mu\text{m}$  wide, and (2) sharp “knife-edge” structures for reliable leak-tight sealing to a PDMS layer above.

The wafer was sealed leak-tight by a 300- $\mu\text{m}$ -thick top sealing PDMS layer spun on a sealing Plexiglas plate, and the SU-8/PDMS junction was compressed by two packaging Plexiglas plates with six pressure-adjustable compression bolts (1/4"-28) hexagonally spaced on the ring and six force tuneable socket screws (1/4"-28) hexagonally spaced on the ring and six force tuneable socket screws

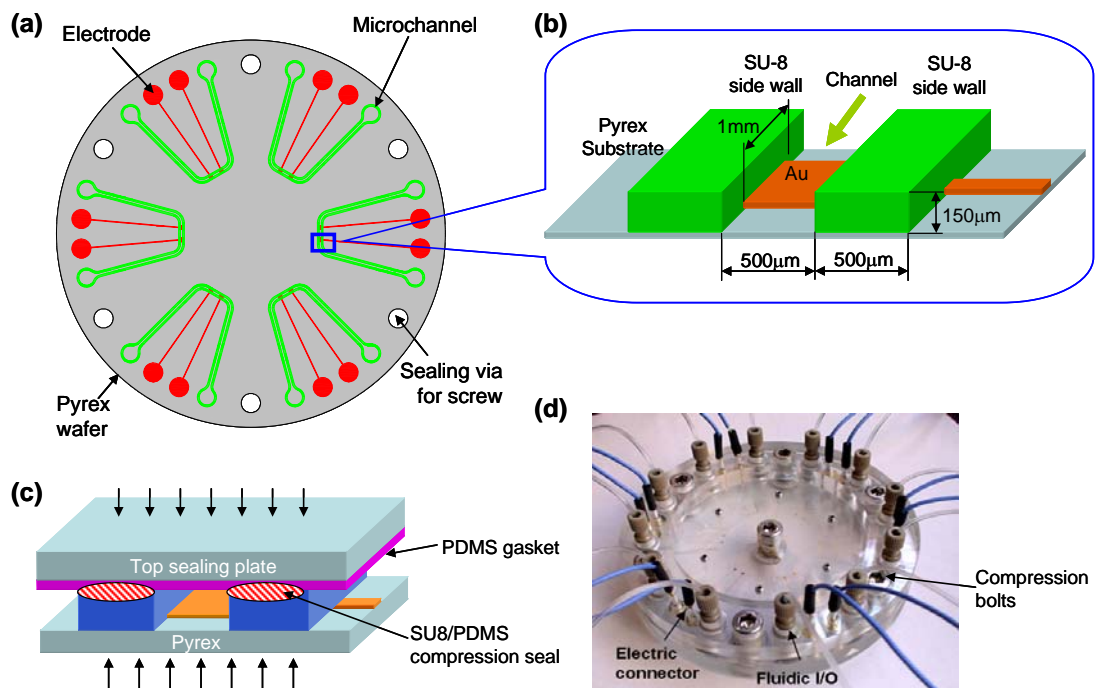


Figure 2-1: The bioMEMS device for biomolecule assembly. (a) Schematic of a 4” Pyrex wafer with 6 SU-8 microchannels with two electrodes underneath each microchannel. (b) 3-D drawing of a microchannel. (c) Non-permanent sealing of a microchannel by a PDMS gasket with pressure. (d) Assembled microfluidic device with electric and fluidic connections.

(4–40) between every two microchannels. Fluidic connectors (Nanoport™ Technologies, Portland, OR) and electric Pogo pins (Interconnect Devices, Kansas City, KS) were assembled through punched holes on the sealing PDMS and drilled-holes through the top sealing and packaging Plexiglas plates, and then connected to external pressure-driven aqueous transport, and electrical signal, correspondingly.

My contribution to the development of this bioMEMS device is mainly in two aspects as shown in Figure 2-2. First, the in-channel reservoirs with curved microchannels (point  $A \rightarrow A'$ ,  $B \rightarrow B'$ ) were replaced so that the fluid flow is smoothed and in-channel fluidic residue is minimized. Second, the alignment of the bioMEMS wafer to external plastic tubing and has been improved and the interconnection reservoirs (point  $C \rightarrow C'$ ,  $D \rightarrow D'$ ) has been shrunken to minimize the dead volume within the interconnections. Further improvements and new bioMEMS designs have been conducted and detailed in Section 5.2 for multi-step biochemical reactions in bioMEMS.

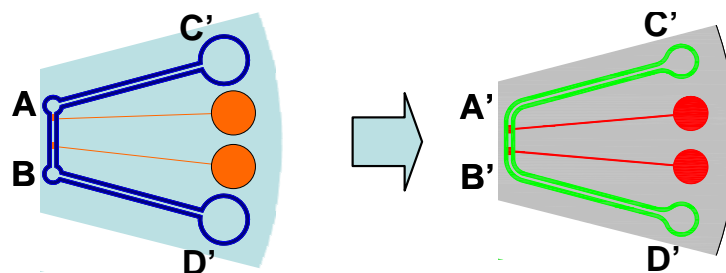


Figure 2-2: Improvements of the bioMEMS device by curving the microchannel ( $A \rightarrow A'$ ,  $B \rightarrow B'$ ) and shrinking the interconnection reservoirs ( $C \rightarrow C'$ ,  $D \rightarrow D'$ ).

## 2.2 BioMEMS system control technology

The biomolecule assembly in bioMEMS of this research normally consists of a series of biochemical processes including preparation steps such as buffer rinsing, non-specific blocking and device biofunctionalization, and the intended biochemical reactions. Repeated reactions are also conducted within the same device as our bioMEMS device has been demonstrated to be reusable.

To better facilitate the multiple-step biochemical process in the bioMEMS device, a bioMEMS control system as shown in Figure 2-3 was built to systematically control the selections from multiple solution sources and the pumping

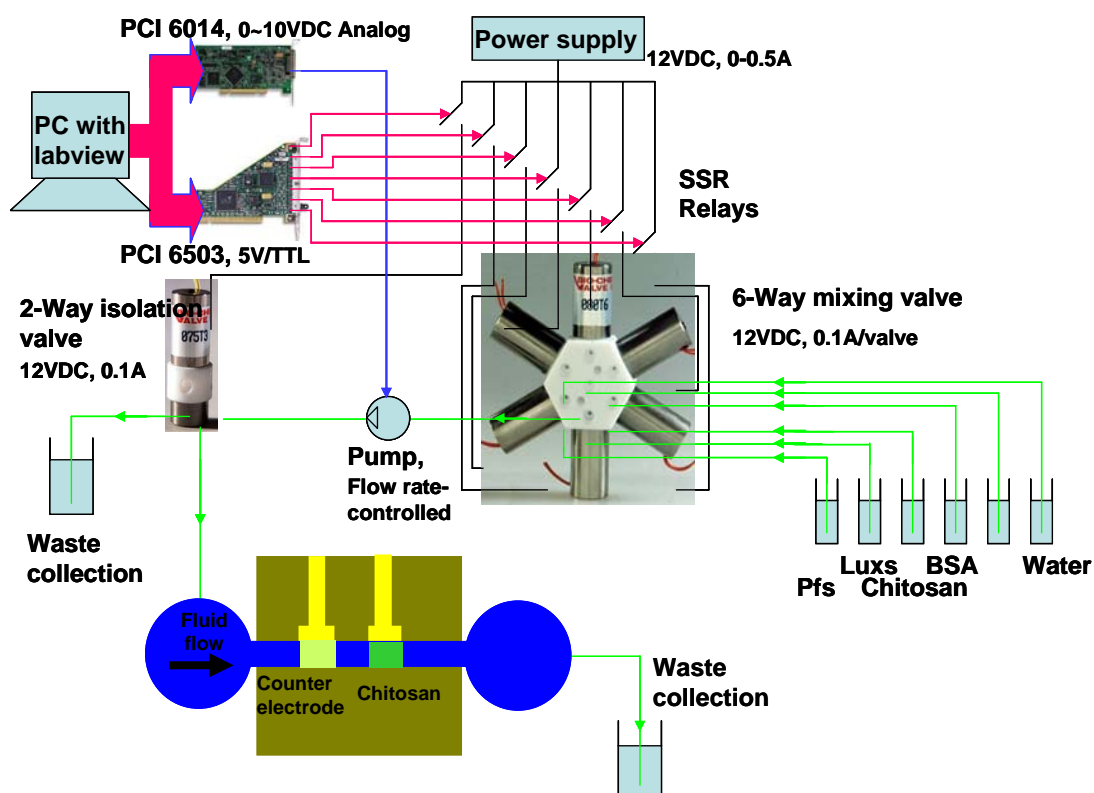


Figure 2-3: BioMEMS control system. The control system controls the selections from multiple solution sources and the pumping flow rate into microfluidic channels.

into microfluidic channels. The control system mainly consists of a peristaltic micropump (Masterflex1 pump drive, Cole-Palmer Instrument Co) with two cartridges in alternating directions on a 8-roller cartridge pump head (Masterflex pump head, Cole-Palmer Instrument Co) to achieve near pulseless combined output flow, a 6-to-1 solenoid valve (Bio-Chem Valve / Omnifit, NJ) with separate tubing (0.19 mm ID, Tygon1) to select solutions from multiple sources, a 1-to-2 isolation valve (Bio-Chem Valve / Omnifit, NJ) to direct the pumping either to waste collection or to the bioMEMS chip, and a LabView-based program which sends digital signals to control the selection of fluidic sources and the on/off switching of the pump, and sends analog signals to control the flow rate.

The assembled bioMEMS control system is shown in Figure 2-4. The system

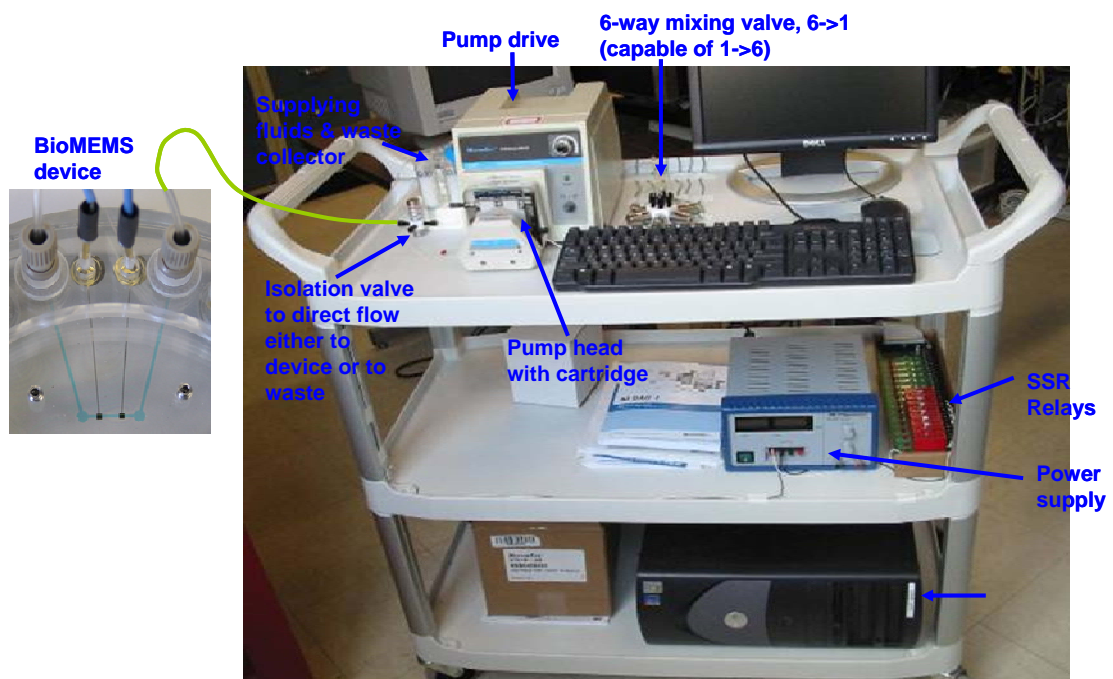


Figure 2-4: BioMEMS control system. The control system controls the selections from multiple solution sources and the pumping flow rate into microfluidic channels.

is capable of controlling the microfluidic flow rate in the range of 2.8–280  $\mu\text{L}/\text{min}$ .

Another LabView program was used to control electrodeposition process and to monitor the voltage of the applied electrical signal (2–3 V measured during the electrodeposition process). A network simulation (VisSim<sup>TM</sup> 3.2, Design Science Inc.) showed that at 5  $\mu\text{L}/\text{min}$  flow rate, the velocity inside the channel (cross section: 500  $\mu\text{m} \times 150 \mu\text{m}$ ) is 1.1 mm/s.



## 2.3 Chitosan as soft interconnect in bioMEMS

Chitosan is a linear  $\beta$ -1, 4-linked polysaccharide that is derived from the partial deacetylation of chitin, an abundant organic material found in the shells of crabs and some insects. The unique structural feature of chitosan is the presence of the high content of primary amines at the C-2 position of the glucosamine residues. These primary amines confer two important properties. First, the solubility of chitosan is pH-responsive, as shown in Figure 2-5(a). At low pH, the primary amine groups

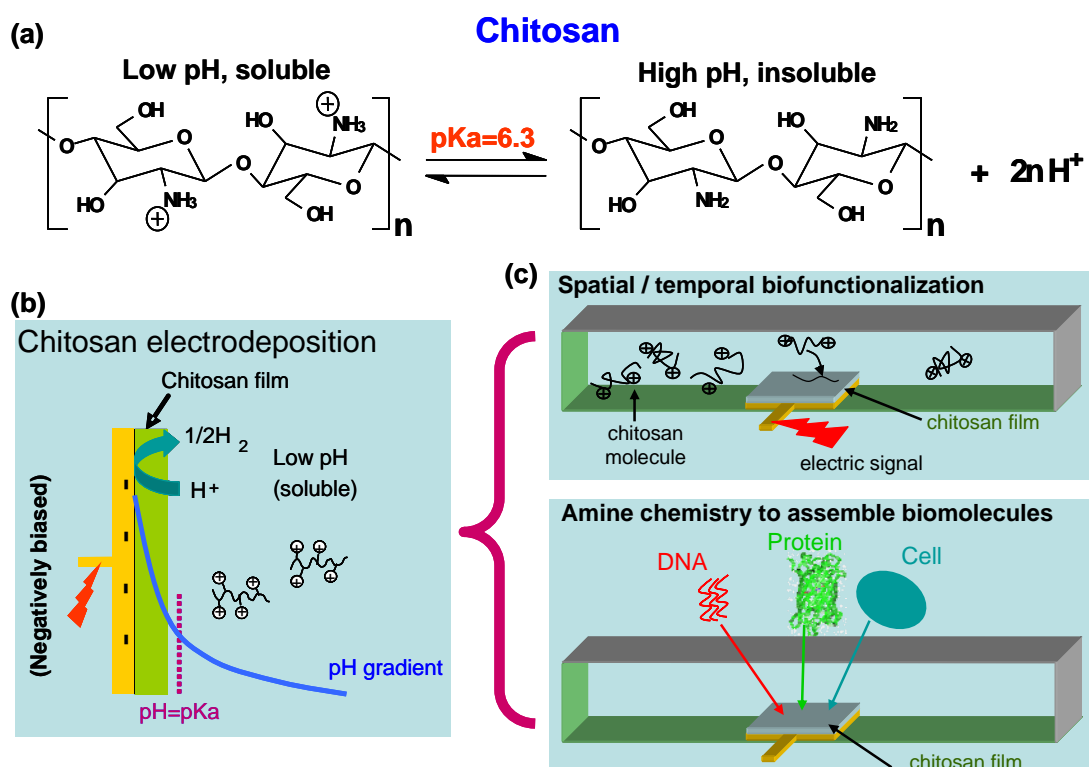


Figure 2-5: Chitosan as the biointerfacial material in microfluidics. (a) Solubility of the polysaccharide chitosan is pH dependent. (b) Electrical signal-guided chitosan deposition at cathode surface where pH gradient is created by negative electrical potential. (c) Chitosan enables spatial/temporal biofunctionalization of bioMEMS device and immobilization of biomolecules in microfluidic channel.

are protonated, making chitosan soluble. As the pH rises above chitosan's pKa value of around 6.5, a particularly convenient range for biological applications, the amines become deprotonated, making chitosan insoluble. By taking advantage of this controlled solubility, chitosan can be electrodeposited onto patterned electrodes guided by electrical signals with spatial and temporal control (Wu et al. 2002, Wu et al. 2003), as shown in Figure 2-5(b).

Second, the abundant reactive amine groups on chitosan allow a range of chemistries to be employed to biofunctionalize chitosan or to cross-link the chitosan backbone to confer elasticity. Therefore, chitosan is an ideal interfacial material between biological molecules and inorganic surfaces, and electrical signals have been applied in many applications to deposit chitosan for the assembly of nucleic acids, proteins, viruses and even cells onto patterned inorganic surface (Yi et al. 2005, Yi et al. 2004, Yi et al. 2005). Chitosan is recognized as a soft component-hard device interconnect for biofabrication (Yi et al. 2005) and a length-scale interconnect for the hierarchical assembly of nano-scale components into macro-scale systems (Payne and Raghavan 2007).

In this research, chitosan is utilized as a programmable platform for biomolecule assembly in the microfluidic environment. As shown in Figure 2-5(c), the electrodeposition of chitosan enables the biofunctionalization of the bioMEMS devices in Section 2.1 with temporal and spatial programmability. Electric signal is applied to electrodeposit chitosan at specific sites in microchannels of prefabricated bioMEMS devices just before introducing and conjugating biomolecules for

biological applications. The amine chemistry of chitosan enables the assembly of biomolecules onto the electrodeposited chitosan scaffold while retaining the biological activity of the assembled biomolecules.

## 2.4 Summary

In summary, microdevices have long shelf life and are normally microfabricated, packaged and stored until the need of biological applications arises. Chitosan as an ideal biointerfacial material has been employed to programmably biofunctionalize the devices on demand for biological applications. The biofunctionalization imparts the bioMEMS devices with the molecular recognition and self-assembly capabilities of labile biology.

In the following chapters demonstrates biomolecule assembly onto specific sites in bioMEMS device, with a particular focus on the assembly and activity of the metabolic pathway enzyme Pfs in prepackaged bioMEMS. Additionally, this research investigates the design optimization of bioMEMS devices and experimental strategy for studies of metabolic pathway enzyme.

## Chapter 3. Programmable Model Protein Assembly and DNA Hybridization in BioMEMS

This chapter reports facile *in situ* biomolecule assembly at readily addressable sites in microfluidic channels of prepackaged BioMEMS devices. As mentioned in Section 2.3, chitosan's pH responsive and chemically reactive properties allow electric signal-guided biomolecule assembly onto conductive inorganic surfaces from the aqueous environment, preserving the activity of the biomolecules. The transparent and nonpermanently packaged bioMEMS device as mentioned in Section 2.1 allows for electrical signal-guided biomolecule assembly onto the patterned gold electrode sites within the microchannels. In this chapter, we demonstrate that chitosan-mediated *in situ* biomolecule assembly is a simple approach to direct the assembly of biological components into prefabricated bioMEMS devices. Specifically, the biomolecules were assembled onto patterned electrodes in microchannels with spatial and temporal programmability. We believe that this strategy holds significant potential as a simple and generic biomolecule assembly approach for future applications in complex biomolecular or biosensing analyses as well as in sophisticated microfluidic networks.

Section 3.1 demonstrates *in situ* green fluorescence protein (GFP) protein assembly onto a chitosan scaffold in a bioMEMS device by chemically activating the amine groups of chitosan with glutaraldehyde. Section 3.2 demonstrates *in situ*

biochemical activation and protein assembly onto a chitosan scaffold in a bioMEMS device. In both demonstrations, the assembled model protein GFP retained fluorescence and hence its 3-dimensional structure. Section 3.3 demonstrates DNA hybridization onto electrodeposited chitosan scaffold by glutaraldehyde activation.

### **3.1 Programmable GFP assembly via glutaraldehyde activation**

*\*\*\*This work was done together with Jung Jin Park. Jin designed and fabricated the bioMEMS device, I designed and built the bioMEMS control system. We worked together to conduct the experiment and analyze the results.\*\*\**

#### **3.1.1 Materials and methods**

Chitosan (minimum 85% deacetylated chitin; molecular weight 200,000 g/mol) from crab shells, phosphate buffered saline (PBS) (2.7 mM KCl, 137 mM NaCl, 1.5 mM  $\text{KH}_2\text{PO}_4$ , 8.1 mM  $\text{Na}_2\text{HPO}_4$ , pH 7.5) and glutaraldehyde (grade I, 50% aqueous solution) were purchased from Sigma (St. Louis, MO). Sodium hydroxide was purchased from J.T. Baker (Phillipsburg, NJ). Bleach was purchased from James Austin Co. (Mars, PA). De-ionized water (ddH<sub>2</sub>O, 18 MVcm, Milli-Q) and PBS (dissolved in de-ionized water) were autoclaved before use. Chitosan solution was prepared by adding chitosan flakes in de-ionized water, with HCl added dropwise to maintain pH ~ 2, and mixing overnight. The pH was then adjusted to 3.5 by adding 1 M NaOH dropwise, and the chitosan solution was then filtered and stored at 48° C. The bioMEMS device fabrication and packaging is discussed in Section 2.1. To

avoid cross contamination between the several solutions, the bioMEMS control system in Section 2.2 is used to control the selection and pumping of different solution into the bioMEMS device.

Programmable green fluorescent protein was assembled onto electrodeposited chitosan scaffold via glutaraldehyde activation of the amine groups of chitosan. First, the experimental microchannel and all connecting tubing (0.02" ID, Tygon) were rinsed with de-ionized water at 50  $\mu\text{L}/\text{min}$  flow rate for 30 min. Chitosan (0.375% (w/w), pH 5) was pumped into the microfluidic system at 5  $\mu\text{L}/\text{min}$  flow rate. After the microchannel was completely filled with chitosan solution, the pump was stopped. The DC power supply (2400 SourceMeter, Keithley Instrument, Cleveland, OH) was then used to maintain negative bias voltage on the gold (working) electrode under constant current conditions of 3  $\text{A}/\text{m}^2$  for 240 sec, while a second gold electrode served as the anode. The chitosan solution was then drained from the system, and the deposited chitosan was neutralized with PBS (30 min at 5  $\mu\text{L}/\text{min}$  flow rate).

After draining the PBS buffer, glutaraldehyde solution (0.5 %) was introduced at 5  $\mu\text{L}/\text{min}$  flow rate for 30 min, followed by PBS buffer rinsing for 30 min. GFP solution was then introduced into the microchannel for 15 min at 5  $\mu\text{L}/\text{min}$  flow rate. For *in situ*, real time observation on the test site, microfluidic system was placed under the microscope during whole process steps. Finally, the microfluidic channel was rinsed at 5  $\mu\text{L}/\text{min}$  PBS for 30 min. For the negative control, we repeated the same processes on a separate channel except that no negative bias was applied (no chitosan electrodeposition). ImageJ analysis software was used to analyze fluorescent 3-D

contour (National Institutes of Health).

### 3.1.2 Results and discussion

The programmable GFP assembly results onto electrodeposited chitosan scaffold via glutaraldehyde activation of the amine groups of chitosan are shown in Figure 3-1. For this, we first electrodeposited chitosan on to a gold electrode in a microfluidic channel followed by introduction of a 0.5% glutaraldehyde solution, an amine group reactive homobiofunctional cross-linker that activates chitosan for covalent coupling with amine groups on proteins. As shown in Figure 3-1(a), no significant fluorescence appears up to this activation step, as expected. Next, we introduced an aqueous solution of green fluorescent protein (GFP) into the microchannel. Figure 3-1(b) illustrates that GFP reacts with and becomes conjugated onto the activated chitosan scaffold. This result shows that electrodeposited chitosan enables post-fabrication, *in situ* assembly of proteins in microfluidic channels through series of simple standard chemical reactions all in aqueous environment. Importantly, the assembled GFP retains the fluorescence, indicating that the structure of the protein is preserved throughout the assembly procedure.

Figure 3-1(c) shows the results of a negative control experiment inside a new microchannel, which underwent the identical procedure as in the previous microchannel except that the electrode was not negatively biased for chitosan electrodeposition. This result confirms that the *in situ* protein assembly requires electrodeposited chitosan as the covalent coupling scaffold. Further, 3-D fluorescent

contour in Figure 3-1(e) shows uniform fluorescent intensity of GFP decorated chitosan film.

Combined these results demonstrate *in situ* protein assembly in the microfluidic device, which could be further exploited for biochemical reactions or biosensing applications based on *in situ* assembled enzymes or antibodies at readily addressable, activated chitosan scaffold sites in microfluidic devices. Particularly important to note is that the sequences of steps and electric signal-guided biomolecule assembly strategy

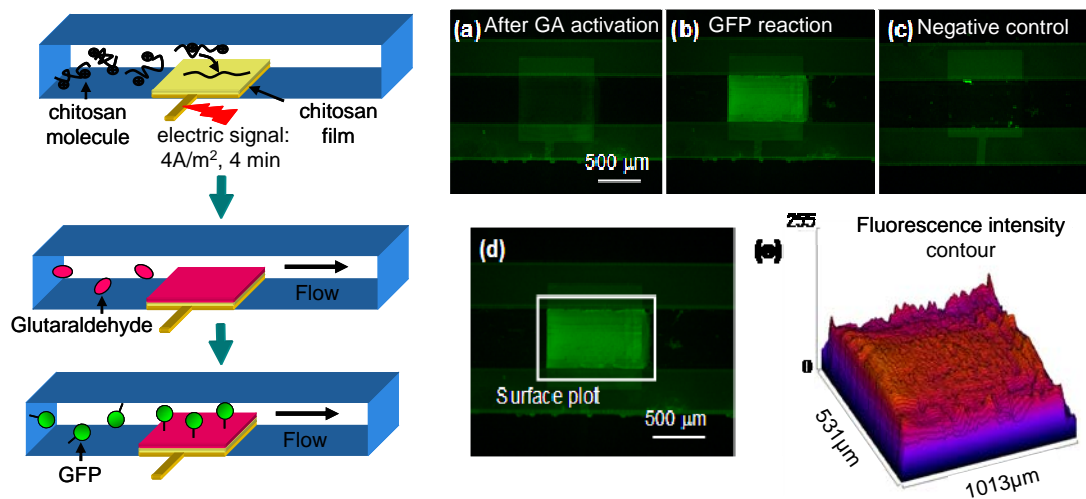


Figure 3-1: Programmable assembly of green fluorescent protein (GFP) via glutaraldehyde activation of chitosan scaffold. Left: Schematic of protein assembly procedure. Right: Fluorescent photographs and intensity contour of protein assembly. allow all-aqueous environment for the protein assembly, preserving the biological activities.



## 3.2 Programmable GFP assembly via *in situ* enzymatic activation

*\*\*\*This work was done together with Angela Lewandowski. Angie prepared the protein solution and other materials, I fabricated the bioMEMS devices. We worked together to conduct the experiment and analyze the experimental results.\*\*\**

The GFP assembly in bioMEMS under flow in the previous section was done by glutaraldehyde activation of the amine groups on electrodeposited chitosan scaffold. In this section, we demonstrate the GFP assembly in bioMEMS under flow via *in situ* enzymatic activation of the genetically fused pentatyrosine pro-tag at its C-terminus. While both surface-assembly approaches enable spatial selectivity in bioMEMS devices, the assembly via enzymatic activation of fusion pro-tag enables orientational control of the assembled protein under mild experimental conditions (Lewandowski et al. 2006).

### 3.2.1 Materials and methods

Tyrosinase from mushroom (1,530 Units/mg solid) was purchased from Sigma (St. Louis, MO). Sodium hydroxide was purchased from J.T. Baker (Phillipsburg, NJ). Acetone, hydrochloric acid, sulfuric acid, and glycerol were purchased from Fisher Chemical (Fair Lawn, NJ). All other materials including chitosan, phosphate buffered saline (PBS), bleach, Sodium hydroxide and De-ionized water were purchased and prepared similarly as in Section 3.1. The bioMEMS device fabrication and packaging is discussed in Section 2.1. The bioMEMS control system

shown in Figure 2-3 was implemented to enhance control over different solutions and processes.

The same device cleaning steps, chitosan electrodeposition, and PBS buffer neutralization steps were performed as described in Section 3.1.1. After draining the PBS buffer, a PBS solution with (His)<sub>6</sub>-GFP-EK-(Tyr)<sub>5</sub> (0.2 mg/mL) and tyrosinase (0.1 mg/mL or 166 Units/mL) was pumped at 5  $\mu$ L/min over the deposited chitosan. As a control, a PBS solution with GFP but without tyrosinase was pumped at 5  $\mu$ L/min flow rate over the deposited chitosan. Between experiments the system was cleaned by rinsing with 1.4 M HCl and then concentrated bleach at 5  $\mu$ L/min flow rate for 10 min each, followed by thorough rinsing with de-ionized water at 50  $\mu$ L/min flow rate for 30 min. For real-time *in situ* fluorescence and observation, the microfluidic device was placed under a microscope (model 310, Carl Zeiss, Thornwood, NY) and a UV source (Zeiss HBO 100). Fluorescence micrographs were acquired every minute from the microscope using a digital camera (Carl Zeiss AxioCam MRc5). Finally, the system was washed with PBS (30 min at 5  $\mu$ L/min flow rate). ImageJ software (National Institutes of Health) was used to analyze the fluorescence intensity of the final fluorescence micrographs.

### 3.2.2 Results and discussion

The *in situ* enzymatic activation and assembly of GFP onto a selected electrode pattern within a completely packaged microfluidic device is shown in Figure 3-2. For this, we fabricated a microfluidic device that features six identical microchannels

evenly distributed on a 4” Pyrex wafer; one microchannel is illustrated in Figure 3-2(a). We electro-assembled chitosan scaffold onto a selected gold electrode pattern within a microchannel by transporting chitosan solution into the channel, and then stopping the pump and applying negative bias to the electrode pattern as shown in Figure 3-2(b). Next, we continually pumped through the channel a PBS solution containing the target protein GFP and the activating enzyme tyrosinase to activate and assemble GFP onto the electro-assembled chitosan scaffold. We observed the fluorescence profile of the 1 mm × 0.5 mm assembly site (scaffold) in real time through an on-site fluorescence microscope.

As illustrated in Figure 3-2(c), the fluorescence intensity of the assembly site gradually increased with time until reaching a maximum constant level. Importantly, the fluorescence remained high even after thorough PBS buffer rinsing, indicating that GFP was covalently bound to the chitosan scaffold. Next, we analyzed the fluorescence intensity of the final micrograph of the assembly site using ImageJ software, which illustrates that GFP assembled relatively uniformly onto the scaffold pattern. These results demonstrate that (1) the target protein GFP assembled only onto the chitosan scaffold with high spatial selectivity, and uniformity, (2) the assembled GFP remained fluorescent after thorough rinsing, and (3) non-specific binding of GFP to other channel surfaces was minimal, as there was no significant fluorescence of the microchannel floor, ceiling, or walls.

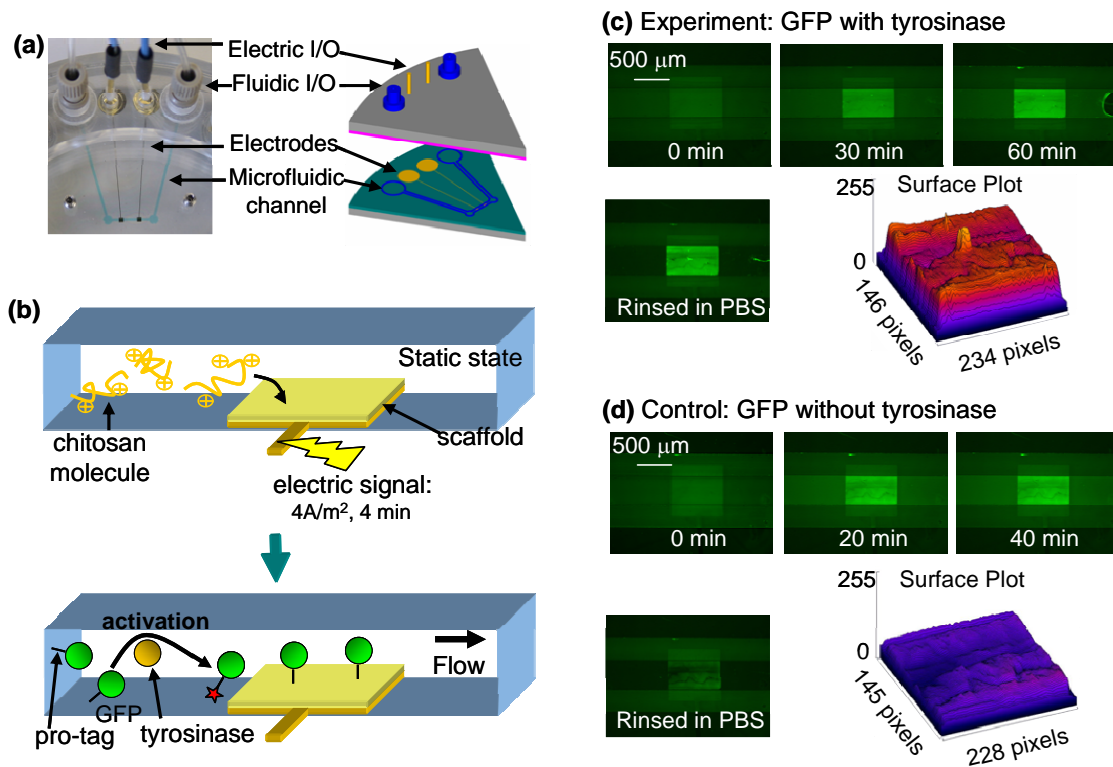


Figure 3-2: Programmable assembly of green fluorescent protein (GFP) via *in situ* enzymatic activation. (a) A microfluidic device. (b) Schematic procedure. (c) Experiment: tyrosinase was added for *in situ* enzymatic activation thereby GFP was covalently assembled on chitosan scaffold. (d) Control: no tyrosinase was added for *in situ* enzymatic activation thereby no GFP was covalently assembled on chitosan scaffold.

Next, we performed control experiments to examine nonspecific binding of unactivated GFP to the electro-assembled scaffold. For this, we reused the same microchannel by removing the scaffold from the previous experiment with dilute hydrochloric acid. We then reassembled the chitosan scaffold onto the electrode pattern, and then continually pumped through the channel a PBS solution containing only the target protein GFP (without the activating enzyme tyrosinase). As illustrated in Figure 3-2(d), the fluorescence intensity of the assembly site gradually increased

with time until reaching a constant level. However, the fluorescence decreased significantly upon PBS buffer rinsing, as illustrated by ImageJ software analysis of the final fluorescence micrograph (the surface plot represents the pixel intensity over the deposition area). Further ImageJ analysis of the micrographs in Figure 3-2(c) and (d) suggests that the final level of GFP upon rinsing after tyrosinase treatment in Figure 3-2(c) was about 92% (e.g., loss from the 60 min time point) and that the final level in Figure 3-2(d) (no tyrosinase) was ~25% of that in Figure 3-2(d). These results indicate that the GFP without tyrosinase was loosely bound to the chitosan scaffold, and easily rinsed off, and confirm that activation of the pro-tag by tyrosinase is required for GFP assembly.

We have demonstrated here, for the first time, *in situ* enzymatic activation, and assembly of a target protein onto a patterned scaffold within a microfluidic channel under flow. The target protein GFP assembled covalently and uniformly in a spatially selective manner, and was not released upon further flow of buffer rinsing. This is significant, as we are unaware of any reports demonstrating the spatially resolved enzymatically activated covalent assembly of proteins in microchannels under flow. Additionally, GFP is assembled predominately through its C-terminal pro-tag, and is in a specific orientation onto the patterned scaffold surface. In contrast, our previous work with microfluidic channels the protein was covalently linked through its native amines to a glutaraldehyde-activated chitosan film surface and in no particular orientation (Park, et al. 2006). Finally, assembly occurs in a completely fabricated and packaged device for reusability, and as mentioned before, occurs under mild

experimental conditions ideal for maintaining protein biological function: in aqueous solution, through enzymatic activation, and at neutral pH. These unique advantages of our assembly strategy combined with the well-known advantages of microfluidic devices (i.e., rapid response time and small volumes of expensive reagents) make this particularly appealing for applications that necessitate microfluidic systems.

In summary, Figure 3-2 demonstrates *in situ* enzymatic activation and assembly of the target protein GFP within a prefabricated and fully packaged bioMEMS device under flow. Assembly is covalent and robust, spatially selective (only onto selected patterned scaffold surfaces), and occurs under mild experimental conditions. Importantly, our assembly approach is readily applicable to microfluidic systems. Combined, these advantages make our assembly approach appealing for a wide variety of bioMEMS applications that require facile device biofunctionalization.

### 3.3 DNA hybridization in bioMEMS

#### 3.3.1 Materials and Methods

PerfectHyb Plus hybridization buffer, saline sodium citrate (SSC) buffer (20X concentrate, molecular biology grade), and Tris-EDTA (TE) buffer (100X concentrate) were all purchased from Sigma (St. Louis, MO). Glacial acetic acid,  $MgCl_2 \cdot 6H_2O$  (enzyme grade), and sodium borohydride powder ( $NaBH_4$ ) were purchased from Fisher Chemical (Fair Lawn, NJ). All other materials including chitosan, glutaraldehyde, phosphate buffered saline (PBS), sodium hydroxide and de-ionized water were purchased and prepared similarly as in Section 3.1. Unless otherwise noted, 1X SSC buffer with 0.1 M  $MgCl_2$  was used for equilibration and rinsing throughout this study. To prepare this SSC buffer, the SSC buffer of 20X concentrate was first distilled with ddH<sub>2</sub>O. After autoclaving, a solution of autoclaved 4 M  $MgCl_2$  was added to adjust the pH to 7.1. All single-stranded DNA (ssDNA) molecules were purchased from Gene Probe Technologies, Inc. (Rockville, MD). These DNAs are HPLC-purified and were used without further purification. The bioMEMS device fabrication and packaging are discussed in Section 2.1. The bioMEMS control system shown in Figure 2-3 was implemented to enhance control over different solutions and processes.

Schematic flow of DNA hybridization process on electrodeposited chitosan scaffold inside a microchannel is shown in Figure 3-3(a). The same device cleaning steps, chitosan electrodeposition, and PBS buffer neutralization steps were performed

as described in Section 3.1.1 (*Step 1*). After draining the PBS buffer, glutaraldehyde solution (0.5 %) was introduced at 5  $\mu\text{L}/\text{min}$  flow rate for 30 min, followed by PBS buffer rinsing for 30 min (*Step 2*). Next, probe ssDNA solution (20  $\mu\text{g}/\text{mL}$ , 5'-amino) was introduced over the activated chitosan in the microchannel for 60 min at 5  $\mu\text{L}/\text{min}$  flow rate, followed by PBS buffer rinsing for 30 min (*Step 3*).  $\text{NaBH}_4$  solution, PBS buffer and hybridization buffer were then introduced into the microchannel in a sequence for 20 min, 30 min and 10 min, respectively.

For the DNA hybridization, mismatch target ssDNA (0.5  $\mu\text{M}$  in hybridization buffer, 5'-FITC) was first flowed over the assembled probe ssDNA on the electrodeposited chitosan scaffold in the microchannel for 30 min at 0.5  $\mu\text{L}/\text{min}$  flow

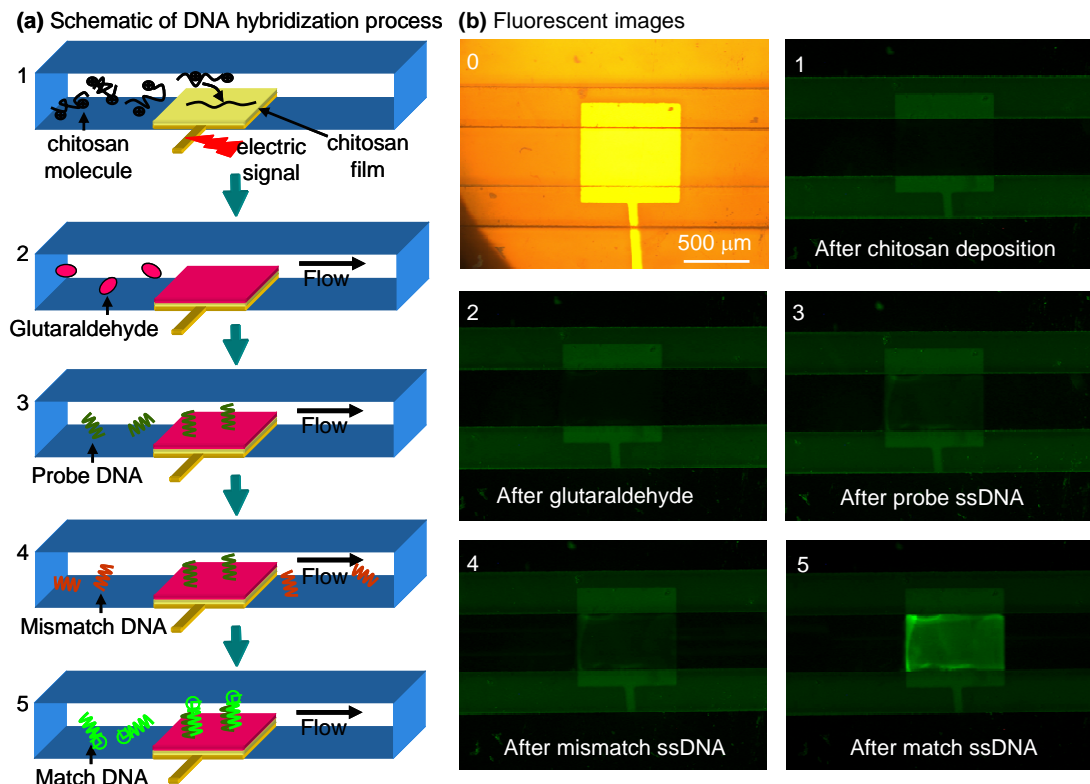


Figure 3-3: DNA hybridization in bioMEMS. (a) Schematic procedure. (b) Fluorescent micrographs.



rate, followed by hybridization buffer conditioning for 10 min (*Step 4*). Then match target ssDNA (0.5  $\mu$ M in hybridization buffer, 5'-FITC) was introduced into the microchannel for 30 min at 0.5  $\mu$ L/min flow rate, followed by hybridization buffer and PBS buffer rinsing for 10 min, respectively (*Step 5*). For *in situ*, real time observation on the test site, the bioMEMS device was placed under the microscope during whole process steps. ImageJ analysis software was used to analyze fluorescent 3-D contour.

### 3.3.2 Results and discussion

The experimental results of *in situ* probe ssDNA assembly onto electrodeposited chitosan scaffold and the subsequent DNA hybridization are shown in Figure 3-3. After chitosan electrodeposition (*step 1*) and glutaraldehyde activation (*step 2*), no significant fluorescence was observed as expected. During the introduction of probe ssDNA, the amine groups at the 5'-end probe was assembled via glutaraldehyde onto the chitosan scaffold (*Step 3*), which shows very weak fluorescence due to the intrinsic fluorescence of the probe DNA in Figure 3-3(b) #3. Next, an aqueous solution of mismatch target DNA was introduced into the microchannel (*Step 4*), up to which the assembly site shows no significant fluorescence, indicating that mismatch target ssDNA didn't hybridize the probe ssDNA, as expected. Finally, the match target ssDNA solution was introduced into the microchannel (*Step 5*). As illustrated in Figure 3-3(b) #5, the match target ssDNA hybridizes with their complementary probe ssDNA assembled on the activated chitosan scaffold. Figure 3-4 shows the sequential micrographs of DNA hybridization during the introduction of match target ssDNA into

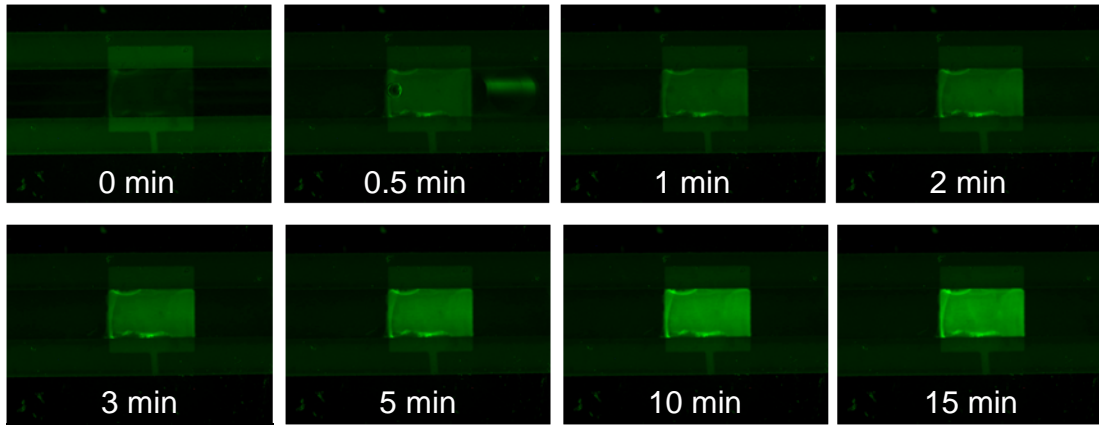


Figure 3-4: DNA hybridization in bioMEMS: Sequential micrographs during introduction of match target ssDNA

the microchannel. The fluorescence signal on chitosan scaffold gradually increased in the first 10 minutes and then reached the plateau after 15 minutes, indicating sufficient match target ssDNA hybridized to the probe until the chitosan scaffold saturated.

These results confirm that electrodeposited chitosan enables post-fabrication, spatially selective DNA hybridization in the microfluidic environment through a series of simple standard chemical reactions, all in an aqueous environment. Signal-directed sequential assembly of DNA onto spatially selective assembly sites is demonstrated in our bioMEMS devices. Importantly, probe DNA on the electrode retained its hybridization capacity throughout the assembly and hybridization procedures.

### 3.4 Conclusions

In this chapter, we demonstrated the *in situ* biomolecule assembly as a simple and versatile approach to direct the assembly of biological components into prefabricated bioMEMS devices. Our approach is based on electro-deposition of the aminopolysaccharide chitosan scaffold as a stable thin film onto patterned conductive surfaces of bioMEMS devices followed by covalent assembly of biomolecules onto the surface of the electrodeposited chitosan scaffold. In the first demonstration, GFP was *in situ* assembled onto chitosan scaffold in a bioMEMS device by chemically activating the amine groups of chitosan with glutaraldehyde. Next, GFP was *in situ* assembled onto chitosan scaffold in a bioMEMS device by enzymatic activation of the genetically fused pentatyrosine pro-tag at the protein's C-terminus. Finally, DNA hybridization was demonstrated on chitosan scaffold by glutaraldehyde activation of the amine groups of chitosan for assembly of probe DNA. Importantly, the biomolecules in all cases were assembled onto patterned electrodes in prepackaged microchannels with spatial and temporal programmability. We believe that this strategy holds significant potential as a simple and generic biomolecule assembly approach for future applications in complex biomolecular or biosensing analyses as well as in sophisticated microfluidic networks.

Our approach for biomolecule assembly in bioMEMS devices offers several unique advantageous capabilities. First, the electric signal-guided nature of the chitosan assembly allows simple *in situ* assembly of biological molecules when and where it is needed, even long after the device is fully manufactured. This capability

may allow biological components to be assembled into complex microfluidic networks (e.g. for high throughput drug screening) with greater ease than conventional assembly methods. Second, biomolecules are assembled from the aqueous environment, thus preserving their biological activities through the assembly procedure. Third, our approach is user friendly since the end-user, namely a biologist or a clinician, does not need complex robotic printing facilities or arduous chemical procedures to achieve selective biomolecule assembly. Forth and finally, our technique offers generic, flexible strategies for different target biomolecules since a wide variety of conjugation schemes can be utilized for different biomolecules. This is clearly demonstrated by the retained fluorescence of assembled GFP and the complementary reaction of target ssDNA onto the assembled ssDNA. Combined, these advantages make our assembly approach appealing for a wide variety of bioMEMS and biosensing applications that require device biofunctionalization.

## Chapter 4. Programmable Enzyme Assembly in Prepackaged BioMEMS

This chapter reports a biofunctionalization strategy for the assembly of catalytically active enzymes within a completely packaged bioMEMS device, through the programmed generation of electrical signals at spatially and temporally defined sites. The enzyme of a bacterial metabolic pathway, *S*-adenosylhomocysteine nucleosidase (Pfs), is genetically fused with a pentatyrosine “pro-tag” at its C-terminus. Signal responsive assembly is based on covalent conjugation of Pfs to the aminopolysaccharide, chitosan, upon biochemical activation of the pro-tag, followed by electrodeposition of the enzyme–chitosan conjugate onto readily addressable sites in microfluidic channels. Compared to traditional physical entrapment and surface immobilization approaches in microfluidic environments, our signal-guided electrochemical assembly is unique in that the enzymes are assembled under mild aqueous conditions with spatial and temporal programmability and orientational control. Significantly, the chitosan-mediated enzyme assembly can be reversed, making the bioMEMS reusable for repeated assembly and catalytic activity. Additionally, the assembled enzymes retain catalytic activity over multiple days, demonstrating enhanced enzyme stability. We envision that this assembly strategy can be applied to rebuild metabolic pathways in microfluidic environments for antimicrobial drug discovery.

## 4.1 Introduction

As discussed in Section 1.3, the microfluidic environment of bioMEMS devices provides unprecedented advantages for enzyme analysis because of the ability to work with smaller reagent volumes, shorter reaction times, and the possibility of parallel operation. Researchers have explored enzyme assembly approaches in microfabricated devices using either entrapment approaches such as packed beads or surface immobilization approaches. However, robust and reproducible enzyme assembly within microfluidic devices remains challenging due to the labile nature of these biological molecules that is incompatible with the lengthy and dry processing conditions often encountered in the device fabrication.

In this chapter, we report a chitosan-mediated biofunctionalization strategy for the assembly of catalytically active enzymes onto spatially and temporally programmed sites within completely packaged and systematically controlled bioMEMS devices. Specifically, we report assembly of the bacterial metabolic pathway enzyme, *S*-adenosylhomocysteine nucleosidase (Pfs), and demonstrate that it retains catalytic activity for small molecule biosynthesis. Pfs catalyzes the irreversible cleavage of *S*-adenosylhomocysteine (SAH) into *S*-ribosylhomocysteine (SRH) and adenine (Duerre 1962), and is a member of the autoinducer-2 (AI-2) biosynthesis pathway, a metabolic pathway found in many bacterial species (Federle and Bassler 2003). As discussed in Section 1.1, AI-2 is a small cell-signaling molecule that serves as a quorum-sensing communicator, through which bacterial populations exhibit altered phenotype. Therefore, the enzyme assembly strategy

reported here provides a template toward rebuilding and interrogating metabolic pathways in microfluidic environments for novel anti-microbial drug discovery.

As opposed to conventional approaches which have immobilized enzymes onto packed beads or on entire surfaces of microchannel walls, our biofunctionalization strategy assembles enzymes at a specific address within a microchannel through the programmed generation of electrical signals at spatially and temporally defined sites. First, the bioMEMS device in Figure 4-1(a) is prefabricated for multiple uses. Second, Pfs-chitosan conjugate solution is prepared by covalently conjugating Pfs to chitosan in solution upon tyrosinase activation of the pro-tag genetically fused at the enzyme's C-terminus, as shown in Figure 4-1(b). This conjugation step confers the pH-responsive properties of chitosan to the enzyme Pfs for one-step electro-assembly

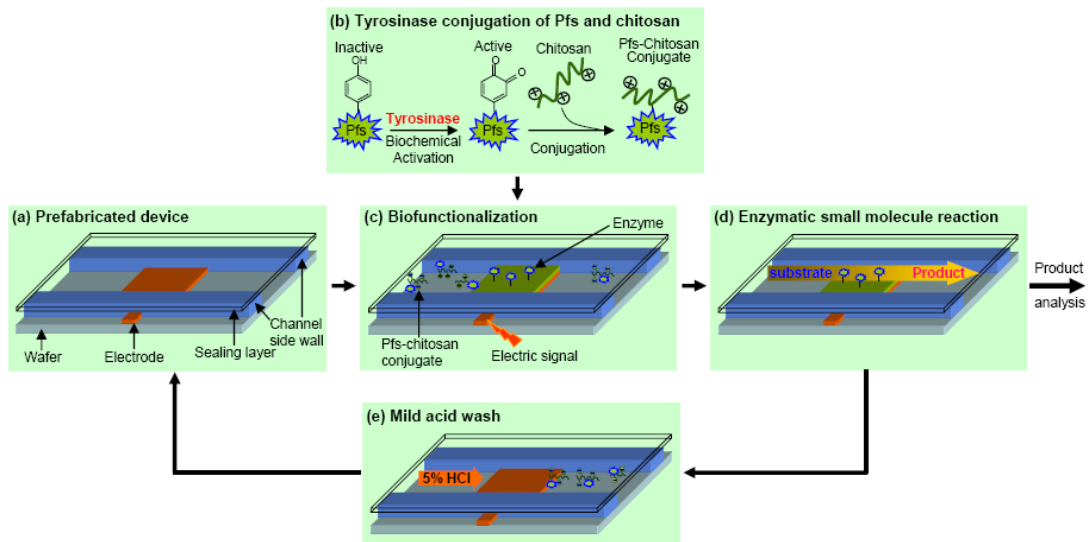


Figure 4-1: Schematic flow of programmable enzyme assembly in a prepackaged reusable bioMEMS device. (a) Prefabricated device, (b) enzyme-chitosan conjugation, (c) electrically programmed assembly of Pfs-chitosan conjugate, (d) enzymatic small-molecule reaction, (e) mild acid wash to remove biofunctionalization and reuse bioMEMS device.

onto the readily addressable sites within the microfluidic channels. Third, the Pfs-chitosan conjugate is electrodeposited onto an assembly site inside a microfluidic channel by applying negatively biased electrical signals, as shown in Figure 4-1(c). With biofunctionalization complete, Figure 4-1(d) shows that the Pfs-catalyzed enzymatic reaction is performed by introducing the enzyme substrate SAH into the microchannel, which is then catalytically converted by the assembled Pfs into products SRH and adenine. After the reaction, Figure 4-1(e) indicates that a mild acid wash removes the assembled Pfs-chitosan conjugate for reuse of the bioMEMS.

The unique features of this work are that we employ localized electrical signals to guide the assembly of a biocatalytically-active enzyme at a specific electrode address within a completely packaged microfluidic channel. This assembly approach is important because it allows device fabrication to be separated from biofunctionalization and enables the prefabricated bioMEMS to be repeatedly biofunctionalized for multiple uses.



## 4.2 Materials and methods

### 4.2.1 Materials

*S*-adenosylhomocysteine (SAH), bovine serum albumin (BSA), chitosan (minimum 85 % deacetylated chitin, molecular weight 200,000 g/mol) from crab shells, imidazole, isopropyl  $\beta$ -D-thiogalactopyranoside (IPTG), nickel sulfate, phosphate buffered saline (PBS) (2.7 mM KCl, 137 mM NaCl, 1.5 mM  $\text{KH}_2\text{PO}_4$ , 8.1 mM  $\text{Na}_2\text{HPO}_4$ , pH 7.5), sodium cyanoborohydride, and tyrosinase from mushroom were purchased from Sigma (St. Louis, MO). Tyrosinase was reported by the manufacturer to have an activity of 1,530 Units/mg solid. LB (Luria broth) medium was purchased from Becton Dickinson (Cockeysville, MD). Acetonitrile (HPLC grade), ampicillin sodium salt, chloroform, glycerol, sodium phosphate (monobasic), sodium phosphate (dibasic), and water (HPLC grade) were purchased from Fisher Chemical (Fair Lawn, NJ). Hydrochloric acid and sodium chloride were purchased from J. T. Baker (Phillipsburg, NJ). Non-fat dry milk was purchased from BioRad (Hercules, CA). Bleach was purchased from James Austin Co. (Mars, PA). De-ionized water (ddH<sub>2</sub>O, 18 M $\Omega$ -cm, Milli-Q) and PBS (dissolved in de-ionized water) were autoclaved before use.

### 4.2.2 Plasmid construction

pTrcHis-Pfs-Tyr plasmid construction has been reported elsewhere (Fernandes et al. 2007). Briefly, the plasmid was constructed by PCR amplification of *pfs* from *E.*

*coli* wild type strain W3110. Following digestion, the PCR products were extracted by gel purification and inserted into pTrcHisC (Invitrogen). DNA sequencing was performed to verify construct integrity. The plasmid was transformed into *E. coli* DH5 $\alpha$  (defective *LuxS* strain).

#### 4.2.3 Purification of (His)<sub>6</sub>-Pfs-(Tyr)<sub>5</sub>

*E. coli* DH5 $\alpha$  containing pTrcHis-Pfs-Tyr was cultured at 37°C and 250 rpm in LB medium supplemented with ampicillin at 50  $\mu$ g/mL concentration. When the OD<sub>600nm</sub> reached 0.5 – 0.6, IPTG was added to induce enzyme production at a final concentration of 1 mM IPTG. After an additional 5 hr, the culture was centrifuged for 10 min at 10,000 g's, and the cell pellet stored at – 20°C. The thawed pellet was resuspended in PBS + 10 mM imidazole, pH 7.5, placed in an ice-water bath, and the cells lysed by sonication (Fisher Scientific Sonic Dismembrator 550). The lysed cells were centrifuged for 10 min at 16,000 g to remove insoluble cell debris, and the supernatant filtered through 0.22  $\mu$ m PES filter. The enzyme was purified from the filtered soluble cell extract by immobilized metal-ion affinity chromatography (IMAC) using a 5 mL HisTrap chelating column (Amersham Biosciences). Prior to loading the filtered extract, the column was charged with Ni<sup>2+</sup> ions using 0.1 M NiSO<sub>4</sub>, washed with de-ionized water, and equilibrated with 3 column volumes (CVs) of 20 mM sodium phosphate, 250 mM NaCl, 10 mM imidazole, pH 7.4. After loading the filtered extract, the column was washed with 3 CVs of the previous buffer, washed again with 3 CVs of 20 mM sodium phosphate, 250 mM NaCl, 50 mM imidazole, pH

7.4, and the protein was eluted using 1.5 CVs of 20 mM sodium phosphate, 250 mM NaCl, 350 mM imidazole, pH 7.4. All steps were performed at 2 mL/min (1 cm/min linear velocity). The eluted sample was dialyzed overnight (16 hr) at 4°C into PBS. Purified protein concentration was determined with a UV/vis spectrophotometer (DU 640, Beckman, Fullerton, CA) using UV light at 280nm wavelength. The protein solution was mixed 2:1 with glycerol, aliquoted and stored at -80°C.

#### **4.2.4 Chitosan and Pfs-chitosan conjugate preparation**

Chitosan solution was prepared by adding chitosan flakes in de-ionized water, with HCl added dropwise to maintain pH ~ 2, and mixing overnight. The pH was then adjusted to pH 4.8 by adding 1 M NaOH dropwise, and the chitosan solution was then filtered and stored at 4° C.

The conjugate was prepared by incubating (His)<sub>6</sub>-Pfs-(Tyr)<sub>5</sub> (0.2 mg/mL), tyrosinase (0.1 mg/mL or 166 Units/mL), and chitosan (0.5 % (w/w)) in 50 mM sodium phosphate buffer (final pH of mixture 6.0) for 2 h at room temperature (23 – 24 °C) and 250 rpm, followed by incubation in sodium cyanoborohydride (0.2 mg/mL) for 30 min at 250 rpm to stabilize Pfs-chitosan binding.

#### **4.2.5 BioMEMS device fabrication and packaging**

The fabrication process of our bioMEMS device with packaging was described in Section 2.1. The bioMEMS device used in these experiments is shown in Figure 4-2. The solution selection and pumping is controlled by the bioMEMS control system as described in Section 2.2.

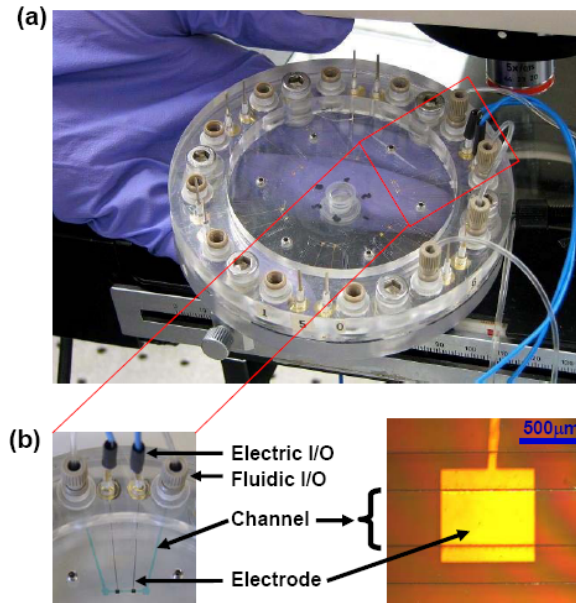


Figure 4-2: BioMEMS device for enzyme assembly. (a) Completely packaged bioMEMS system with electric connectors and fluidic inputs/outputs. (b) Color ink running through one microfluidic channel (left) and zoom-in view of one electrode at the bottom of the channel (right).

#### 4.2.6 One-step electrodeposition of enzyme-chitosan conjugate and sequential enzymatic reactions

As shown in Table 4-1, the microchannel and all the connecting tubing were first rinsed with DI water at 50  $\mu\text{L}/\text{min}$  flow rate for 30 min. Then, Bovine Serum Albumin (BSA) solution (1 % (w/v) in PBS buffer) was pumped into the microchannel at 3  $\mu\text{L}/\text{min}$  flow rate for 2 hours to block non-specific binding. After PBS buffer rinsing at 3  $\mu\text{L}/\text{min}$  flow rate for 30 min, Pfs-chitosan conjugate solution was pumped into the microchannel at 5  $\mu\text{L}/\text{min}$  flow rate. After the microchannel was completely filled, the pump was stopped and an electrical signal of constant current density 3  $\text{A}/\text{m}^2$  was applied to maintain negative bias voltage on the gold

(working) electrode for 240 seconds, while a second gold electrode served as the anode (counter).

The Pfs-chitosan conjugate solution was then drained from the system, and the electrodeposited Pfs-chitosan conjugate was washed with PBS buffer at 5  $\mu\text{L}/\text{min}$  and then at 20  $\mu\text{L}/\text{min}$  flow rates, each for 15 min. Next, enzymatic reactions were performed by continuously pumping the SAH substrate solution (1 mM SAH in 50 mM sodium phosphate buffer pH 7.2) for 2 hours at each flow rate. During the second hour of each flow rate, samples were collected every 10 min for 3 min each. They were then extracted with chloroform and stored at  $-20^{\circ}\text{C}$  before analyzing by HPLC.

Table 4-1: Experimental procedure to demonstrate programmable assembly of a catalytically active enzyme and its reproducibility<sup>a</sup>

|         | Step # | Procedure                       | Flow rate ( $\mu\text{L}/\text{min}$ ) | Time (min) |
|---------|--------|---------------------------------|--|------------|
| Day 1   | 1      | DI water cleaning               | 50                                     |            |
|         | 2      | BSA                             | 3                                      | 120        |
|         | 3      | PBS buffer                      | 3                                      | 30         |
|         | 4      | <b>Pfs-chitosan assembly</b>    | <b>static</b>                          | <b>4</b>   |
|         | 5      | PBS buffer                      | 5, 20                                  | 30         |
| Day 2   | 6      | <b>Enzymatic reaction (SAH)</b> | <b>3, 22</b>                           | <b>600</b> |
|         | 7      | HCl wash                        | 22                                     | 10         |
|         | 8      | DI water cleaning               | 50                                     | 90         |
| Day 3   | 9      | <b>Enzymatic reaction (SAH)</b> | <b>3</b>                               | <b>120</b> |
|         | 10     | DI water cleaning               | 50                                     | 60         |
|         | 11     | BSA                             | 5                                      | 120        |
|         | 12     | PBS buffer                      | 5                                      | 30         |
|         | 13     | <b>Pfs-chitosan re-assembly</b> | <b>static</b>                          | <b>4</b>   |
| Day 4   | 14     | PBS buffer                      | 5, 20                                  | 30         |
| Day 4   | 15     | <b>Enzymatic reaction (SAH)</b> | <b>3, 22</b>                           | <b>600</b> |
| Day 5-7 | 16     | In PBS buffer                   | static                                 | 3 days     |
| Day 8   | 17     | <b>Enzymatic reaction (SAH)</b> | <b>3, 22</b>                           | <b>360</b> |
|         | 18     | Cleaning                        | 50                                     |            |

<sup>a</sup> The background colors of each step correspond to that in Figure 4-3.

#### 4.2.7 Negative controls

Several control experiments were run to evaluate the signal-directed assembly of the conjugate and free enzyme within the bioMEMS. For control Set #1, the microchannel was incubated for 240 seconds with free Pfs solution (0.2 mg/mL) without chitosan (therefore no need of electrical bias) and without tyrosinase. For control Set #2, an electrical signal of constant current density  $3 \text{ A/m}^2$  was first applied for 240 seconds to electrodeposit chitosan scaffold onto the assembly electrode, then the microchannel was filled with a 5% (w/v) milk-PBS solution to block non-specific binding of Pfs to chitosan and the channel surfaces. Next, a solution of free Pfs solution (0.2 mg/mL) without tyrosinase was pumped into the microchannel at  $5 \mu\text{L}/\text{min}$  flow rate for 60 minutes. For the corresponding experiment, a mixed solution of Pfs (0.2 mg/mL) and tyrosinase (0.1 mg/mL or 166 Units/mL) was pumped into the microchannel at  $5 \mu\text{L}/\text{min}$  for 60 minutes to activate the pro-tag of Pfs *in situ* for its covalent assembly onto the electrodeposited chitosan scaffold. For control Set #3, the process was similar to that shown in Table 4-1, except there was no electrical signal applied when incubating the microchannel with the same batch of Pfs-chitosan conjugate solution for 240 seconds. Finally, enzymatic reactions were performed for all sets of controls and the corresponding experiments, and the downstream reaction products were collected and analyzed by HPLC.

#### 4.2.8 Analysis of enzymatic reaction products

A Waters Spherisorb Silica column ( $250 \times 4.6 \text{ mm}$ ) with  $5 \mu\text{m}$  beads ( $80 \text{ \AA}$  pore)

was used in reversed-phase mode with 5  $\mu$ L sample injection size and a mobile phase of 70:30 acetonitrile:water at 0.5 mL/min. Conversion was calculated from elution data at 210 nm. The HPLC system consisted of two Dynamax model SD-200 pumps (with 10 mL pump heads and mixing valve) and a Dynamax Absorbance Detector model UV-D II. The conversion data was analyzed using Star 5.5 Chromatography Software (Rainin).

## 4.3 Results

### 4.3.1 One-step electrodeposition of enzyme-chitosan conjugate and sequential enzymatic reactions

We demonstrate assembly of Pfs enzyme onto a readily addressable site in a prefabricated and packaged microfluidic channel by one-step electrodeposition of Pfs-chitosan conjugate. Additionally, we demonstrate retention of catalytic activity of the assembled Pfs, and robustness and stability of the assembled Pfs throughout repeated flow cycles over extended time. For this, we first prepared the Pfs-chitosan conjugate solution by incubating chitosan (buffered to pH 6.0 by the addition of sodium phosphate buffer), tyrosinase, and the pro-tagged Pfs as in Figure 4-1(b). Tyrosinase activates the pro-tag to covalently conjugate Pfs to the chitosan in solution. Next, we electrodeposited Pfs-chitosan conjugate onto the patterned assembly site inside a microfluidic channel by filling the microchannel with Pfs-chitosan conjugate solution and then applying negatively biased electrical signals to the patterned electrode as in Figure 4-1(c). This microchannel was previously incubated in BSA solution to block non-specific binding of Pfs to the channel surfaces. Next, we continually transported through the microchannel a solution containing the substrate SAH, which was catalytically converted into reaction products SRH and adenine by the assembled Pfs as in Figure 4-1(d). Finally, we performed HPLC analysis of the enzymatic reaction mixtures collected downstream.



As shown in Figure 4-3(a), Pfs-chitosan conjugate was first assembled onto the assembly site in the microchannel by applying negatively-biased electrical signals (day 1), and enzymatic reactions were performed by continuously pumping SAH solution through the channel in a cyclic manner between 3  $\mu\text{L}/\text{min}$  and 22  $\mu\text{L}/\text{min}$ , as shown in Figure 4-3(b) (day 2). Reaction mixtures collected downstream were analyzed by HPLC. Next, Pfs enzyme was disassembled by mild acid solution (day 2), SAH was continuously pumped through the channel (day 3), and HPLC analysis was performed on the solutions collected downstream to demonstrate that Pfs enzyme was in fact completely disassembled and the device was cleaned for reuse. With the

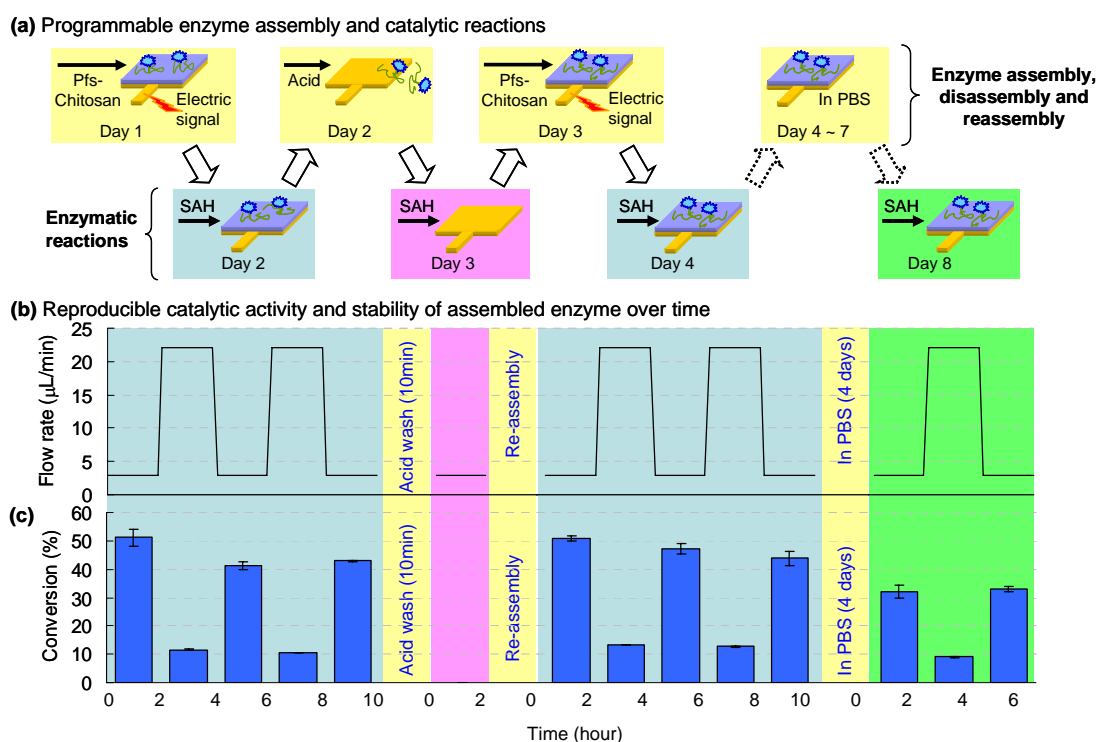


Figure 4-3: Programmable enzyme assembly, reproducibility after removal and robustness over time. (a) Schematic of programmable enzyme assembly, disassembly and reassembly and the corresponding enzymatic reactions. (b) Flow rates. (c) Reproducible catalytic activity after enzyme assembly, disassembly and re-assembly, and stability of assembled enzyme after 4 days.

acid wash completed, Pfs-chitosan conjugate from the same solution batch was re-assembled (day 3), and enzymatic reactions were performed at the same flow rates, as shown in Figure 4-3(b) (day 4), to demonstrate reproducible enzyme assembly and catalytic activity. Finally, the assembled enzyme was left in PBS buffer for 4 days at room temperature (days 4 – 7) before the final cycle of enzymatic reactions were performed (day 8) to demonstrate the stability of the assembled enzyme with extended time.

The HPLC analysis results in Figure 4-3(c) show the following behavior. (1) By varying the flow rate in a cyclic manner between 3  $\mu\text{L}/\text{min}$  (low flow rate) and 22  $\mu\text{L}/\text{min}$  (high flow rate), the SAH conversion correspondingly cycled between  $46 \pm 4\%$  at the low flow rate and  $12 \pm 1\%$  at the high flow rate (day 2). (2) After cleaning the channel with mild acid solution, there is no conversion (day 3), demonstrating that the assembled enzyme was in fact completely removed, and thus allowing for repeated biofunctionalization and reuse of the bioMEMS device. (3) After re-assembly of Pfs enzyme, the SAH conversion recovered back to the cyclic behavior alternating between  $46 \pm 4\%$  and  $12 \pm 1\%$  (day 4), demonstrating reproducible enzyme assembly and catalytic activity. (4) After leaving the enzyme in the microfluidic environment at room temperature for 4 days (days 4 – 7), the conversion cycled between  $33 \pm 2\%$  and  $9\%$  (day 8). Specifically, the  $33 \pm 2\%$  conversion represents  $> 70\%$  of the original conversion ( $46 \pm 4\%$ ), demonstrating the stability of the enzyme over extended time. These results show that our model enzyme Pfs was successfully and robustly assembled onto readily addressable sites

within prefabricated and packaged microfluidic channels by one-step electrodeposition of the Pfs-chitosan conjugate. Importantly, the assembled enzyme retained reproducible activity throughout the repeated flow cycles.

Combined, these results demonstrate the reproducibility of enzyme catalytic activity, the spatial and temporal programmability of our enzyme assembly process, the robustness and stability of the assembled enzyme with time, and the reusability of the devices when using our electrochemical enzyme assembly process.

#### **4.3.2 Negative controls to examine non-specific binding and dead volume**

We next examined what portion, if any, of the SAH conversion in Figure 4-3(c) was a result of Pfs non-specifically assembled onto the microchannel surfaces and/or of solution-phase Pfs retained in the dead volume of the bioMEMS. For this, we designed the following three sets of experiments as shown in Figure 4-4(a).

The simplest experiment set #1 was designed to test the non-specific binding of free, unconjugated, solution-phase Pfs to the bioMEMS surfaces. In the experiment, Pfs-chitosan conjugate was electrodeposited, as shown in Figure 4-3 (day 2), while the negative control was performed in the same microchannel after rinsing with acid solution. The negative control only differed from the experiment in that the microchannel was incubated with Pfs solution without chitosan and without tyrosinase. The HPLC analysis results in Figure 4-4(d) show that at 3  $\mu\text{L}/\text{min}$  flow rate, there was  $16 \pm 3\%$  conversion of SAH to SRH and adenine for the negative control, while there was  $48 \pm 2\%$  conversion for the experiment on day 2 in Figure

4-3(c).

Experiment set #2 was designed to compare the non-specific binding versus covalent binding of free Pfs to an already electrodeposited chitosan scaffold in the bioMEMS. For this, we first applied electrical signals to electrodeposit chitosan scaffold onto the assembly electrode, then incubated the microchannel in milk solution to block non-specific binding of Pfs to chitosan and the channel surfaces. Next, we incubated the microchannel with a mixed solution of Pfs and tyrosinase to *in situ* activate the pro-tag of Pfs for its covalent assembly onto the electrodeposited chitosan scaffold, and finally we performed enzymatic reactions. Following the

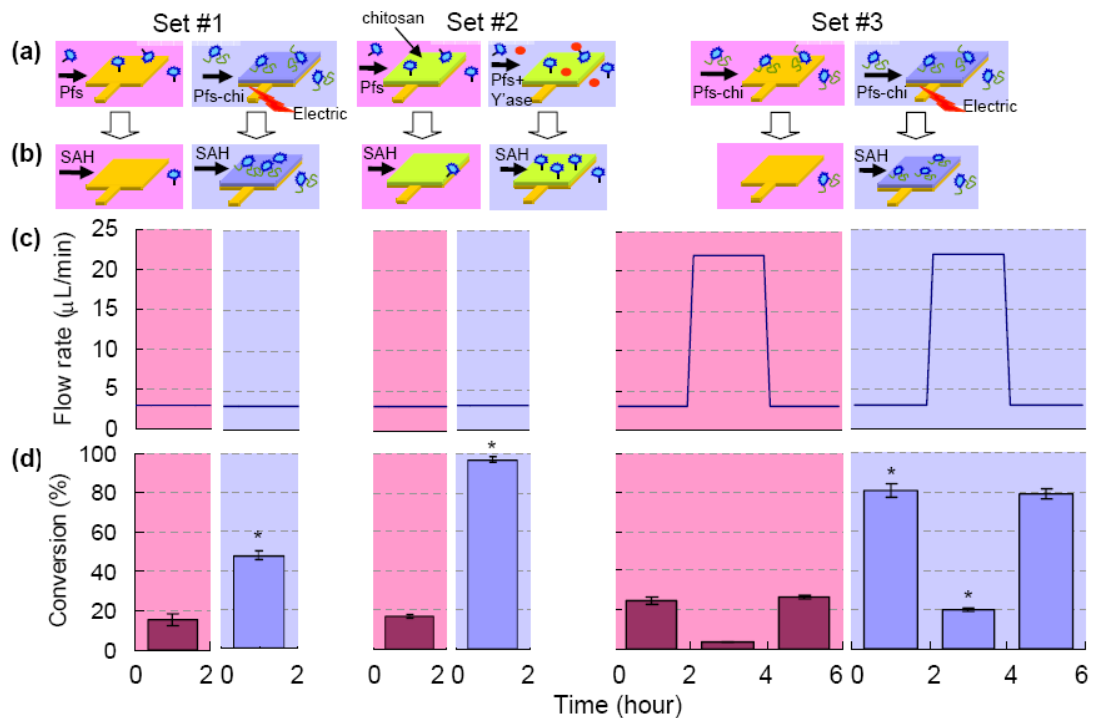


Figure 4-4: Negative controls and corresponding experiments. (a) Preparation of assembly site surface. Green = pure chitosan, blue = Pfs-chitosan conjugate. (b) Enzymatic reactions. (c) Flow rates. (d) Enzymatic conversions. The \* denotes a statistical difference ( $p < 0.01$  in all cases).

same procedure, the negative control was performed in the same microchannel after rinsing with acid solution, except that no tyrosinase was added to the free Pfs solution. The HPLC results in Figure 4-4(d) show that at 3  $\mu\text{L}/\text{min}$  flow rate, there was  $17 \pm 1\%$  conversion of SAH to SRH and adenine for the negative control, while there was  $97 \pm 2\%$  conversion for the experiment. The higher conversion in the experiment of set #2 ( $97 \pm 2\%$ ) compared to that of set #1 ( $48 \pm 2\%$ ) might be due to the facts that in experiment set #1, (1) the Pfs molecules might be partially buried in the electrodeposited Pfs-chitosan matrix, making them less accessible to SAH substrate, and (2) Pfs molecules might be exposed to high pH during the electrodeposition.

This work focus on the conjugate assembly (set #1) as more advantageous than *in situ* activation and assembly (set #2) in that this strategy will ultimately enable sequential assembly of multiple enzymes within the same microfluidic channel representing a metabolic pathway onto different assembly sites. That is, each enzyme of the pathway can be conjugated to chitosan separately, and then each conjugate can be electrodeposited onto its own assembly site within a microchannel.

We believe the most stringent control was in experiment set #3 that was designed to test the non-specific binding of Pfs-chitosan conjugate in bioMEMS without biasing the assembly electrode. This was performed in a new microchannel and with a new batch of Pfs-chitosan conjugate solution. Following the similar experimental procedure shown in Table 4-1, we first incubated the microchannel in BSA solution to block non-specific binding of Pfs to the channel surfaces. Next, we performed the experiment by electrodepositing Pfs-chitosan conjugate onto the patterned assembly

site, and conducting enzymatic reactions by cycling the SAH flow rate between 3  $\mu\text{L}/\text{min}$  and 22  $\mu\text{L}/\text{min}$  flow rates and analyzed the reaction products by HPLC. Following the same procedure, the negative control was performed in the same microchannel after rinsing with acid solution, except that no electrical signal was applied during Pfs-chitosan conjugate incubation. The HPLC analysis of the enzymatic reaction products in Figure 4-4(d) shows that at 3  $\mu\text{L}/\text{min}$  flow rate, there was  $25 \pm 3\%$  conversion of SAH into SRH and adenine in the negative control, while there was  $79 \pm 4\%$  conversion in the experiment. At 22  $\mu\text{L}/\text{min}$  flow rate there was  $3 \pm 1\%$  conversion in the negative control and  $19 \pm 1\%$  conversion in the experiment. The conversion difference at 3  $\mu\text{L}/\text{min}$  flow rate in experiment set #1 ( $48 \pm 2\%$ ) versus set #3 ( $79 \pm 4\%$ ) might be because the experiment set #3 was performed within a different microchannel and with a new batch of Pfs-chitosan conjugate solution.

#### **4.3.3 Performance of enzyme assembled on electrodes**

In all three experimental sets shown in Figure 4-4, the results consistently yield 3~6 times more conversion than the corresponding negative controls, which demonstrates that the majority of conversion resulted from catalytic reactions at the target electrode sites. We confirmed that there was a significant statistical difference between the enzymatic conversion of the negative control and that of the experiment in each set by analyzing via single-factor ANOVA tests and multiple comparison tests ( $p < 0.01$ ). For set #3, this analysis was performed on conversions at both 3 and 22  $\mu\text{L}/\text{min}$  flow rates. This is particularly striking because (1) the electrode site

comprises only 0.2 % of the total surface area within the bioMEMS device available for non-specific binding of the enzyme, and (2) the fluid volume above the electrode site comprises only 0.3 % of the total fluid volume in the bioMEMS available for trapping free, unattached, solution-phase enzyme. In other words, these results demonstrated that the enzyme intentionally assembled on the electrode is far more ( $> 10^3 = 3\sim 6 / 0.2\%$ ) efficient than the enzyme at non-specific binding sites in the entire microchannel.

We are currently optimizing our bioMEMS design to further minimize system dead volume, and are investigating alternative methods for blocking non-specific enzyme attachment. Nonetheless, non-specific protein attachment and system dead volume are issues common in biofunctionalized bioMEMS systems due to the structural characteristics of enzymes and other proteins, the high surface area to volume ratio of the system, and the minimal mixing due to the laminar flow characteristics of the system (Beebe, et al. 2002, Holden et al. 2004, Ku, et al. 2006, Mao, et al. 2002).

#### **4.3.4 Enzyme stability and activity**

The experimental results in Figure 4-3(c) show that the assembled enzyme on the selected site in the microfluidic channel retained substantial catalytic activity for at least four days. We further examined Pfs stability by comparing specific catalytic activities over 4 days of the surface-assembled Pfs-chitosan conjugate at the electrode in a microchannel to (1) unassembled Pfs-chitosan conjugate solution and to (2) free

and unconjugated Pfs solution (Table 4-2).

For this, we reacted the Pfs solutions (1) and (2) with SAH on day 1 and then re-reacted the same Pfs solutions with fresh SAH on day 5. The free Pfs-chitosan conjugate formed a suspension when it was mixed with SAH substrate (due to the higher pH of SAH solution). All reaction mixtures were analyzed by HPLC. Shown in Table 4-2 are the specific activities of the experiments on day 1 and on day 5 after remaining 4 days at room temperature in PBS buffer, calculated as  $\mu\text{mol SAH}$  converted per min per mg Pfs. For the case of the unassembled conjugate, we assumed that all of the initially available Pfs had conjugated to chitosan during the

Table 4-2: Estimated specific catalytic activities of assembled Pfs-chitosan conjugate in microchannel, Pfs-chitosan conjugate suspension, and free unconjugated Pfs enzyme solution on day 1 and on day 5 after 4 days in PBS buffer at room temperature.

| Enzyme conditions  |                                     | Specific activity day 1 ( $\mu\text{mol SAH}/\text{min}/\text{mg Pfs}$ ) | Specific activity day 5 ( $\mu\text{mol SAH}/\text{min}/\text{mg Pfs}$ ) | % activity after 4 days |
|--|-------------------------------------|--|--|-------------------------|
| <i>Heterogeneous:</i><br>Assembled Pfs-chitosan conjugate in bioMEMS |                                     | 3.7 <sup>a</sup>   | 2.6 <sup>a</sup>   | 70.4                    |
| <i>Homogeneous:</i><br>Unassembled enzyme in batch reactors          | Pfs-chitosan conjugate <sup>b</sup> | 12.1   | 3.2  | 26.4                    |
|  | unconjugated free Pfs               | 12.0   | 1.5  | 12.8                    |

<sup>a</sup> The enzymatic reaction by the assembled Pfs-chitosan conjugate on spatially selected sites in a bioMEMS channel is heterogeneous. Quantification of the specific activities is more difficult than that in homogeneous reactions and is the focus of ongoing research. Assumptions were made to estimate the specific activities shown in the table, and more details are available in 6Appendix I: Estimation of enzyme specific activity.

<sup>b</sup> Free Pfs-chitosan conjugate forms a suspension when it was mixed with SAH due to the higher pH of SAH solution.



conjugation reaction (as chitosan was added in excess of Pfs). For the case of the assembled conjugate, the milligrams of Pfs assembled was estimated by electrodepositing Pfs-chitosan conjugate onto a microfabricated chip under the same conditions, then resolubilizing the conjugate with dilute hydrochloric acid and performing Western blot analysis. Further information can be found in 6Appendix I.

Table 4-2 shows that on the first day the specific activity of the assembled Pfs-chitosan conjugate is 1.8  $\mu\text{mol SAH/ min/ mg Pfs}$ , while the specific activities of the unassembled conjugate suspension and the free unconjugated Pfs solution are 12  $\mu\text{mol SAH/ min/ mg Pfs}$ . Both values are within the range of reported Pfs specific activities, which vary over 3 orders of magnitude (Duerre 1962, Ferro et al. 1976, Ragione et al. 1985). The decrease in activity upon assembly is not surprising, given the steric hindrance effects of immobilized enzymes, and the diffusional limitations due to the minimal mixing associated with laminar flow in bioMEMS systems.

However, Table 4-2 demonstrates that the activity of the assembled Pfs-chitosan conjugate is better retained with time, as shown by the % activities remaining after 4 days incubation in PBS buffer at room temperature: 70 % remaining for the assembled conjugate, only 26 % remaining for the conjugate suspension, and only 13 % remaining for the free unconjugated enzyme. We conclude that the assembled enzymes in our bioMEMS are more stable and resistant to environmental changes for better retention of catalytic activities with time than are the bulk free or chitosan-conjugated enzyme solutions. Therefore, our approach allows for repeated use of the bioMEMS in continuous or intermittent processes. This stability

advantage for surface-assembled enzyme over those in bulk solution is consistent to what has been observed in literature (Cao 2005).

#### 4.3.5 Transient response

Using our current bioMEMS packaging system, we observed a time delay between changing the flow rate over the reaction site (assembled with Pfs enzyme) and measuring the corresponding change in SAH concentration at the sample collection point downstream. To further understand the transient system response, we performed numerical modeling of the bioMEMS by simulating the mixing purely due to mass diffusion and laminar transport (Reynolds number = 0.1).

The simulation result in Figure 4-5 shows that in the low flow rate case (3  $\mu\text{L}/\text{min}$ ) it takes 10 minutes for a concentration change at the reaction site to travel downstream and arrive at the sample collection site, and it takes 25 minutes for the concentration response at the sample collection site to reach 95% of the concentration change at the reaction site. This is mainly due to dead volume ( $\sim 20 \mu\text{L}$ ) in the packaging between the microchannel and the external tubing. This transient response of the bioMEMS justifies that we collected the samples for HPLC analysis only at the 2<sup>nd</sup> hour in each flow rate step after the concentration completely stabilized. The response time of the current system design also partially explains the conversions in the control experiment as any enzyme in the dead volume contributes to the enzymatic conversion. The minimization or elimination of dead volume is also under investigation and will be a focus of subsequent studies.

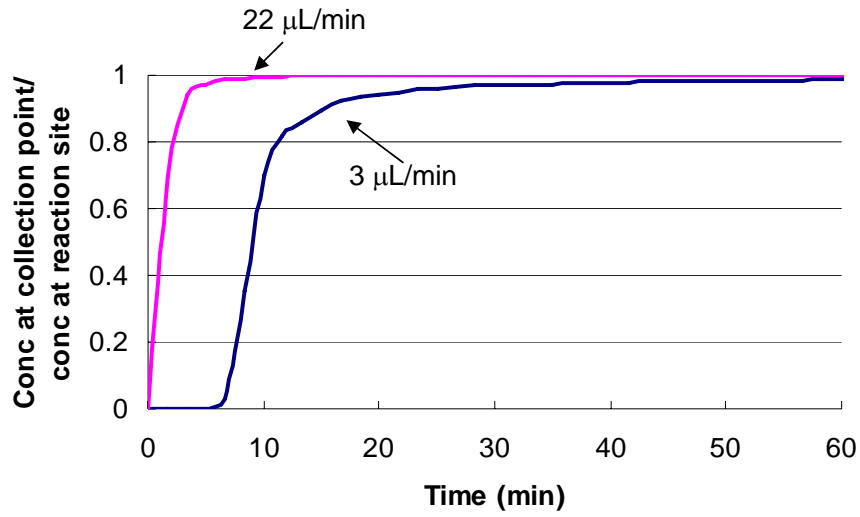


Figure 4-5: Simulation of the transient concentration response at sample collection point to the concentration change at reaction site. (a) At 3  $\mu\text{L}/\text{min}$  flow rate (blue). (b) At 22  $\mu\text{L}/\text{min}$  flow rate (purple).

## 4.4 Discussions

### 4.4.1 Enzyme assembly and activity in bioMEMS

Here we report an enzyme assembly strategy and demonstrate corresponding enzymatic activity based on electrodeposition of the enzyme-chitosan conjugate onto readily addressable electrode sites into a microchannel of a prefabricated and packaged bioMEMS device. Specifically, we report assembly of Pfs enzyme, a member of the AI-2 biosynthesis pathway, which catalyzes the cleavage of SAH into SRH and adenine. The significance of this result is that enzymes can be programmably assembled within a bioMEMS while maintaining their catalytic activity over time. This provides the underpinnings for a viable bioMEMS technology platform to support metabolic engineering research and development for applications from elucidating biochemical reaction kinetics to discovering new drugs.

Our enzyme assembly strategy described here offers several unique advantages over conventional techniques such as microcontact printing (Quist, et al. 2005) and self assembly layers (Chaki and Vijayamohanan 2002). First, the enzymes conjugated to chitosan are covalently bonded, and the assembly of the enzyme-chitosan conjugate onto the patterned electrode in the microchannel can be programmed conveniently by electrical signals. Second, the enzyme assembly is performed in mild aqueous conditions inside prefabricated and completely packaged bioMEMS devices, thus avoiding direct contact and complex facilities. Third, we achieve temporal programmability since we are able to assemble the enzymes just

prior to using the enzyme for small molecule biocatalysis. This is advantageous for biological components that have limited shelf life.

#### 4.4.2 Quantification

While the purpose of this chapter was to demonstrate the assembly and activity of enzymes within the bioMEMS, quantification of the activity and comparison to alternatives is a natural and important question. Such quantification is challenging and is the subject of ongoing research. In the meantime, it is possible here to identify or estimate several semi-quantitative results of note.

Figure 4-4(d) shows that some parasitic or background reaction occurs, presumably through non-specific enzyme assembly onto the microchannel surfaces<sup>13-25</sup> or through any free, unattached, solution-phase enzyme. Figure 4-4(d) also demonstrates that such conversion is significantly less, and statistically different compared to the conversion achieved by the electrodeposited enzyme-chitosan conjugate. Additionally, the electrode, with only 0.5 mm<sup>2</sup> area, represents only 0.2% of the total microenvironment surface (221 mm<sup>2</sup>), and the volume above the electrode site (0.075 μL) represents only 0.3% of the total microenvironment volume (23.9 μL). Therefore, the enzyme-activated electrode is > 3 orders of magnitude more efficient in executing the catalytic reaction than other areas of the microfluidic environment.

In a meaningful sense, these quantitative results are already encouraging. An overriding concern with microfluidics technology and applications is that the vastly enhanced surface/volume ratio cf. conventional chemical reactors may dramatically

alter pathways and kinetics, rendering microfluidic environments not viable. For localized reaction sites in a bioMEMS, the concern takes two somewhat different but equally important forms: (1) will nonspecific binding at the large area of channel surface dominate over the small area of active electrode? and (2) will parasitic reaction of enzyme in the aqueous phase of the entire channel volume dominate over that at the electrode? Results here show that the assembled enzyme on the small electrode can control the catalytic conversion of small molecules in the bioMEMS.

#### **4.4.3 Optimization**

There is ample opportunity to optimize conversion rates in our bioMEMS environments (Lewandowski et al. 2008). One means is through process parameters such as flow rates, process time, concentrations, surface passivation, and pH. Another is through device design, such as channel dimensions and geometry, reduction of dead volumes such as reservoirs, and new network designs which minimize cross-talk between enzyme assembly and subsequent catalytic conversion. With present conversion rates of 46 %, there is room to improve the efficiency of enzyme conversion at the electrode, and reduction of parasitic conversion pathways (non-specific binding at channel surfaces and/or reaction in aqueous volumes), control and specificity of reaction at the active electrode sites can be improved as well.

## 4.5 Conclusions

This work demonstrates a chitosan-mediated biofunctionalization strategy for the assembly of catalytically active enzymes onto spatially and temporally programmed sites within a completely packaged and systematically controlled bioMEMS device. The HPLC analysis of downstream reaction mixtures demonstrates that the assembled enzymes are catalytically active, robust, and stable with time, and that our strategy is reproducible, allowing for multiple uses of bioMEMS devices. While further quantification is needed, the assembled enzyme at the small active electrode is much more effective overall in catalytic conversion of the SAH substrate than are parasitic channels associated with non-specific enzyme attachment to the channel surfaces or with solution-phase enzyme. In any case, we report here for the first time the signal-guided assembly of catalytically active enzymes at localized sites which can be programmed both spatially and temporally within a prepackaged bioMEMS. The demonstration of their catalytic activity represents a key step in progress toward a bioMEMS technology to support metabolic engineering research and development, where multi-step biochemical reactions are common and separation of these steps is highly desirable for understanding reaction details and modifying pathways and kinetics for various applications (e.g. drug discovery).

This novel strategy of enzyme assembly was achieved through two unique techniques: (1) the covalent conjugation of the enzyme to chitosan in solution upon biochemical activation of a pro-tag and (2) the electrodeposition of the resulting enzyme-chitosan conjugate. Because the assembly of biological elements is

signal-guided through the electrodeposition process, the active biology (enzyme-chitosan conjugate) can be introduced into prefabrication bioMEMS devices upon demand. We anticipate that the methodology can be extended to multiple sites and with different enzymes to accommodate multi-step metabolic pathways (Jung and Stephanopoulos 2004), as would be valuable for replicating specific bacterial pathways and seeking new antimicrobial drugs that modify or suppress those pathways.



## Chapter 5. BioMEMS Optimization for Enzyme Assembly and Activity

Biological microelectromechanical systems (bioMEMS) provide an attractive approach to understanding and modifying enzymatic pathways by separating and interrogating individual reaction steps at localized sites in a microfluidic network. Chapter 4 has shown that electrodeposited chitosan enables immobilization of an enzyme at a specific site while maintaining its catalytic activity. While promising as a methodology to replicate metabolic pathways and search for inhibitors as drug candidates, these investigations also revealed unintended (or parasitic) effects, including products generated by the enzyme either (1) in the homogeneous phase (in the liquid), or (2) nonspecifically bound to microchannel surfaces, i.e., in the heterogeneous phase. Here we report on bioMEMS designs which significantly suppress these parasitic effects.

To reduce homogeneous reactions we have developed a new packaging and assembly strategy which eliminates fluid reservoirs that are commonly used for fluidic interconnects with external tubing. To suppress reactions by nonspecifically bound enzyme on microchannel walls we have implemented a cross-flow microfluidic network design so that enzyme flow for assembly and substrate/product flow for reaction share only the region where the enzyme is immobilized at the intended reaction site. Our results show that the signal-to-background ratio of sequential enzymatic reactions increases from 0.72 to 1.28 by eliminating the

packaging reservoirs, and increases to 2.43 by separating the flow direction of enzymatic reaction from that of enzyme assembly step. These techniques can be easily applied to versatile microfluidic devices to minimize parasitic reactions in sequential biochemical reactions.

## 5.1 Introduction

### 5.1.1 Motivation: enzymatic reactions and metabolic pathways in bioMEMS

Microfluidic devices and polydimethylsiloxane (PDMS) soft lithography fabrication have reduced the size, reagent quantity, and cost of many standard biochemical analytical protocols, by handling nanoliter volumes (Janasek et al. 2006, Quake and Scherer 2000). Biological micro-electromechanical systems (bioMEMS) are an important subset of these devices that are able to recreate biomolecular reaction pathways. Of particular interest are pathways that play a critical role in the functionality and behavior of living cells. Enzyme catalysis is central to many of these pathways, and accordingly it has been a major goal to develop means to isolate enzymes at specific locations in a microfluidic system, and confirm that their catalytic action is maintained in this artificial setting. This would provide an attractive testbed for understanding the details of reaction pathways and kinetics, and for identifying means to modify pathways (e.g., for discovery of a drug that can significantly suppress, enhance, or modify the dominant pathway).

Our group has demonstrated bioMEMS technology that enables the programmable assembly of biomolecules on localized assembly sites in microchannels (Park, et al. 2006) using electrodeposition of the amine-rich polysaccharide chitosan to direct the assembly. As discussed in Chapter 4, we

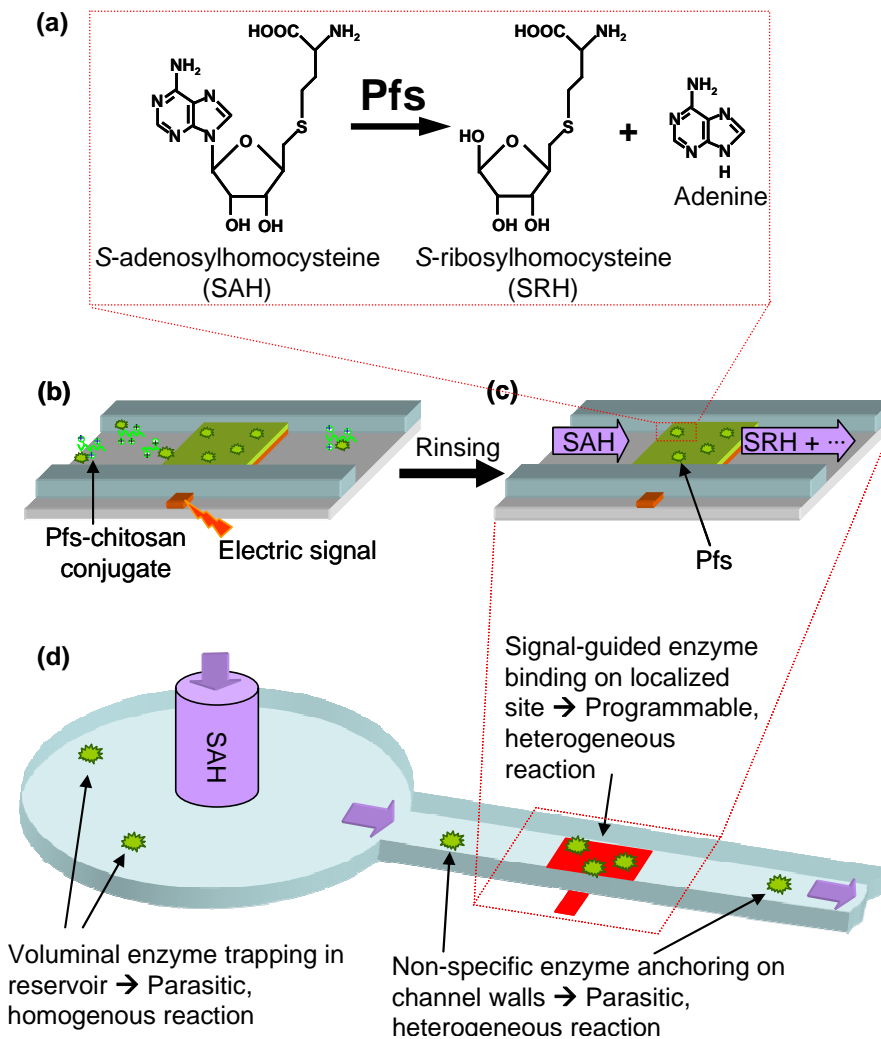


Figure 5-1: Parasitic reactions in microfluidics due to enzyme trapped in interconnect reservoirs and non-specifically bound on microchannel walls. (a) Pfs enzyme converts SAH substrate into products SRH and adenine. (b) Assembly of Pfs-chitosan conjugate onto a localized assembly electrode in a microchannel. (c) Sequential enzymatic reaction in continuous flow. (d) Parasitic reactions in reservoirs and on microchannel wall as well as programmable reactions on enzyme assembly site.

recently demonstrated that the metabolic pathway enzyme *S*-adenosylhomocysteine nucleosidase (Pfs) can be assembled in this way and that its catalytic action is retained in the microfluidic environment, shown by conversion of substrate *S*-adenosylhomocysteine (SAH) into products *S*-ribosylhomocysteine (SRH) and adenine, as illustrated in Figure 5-1 (a)-(c) (Luo et al. 2008).

This reaction step is known to be one of two enzyme reaction steps by which bacteria produce autoinducer-2 (AI-2), a small cell-signaling molecule that serves as a quorum sensing communicator, through which bacterial populations exhibit altered phenotype. Our ultimate goal is to use the bioMEMS environment as a testbed for discovery of molecules that inhibit quorum sensing. These would be good candidates for a new type of antimicrobial drug that would work by interfering with bacterial communication rather than by killing bacteria, hopefully avoiding drug-resistant mutations that are too often generated by direct attack on the bacteria.

### **5.1.2 Limitations and goals**

While these results showed clear enzyme activity at the assembled active sites, it was accompanied by notable (~15-30%) background (or “parasitic”) reaction that occurred elsewhere in the microfluidic system (signal/background, or S/B, =3-6X). This is not surprising, given that the surface area and volume at the reaction site comprised only ~0.2% of the total wall area and volume of the microfluidic system. The result indicates that the active site is >1000X more efficient than unintended (parasitic) sites in the microfluidic network. These background signals appear in

control experiments and are not associated with the intended catalytic action at the enzyme assembly sites. Accordingly we refer to these background reaction channels as “parasitic” in that they produce reactions that add to and interfere with efforts to localize reactions at the electrode sites.

The purpose of the present work is to reduce two significant parasitic reaction mechanisms in our bioMEMS. One is a homogeneous reaction mechanism, in that substrate and enzyme react while in the fluid phase. It occurs because active enzyme is retained in reservoir areas where fluidic interconnects are made at the packaging level. The other is a heterogeneous reaction mechanism, in which enzyme nonspecifically bound to microfluidic channel walls reacts with substrate impinging from the fluid phase. These mechanisms are depicted schematically in Figure 5-1(d).

### **5.1.3 Eliminating reservoir dead volume**

Connections between a bioMEMS device and external sources of fluids are essential to operate the device. However, alignment of fluidic inputs/outputs (I/O's) to the microchannels can be challenging. A conventional approach is to design a larger fluidic reservoir as an interface between on-chip microfluidic channels and external fluidic connections at the packaging level, reducing the precision needed for alignment. This approach has been used for tubing connection in microfluidics from individual microsystems (Bilitewski, et al. 2003, Han et al. 2005, Kim et al. 2007, Long et al. 2007) to large-scale integration (McDonald and Whitesides 2002, Thorsen, et al. 2002, Urban, et al. 2006). However, in the case of more than one substrate was

sequentially introduced from the same input into the microchannel, which is almost unavoidable for multi-step biochemical reactions, the reservoirs are not readily flushed since their geometry leaves dead volume regions which entrap reactive biomolecules (e.g. enzymes) for extended periods of time, causing homogeneous parasitic reactions and altering the apparent conversion efficiency and time dependence of intended enzyme reaction steps (Ku, et al. 2006, Luo, et al. 2008).

To avoid the homogenous parasitic reactions in interconnect dead volume, we implemented a new packaging technique that involves fabricating aligners on soft lithography molds to improve the alignment capability for interfacing between in-plane microfluidic channels and external tubing. Frederickson and Fan have reviewed the macro-scale packaging and assembly technology issues and their effect on microfluidic performance (Fredrickson and Fan 2004). Our design eliminates the interconnection reservoirs by fabricating on-chip SU-8 aligner plugs, analogous to Si plugs made by DRIE (Gray et al. 2004), to guide microfluidic packaging connections. The relevant properties of PDMS which enable this technique are given elsewhere (McDonald and Whitesides 2002). Here we show PDMS sealing around tubing 20% larger than the nominal hole diameter, building on the demonstration in the literature (Christensen et al. 2005). We employ two rigid Plexiglas plates to clamp the PDMS-glass device, and stabilize the pogo pins on their electrode contacts, similar to the demonstration by Bhagat et al where rigid clamps were employed to mechanically stabilize the tubing (Bhagat et al. 2007). We demonstrate that background biochemical activity is reduced by 33% in the new design.

#### 5.1.4 Reducing impact of nonspecifically bound enzyme

The presence of microfluidic channel walls with area far in excess of that of the intended enzyme reaction site is intrinsic to the geometry of bioMEMS. As indicated in Figure 5-1(d), however, our bioMEMS design employed a single channel to (1) first activate the enzyme to react with chitosan, and then deliver the enzyme-chitosan conjugate to be immobilized on the assembly site by electrical signal, and (2) subsequently to transport substrate to the active site and product away from it to a downstream collection point. This configuration exposed substrate to nonspecifically bound enzyme through the full length of the channel prior to its collection.

To reduce the contribution of enzyme nonspecifically bound on channel walls, we have implemented a cross-flow bioMEMS channel design. The channel that carries the enzyme-chitosan conjugate for immobilization is orthogonal to a second channel that carries substrate and product downstream to an exhaust location for analysis of enzyme conversion rate. Thus, substrate is exposed to enzyme only at the active site, suppressing the contribution of nonspecifically bound enzyme to measured conversion rates.

This experimental strategy utilizing cross-flow microchannels to separate flow directions for sequential biochemical reactions has been broadly used in DNA/protein separation (Long, et al. 2007), droplet formation (Tan et al. 2006) and enzymatic reaction (Bilitewski, et al. 2003), where the cross area is the focus point for sample manipulation or for reagent introduction. In this work, we spatially assemble

metabolic enzyme Pfs at the intersection between two flow channels so that we can separate the flow direction for enzyme assembly from the subsequent flow direction for enzymatic reaction. This design enhancement is an important advance toward our goal of reconstructing multiple metabolic pathway enzymes. Spatially separating individual reaction steps in microfluidics allows for better understanding of reaction details and testing of molecules that can modify pathways and kinetics. In drug discovery, for example, a molecular species which inhibits a bacterial signaling pathway enzyme can be a candidate for an antimicrobial drug whose action is to interfere with cell signaling or quorum sensing. By using a cross-flow design to separate flow directions, we significantly suppress non-specific heterogeneous reactions on microchannel walls and reduce the background signal by an additional 50%. Together bioMEMS design modifications for these two effects result in a combined enhancement of 3.38X in signal/background (from 0.72 to 2.43).



## 5.2 Detailed design, fabrication and packaging

For this work we have employed a soft lithography molding approach (McDonald and Whitesides 2002) to the fabrication of the bioMEMS, in contrast to our previous work on enzyme reactions in bioMEMS (Luo, et al. 2008). This accelerates development and testing of the concept, while removes some of the benefits of our earlier design (Park, et al. 2006).

### 5.2.1 Packaging aligners to eliminate interconnection reservoirs

To avoid homogeneous parasitic reaction in interconnect dead volume, minimal or no interconnection reservoir is desired. To achieve this goal, we designed and fabricated packaging aligners using a soft lithography molding process. As shown in Figure 5-2(a), packaging aligners of 500 $\mu\text{m}$  in diameter were patterned from a 200 $\mu\text{m}$ -thick SU-8 layer on the top of the 150 $\mu\text{m}$ -thick SU-8 mold layer used to define the 500 $\mu\text{m}$ -wide microchannels. A design offset of 1.07% was applied in the photomask to adjust the shrinkage ratio of PDMS (Lee and Lee 2008). Figure 5-3(a) shows the fabricated prototype mold with packaging aligners.

Three ways of PDMS curing and packaging have been explored to assemble the final device without interconnection reservoirs to external tubing. In Figure 5-2(b), a sharpened coupler (fabricated in-house from a 25ga coupler, 0.020" OD) was used to punch through the 3mm-thick PDMS layer along the pits formed by the packaging aligners during the PDMS curing process. Holes for electrical contact (0.1" diameter) were also punched in the PDMS before the microchannel side was wetted with

methanol and bonded to a glass slide (2x1"). The whole device was then sandwiched with screws between two Plexiglas clamp plates, and with pogo pins inserted through holes in the top plate for electrical connection. Finally, flat-end couplers of the same size were inserted into the punched holes and connected to external PE tubing (0.015"ID).

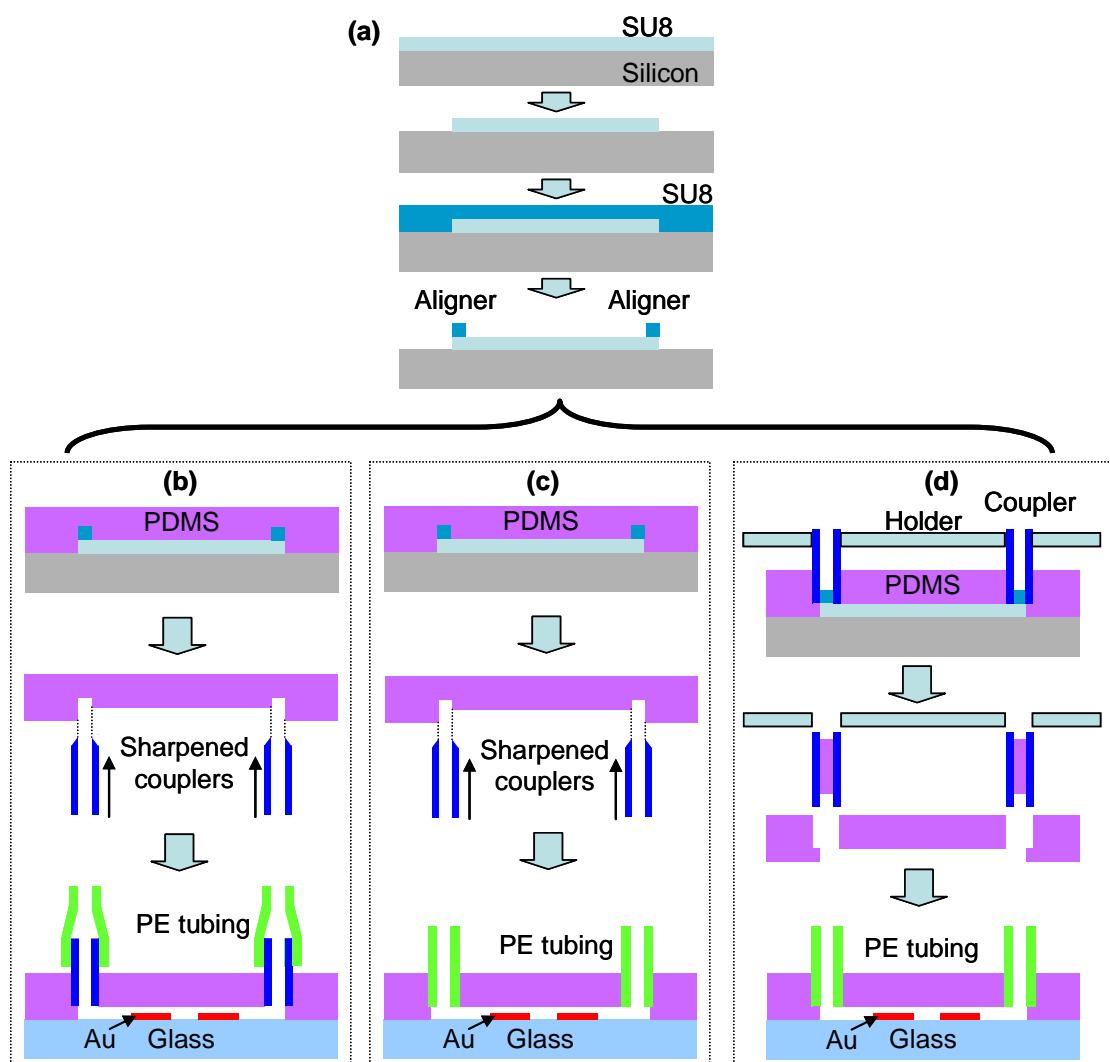


Figure 5-2: Eliminating interconnection reservoirs by aligners on prototype mold to guide microfluidic packaging. (a) Aligners on prototype mold. (b) Packaging way #1: punch holes via PDMS followed by coupler insertion. (c) Packaging way #2: punch holes via PDMS followed by tubing insertion. (d) Packaging way #3: align couplers for PDMS curing followed by coupler removal and tubing insertion.

Figure 5-2(c) shows the same strategy as Figure 5-2(b) except that the external tubing was directly inserted into the punched holes in PDMS. In Figure 5-2(d), couplers with inner-diameter of 0.024" (20ga, 0.036" OD) were gently placed onto the aligners of 0.5mm OD and stabilized with a Plexiglas coupling holder during while the PDMS was cured. Then the couplers were removed and external microbore PTFE tubing (0.022" ID, 0.042" OD) was inserted into the well-defined connection holes (0.036" OD). Due to capillary action, couplers were normally filled with PDMS after curing, which was advantageous because it allowed a slug of PDMS to be removed, facilitating better sealing. A packaged device following the procedure of Figure 5-2(d) is shown in Figure 5-3(b) with blue dye flowing through the cross channel.

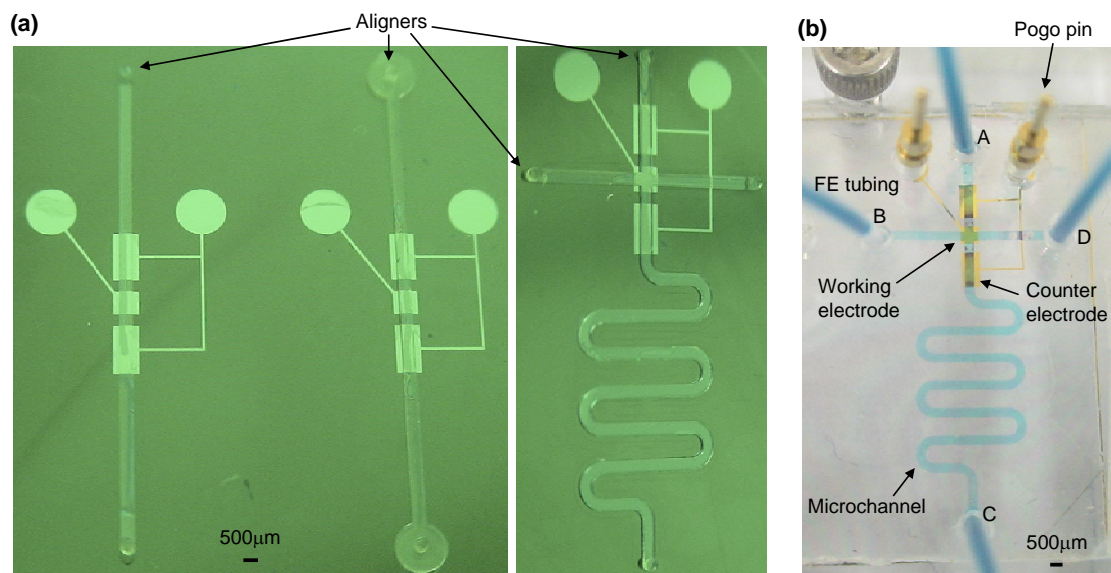


Figure 5-3: Device and packaging. (a) Fabricated aligners on prototype mold. (b) Blue dye solution flowing through a packaged cross-channel without interconnection reservoirs. PE tubing was inserted. In experiment, enzyme solution flowed A→C, substrate solution flowed B→D.

Finally, leak testing showed that all three strategies provide leak-tight sealing. The designs (b) and (c) in Figure 5-2 were predominantly used in our experiments since they minimized the dead volume between the coupler and tubing as well.

### **5.2.2 Cross-channel design to separate sequential flow directions**

Cross channels (500 $\mu\text{m}$ -wide, 150 $\mu\text{m}$ -high) as shown in Figure 5-3 (b) were designed to separate the sequential flow direction of enzyme assembly ( $A \rightarrow C$ ) from the flow direction of the subsequent enzymatic reaction ( $B \rightarrow D$ ). No on-chip valves were included for this test-of-concept design. Parafilm was used to seal the connecting couplers/tubing that are not being used for a given experiment step to minimize the flow into these channels. After enzyme assembly, PBS buffer was pumped into the top three ports of the device in Figure 5-3(b) to rinse the channels. In the following experiment, substrate was continuously pumped through the reaction site at the intersection for  $\sim 10$  hours. The serpentine channel connecting the bottom port was included to increase channel length in an efficient manner to prevent any enzyme from defusing back to the reaction site. The packaging aligners described above were also included for this cross-channel design.

## 5.3 Experimental methods

### 5.3.1 Materials

*S*-adenosylhomocysteine (SAH), bovine serum albumin (BSA), chitosan (minimum 85 % deacetylated chitin, molecular weight 200,000 g/mol) from crab shells, imidazole, isopropyl  $\beta$ -D-thiogalactopyranoside (IPTG), nickel sulfate, phosphate buffered saline (PBS) (2.7 mM KCl, 137 mM NaCl, 1.5 mM  $\text{KH}_2\text{PO}_4$ , 8.1 mM  $\text{Na}_2\text{HPO}_4$ , pH 7.5), sodium cyanoborohydride, and tyrosinase from mushroom were purchased from Sigma (St. Louis, MO). Tyrosinase was reported by the manufacturer to have an activity of 1,530 Units/mg solid. LB (Luria broth) medium was purchased from Becton Dickinson (Cockeysville, MD). Acetonitrile (HPLC grade), ampicillin sodium salt, chloroform, glycerol, sodium phosphate (monobasic), sodium phosphate (dibasic), and water (HPLC grade) were purchased from Fisher Chemical (Fair Lawn, NJ). Hydrochloric acid and sodium chloride were purchased from J. T. Baker (Phillipsburg, NJ). Non-fat dry milk was purchased from BioRad (Hercules, CA). Bleach was purchased from James Austin Co. (Mars, PA). De-ionized water (ddH<sub>2</sub>O, 18 M $\Omega$ -cm, Milli-Q) and PBS (dissolved in de-ionized water) were autoclaved before use.

Silicon wafers were purchased from University Wafer (South Boston, MA). Plain and frosted micro slides, Single-Use Syringes/BD Needle Combinations, Microcentrifuge tubes were purchased from VWR (West Chester, PA). SU-8 photoresist was purchase from MicroChem (Newton, MA). Sylgard<sup>®</sup> 184 silicone

elastomer kit was purchased from Robert McKeown (Branchburg, NJ). Steel couplers (25ga, 20ga) and PE tubing were purchased from Instech Laboratories (Plymouth Meeting, PA). Microbore PTFE tubing was purchased from ColeParmer (Vernon Hills, Illinois). Genie Plus syringe pumps were purchased from Kent Scientific (Torrington, CT).

### 5.3.2 Pfs-chitosan conjugate preparation

Chitosan, enzyme Pfs and Pfs-chitosan conjugate preparation procedures were reported elsewhere (Lewandowski, et al. 2006, Luo, et al. 2008). Briefly, Chitosan solution was prepared by dissolving chitosan flakes in HCl solution at pH ~ 2 overnight, then the pH was adjusted to pH 4.8 by adding 1 M NaOH dropwise before being filtered and stored at 4° C. Plasmid pTrcHis-Pfs-Tyr was first constructed by PCR amplification of *pfs* from *E. coli* wild type strain W3110. Following digestion, the PCR products were extracted by gel purification and inserted into pTrcHisC (Invitrogen). DNA sequencing was performed to verify construct integrity. The plasmid was transformed into *E. coli* DH5 $\alpha$  (defective *luxS* strain). *E. coli* DH5 $\alpha$  containing pTrcHis-Pfs-Tyr was cultured and enzyme production was induced before the cells were lysed by sonication. Next, the enzyme was purified by ion-metal affinity chromatography (IMAC) before being mixed 2:1 with glycerol, divided into aliquots, and stored at -80°C. The conjugate was prepared by incubating enzyme Pfs, tyrosinase, and chitosan in sodium phosphate buffer for 2 h at room temperature followed by incubation in sodium cyanoborohydride for 30 min to stabilize

Pfs-chitosan binding.

### 5.3.3 Enzyme assembly and enzymatic reactions

After leak-testing of the assembled microfluidic device, the microchannel and all the connecting tubing were rinsed with DI water at 50  $\mu\text{L}/\text{min}$  flow rate for 30 minutes. Then, Bovine Serum Albumin (BSA) solution (1 % (w/v) in PBS buffer) was pumped into the microchannel at 3  $\mu\text{L}/\text{min}$  flow rate for 2 hours to block non-specific binding. After PBS buffer rinsing for 15 min at 5  $\mu\text{L}/\text{min}$  flow rate, Pfs-chitosan conjugate solution was pumped at the same flow rate until the microchannel was completely filled before the pump was stopped. For all the control experiments to test the background signals, no electrical signal was applied to the working electrode during incubation of 240 seconds, as shown in Figure 5-4. The Pfs-chitosan conjugate solution was then drained from the system, and the electrodeposited Pfs-chitosan conjugate was washed with PBS buffer at 5  $\mu\text{L}/\text{min}$  flow rate for 30 min. Next, enzymatic reactions were performed by continuously pumping the SAH substrate solution (1 mM SAH in 50 mM sodium phosphate buffer, pH 7.2) for 2 h at 0.4, 1 and 4  $\mu\text{L}/\text{min}$  flow rates by a Genie Plus syringe pump. During the second hour at each flow rate, samples were collected every 20 min. They were then extracted with chloroform and stored at  $-20^{\circ}\text{C}$  before analyzing by HPLC.

For the experiments to test the overall conversion by site-specifically assembled enzyme and non-specifically assembled enzyme, an electrical signal of constant current density 3  $\text{A}/\text{m}^2$  was applied to maintain negative bias voltage on the working

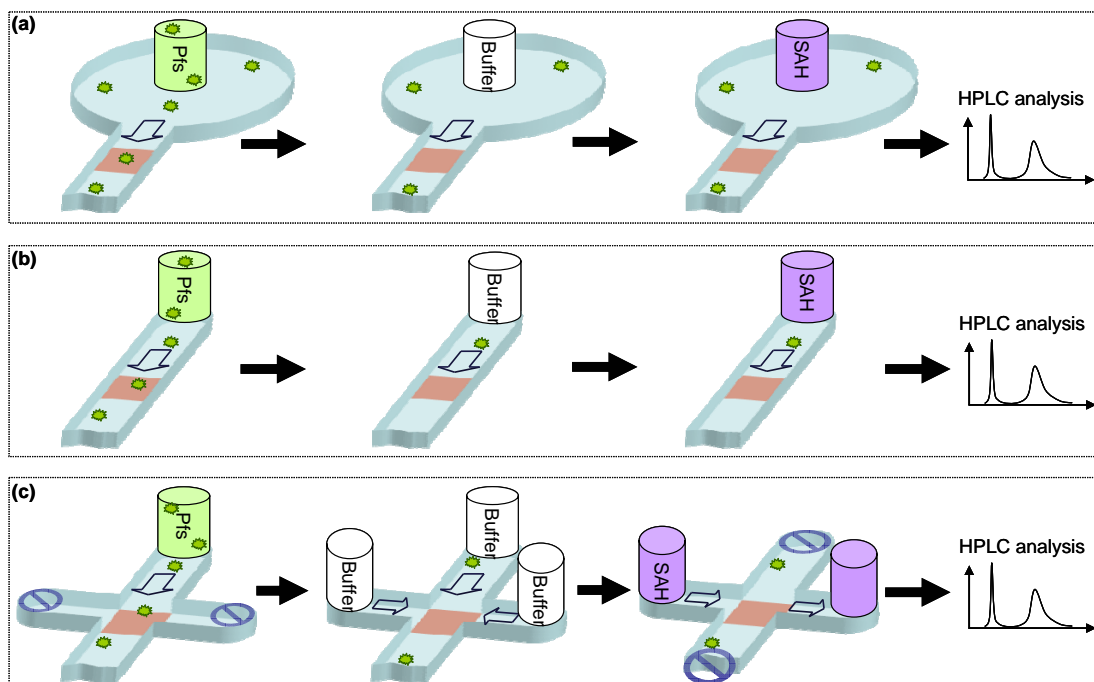


Figure 5-4: Minimize parasitic reactions by eliminating interconnection reservoirs and by separating sequential flow directions in cross channels. To test the background signal by parasitic reactions, Pfs enzyme solution was introduced without electro-assembly followed by buffer rinsing, then enzymatic substrate SAH was introduced and products were collected downstream to be analyzed by HPLC. (a) Single channel with interconnection reservoirs. (b) Single channel without interconnection reservoirs. (c) Cross-channel without interconnection reservoirs.

electrode for 240 seconds, while a second electrode served as the counter electrode.

All other steps followed the same aforementioned procedure.

### 5.3.4 Analysis of enzymatic reaction products

A Waters Spherisorb Silica column (250 × 4.6 mm) with 5 μm beads (80 Å pore) was used in reversed-phase mode with 5 μL sample injection size and a mobile phase of 70:30 acetonitrile:water at 0.5 mL/min. The HPLC system consisted of two



Dynamax model SD-200 pumps (with 10 mL pump heads and mixing valve) and a Dynamax Absorbance Detector model UV-D II, and data was analyzed using Star 5.5 Chromatography Software (Rainin). Conversion was calculated from elution data at 210 nm absorbance.

## 5.4 Quantification and simulation of interconnect dead volume

To better understand the degree to which interconnect dead volume affects the system response at a specific reaction site, we quantified and measured the changes in fluorescent dye intensity in the microchannel under flow, at a point 8.75 mm downstream of the interconnect point over the active electrode. As shown in Figure 5-5(a), the interconnect reservoir is 2 mm in diameter and 0.15 mm high, and the microchannel is 0.5 mm wide. The upstream external tubing was first filled with dye solution (Cy5) before inserting into the PDMS device. The dye solution was pumped into the microchannel at 1  $\mu\text{L}/\text{min}$  flow rate by a syringe pump, and a fluorescent microscope simultaneously recorded the dye intensity over the electrode. The microscope monitors the changes in relative intensity over the electrode in the microchannel. The microscope images were converted into grayscale images and processed by ImageJ software (National Institutes of Health). As a comparison, quantification was also performed for a microchannel of the same dimension without the interconnect reservoir as in Figure 5-5(b).

The experimental results show that it takes about 50 sec for the dye solution to reach the electrodes. The experimental curve in Figure 5-5(a, purple dashed line) shows that for a microchannel with interconnect reservoirs, it takes 61 sec for the dye intensity to increase from 10% to 90%. In comparison, for a microchannel without interconnect reservoirs it only takes 32 sec for the dye intensity to increase from 10% to 90%, as shown in Figure 5-5(b, purple dashed line).

Finite element simulation was also performed to investigate the effects of the interconnection reservoirs on the system response at the same location as in the experimental quantification. The simulation was performed using COMSOL Multi-Physics by modeling the switching of incoming flow into dye solution at the

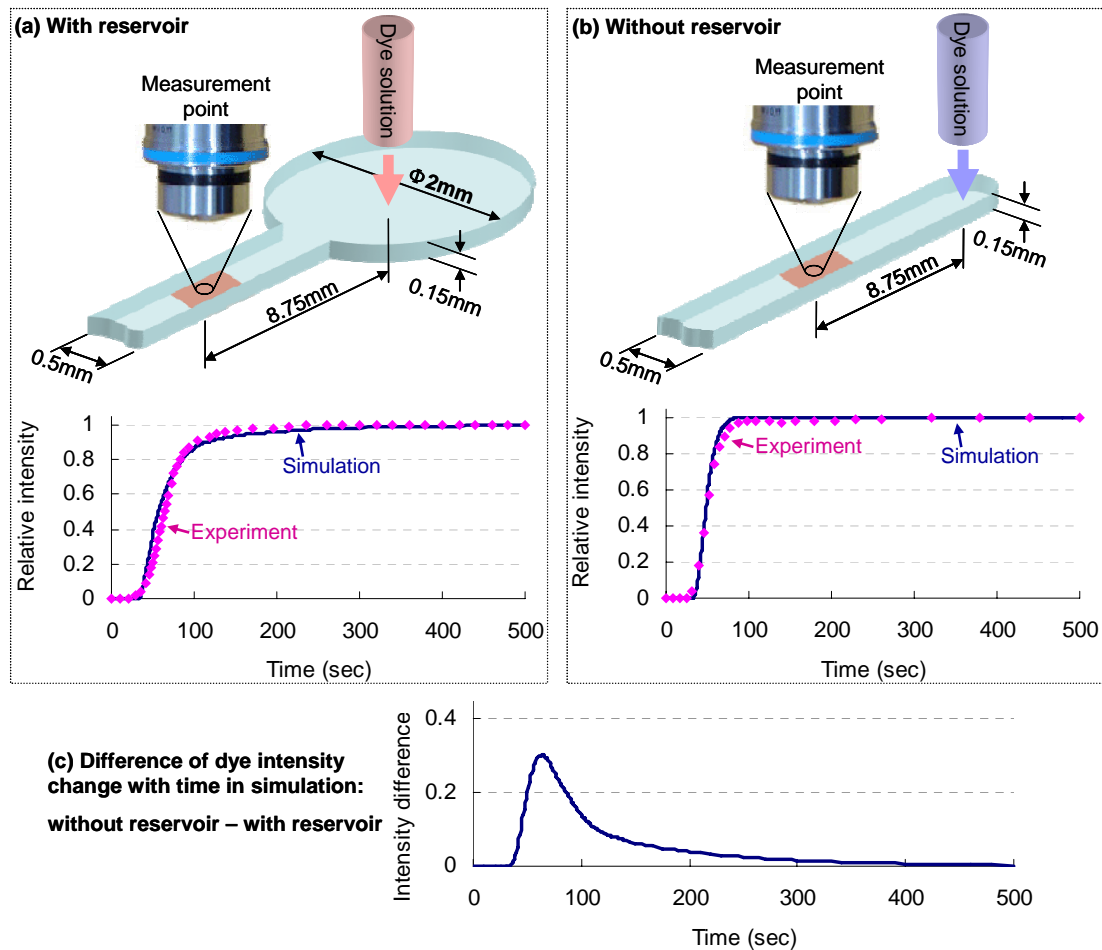


Figure 5-5: Quantification and simulation of dye intensity change from the interconnect point. Dye intensity was monitored over electrode patches 12mm downstream the microchannels. (a) Dye intensity change from 10% to 90% for the interconnect with reservoir takes 61 sec in experiment (purple dashed line) and 75 sec in simulation (blue solid line). (b) Dye intensity change from 10% to 90% for the interconnect without reservoir takes 32 sec in experiment (purple dashed line) and 25 sec in simulation (blue solid line). (c) The difference of intensity change in simulation from interconnects with and without reservoir

interconnection point, and by integrating the dye intensity over the electrode. The simulation curves in Figure 5-5(a, blue solid line) shows that for a microchannel with an interconnection reservoir it takes 75 sec for the dye intensity to increase from 10% to 90%, while for a microchannel without an interconnection reservoir it only takes 25 sec as shown in Figure 5-5(b, blue solid line). Figure 5-5(c) is the intensity difference in the microchannels with and without reservoir over time in simulation, which shows that the intensity over this specific electrode site differs for more than 100 sec before it reaches plateau with the maximum value 0.30.

Together, both the experimental quantification and the finite element simulation confirm that the system response (as measured downstream at the reaction site) has improved 2~3 times by eliminating the dead volume in interconnection reservoirs, therefore avoiding the homogenous parasitic reactions in the dead volume.

## 5.5 Quantification of parasitic reactions and overall analysis

### 5.5.1 Enzyme reaction and controls

To determine the benefit of the design changes detailed above which focus on microfluidics, we compared enzymatic conversions in these various designs to test the effects of parasitic reactions. This is schematically indicated in Figure 5-4 for the cases of (1) single channel with interconnect reservoirs, (2) single channel without interconnect reservoirs and (3) cross channel without reservoirs. The microchannels were first filled with Pfs enzyme solution, and then incubated in the enzyme solution in a static state for 4 min without applying an electrical signal to the assembly site (no electrodeposition). Next, enzyme solution was drained from the microchannel, and buffer solution was introduced to rinse the channel. Finally, enzymatic substrate SAH was introduced and the downstream solution was collected for HPLC analysis.

The experimental results of parasitic reactions for the afore-mentioned three cases are shown in Figure 5-6. In the case of single channel with reservoirs, the conversion of SAH into SRH and adenine was  $44.5 \pm 2.9\%$ ,  $19.3 \pm 0.4\%$  and  $5.0 \pm 0.3\%$  at 0.4  $\mu\text{L}/\text{min}$ , 1  $\mu\text{L}/\text{min}$  and 4  $\mu\text{L}/\text{min}$  flow rates, respectively. In the case of single channel without reservoirs, the conversion was  $29.7 \pm 1.8\%$ ,  $13.4 \pm 0.7\%$  and  $4.1 \pm 0.3\%$  at 0.4  $\mu\text{L}/\text{min}$ , 1  $\mu\text{L}/\text{min}$  and 4  $\mu\text{L}/\text{min}$  flow rates, respectively. In the case of cross channel without reservoirs, the conversion was  $13.3 \pm 0.2\%$ ,  $6.8 \pm 0.3\%$  and  $1.5 \pm 0.2\%$  at 0.4  $\mu\text{L}/\text{min}$ , 1  $\mu\text{L}/\text{min}$  and 4  $\mu\text{L}/\text{min}$  flow rates, respectively.

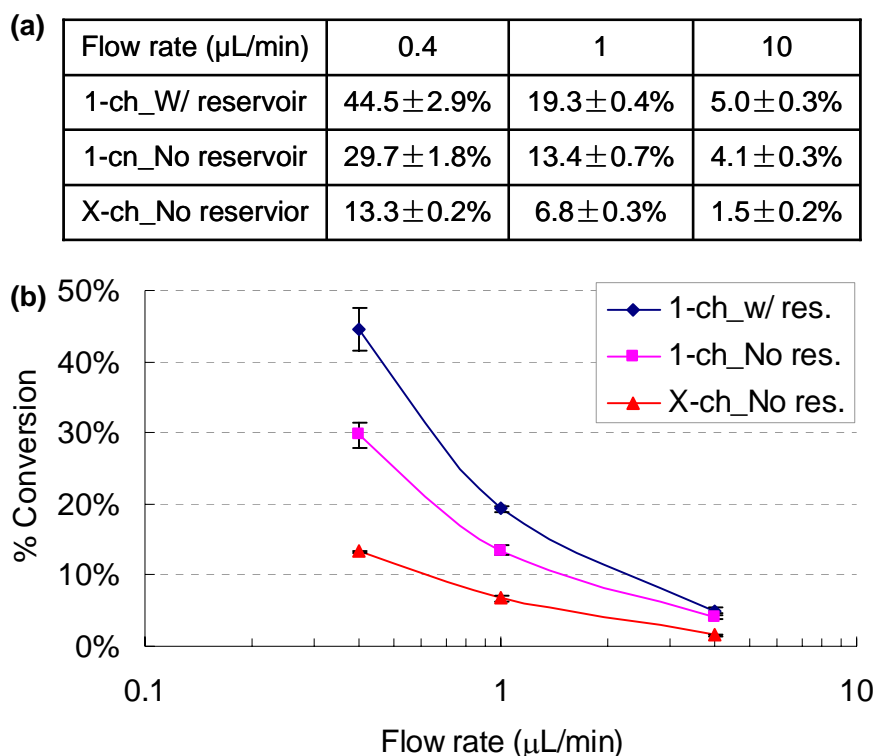


Figure 5-6: Background signals (parasitic enzymatic conversion) at different flow rates. Enzyme Pfs solution was introduced without electro-assembly followed by buffer rinsing, then enzymatic substrate SAH was introduced and products were collected downstream to be analyzed by HPLC. Legend: 1-ch\_w/ res.: single channel with interconnection reservoirs (blue); 1-ch\_No res.: single channel without interconnection reservoirs (pink); X-ch\_No res.: cross-channel without interconnection reservoirs (red).

Combined, these results demonstrate that by eliminating the reservoirs, the background signal from homogeneous parasitic reactions in the dead volume of interconnects decreases by 33%. By separating the flow directions with the cross channel configuration, the background signals from heterogeneous parasitic reactions on the microchannel walls further decreases by 63%. The total decrease of background signal from the configuration of Figure 5-4(a) to that of Figure 5-4(c) is 65~70% for the three flow rates tested.

### 5.5.2 Enzyme conversion signal/background

To better understand the improvements realized by eliminating interconnect dead volume and separating the flow directions for sequential enzymatic reactions, site-specific heterogeneous enzymatic reactions on the assembly electrode were also performed side by side to compare with the control experiments. The experiments differ from the control experiments only in that an electrical signal of  $3\text{A/m}^2$  current density was applied to electrodeposit Pfs-chitosan conjugate onto the assembly electrodes during the 4-min incubation of enzyme solution in the channels. The experiments were performed at  $0.4\ \mu\text{L}/\text{min}$  flow rate for all the three configurations shown in Figure 5-4. The enzyme solution for all the experiments and controls was from the same batch, while the conjugate solution was made right before experiments. The background signal was taken from Figure 5-6 at the flow rate of  $0.4\ \mu\text{L}/\text{min}$ .

The experiment results in Figure 5-7 show that in the case of the single channel with reservoirs, the site-specific conversion is  $32.0 \pm 1.6\%$  and the background signal is as high as  $44.5 \pm 2.9\%$  yielding a signal-to-background (S/B) ratio of 0.72. For the single channel without reservoirs design, the site-specific conversion is  $38.1 \pm 0.6\%$  while the background signal is  $29.7 \pm 1.8\%$  with the S/B ratio of 1.28. In the case of the cross channel without reservoirs design, the site-specific conversion is  $32.3 \pm 3.5\%$  while the background signal is as low as  $13.4 \pm 0.7\%$  with the S/B ratio of 2.43. The cross hatched area in Fig. 7 (X-ch\_No res) represents calculated missing reaction correction due to a slight reduction in electrode area upon alignment of intersection channels onto electrode (see 6Appendix II: Calculation of the missing enzymatic

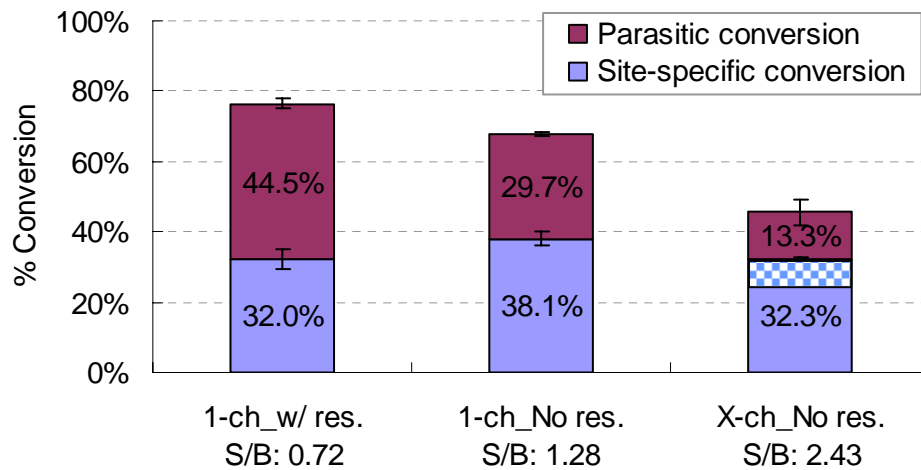


Figure 5-7: Conversions by non-specifically bound or trapped enzyme (blue) and conversions by site-specifically assembled enzymes (red) at 0.4  $\mu\text{L}/\text{min}$  flow rate. For the non-specific conversion, no electrical signal was applied to electrodeposit Pfs-chitosan conjugate. For the total conversion, a electrical signal of  $3\text{A}/\text{m}^2$  current density was applied for 4 minutes to electrodeposit Pfs-chitosan conjugate onto the assembly electrodes.

conversion of intersection-channels). Note, however, the electrode with only  $0.75\text{ mm}^2$  area represents only 1% of the total microchannel surface ( $77.15\text{ mm}^2$ ), and the volume above the electrode site ( $0.11\text{ }\mu\text{L}$ ) represents only 2.5% of the total microenvironment volume ( $4.45\text{ }\mu\text{L}$ ). Therefore, the conversion on the enzyme-activated electrode is  $> 2$  orders of magnitude faster per unit area than the background signal resulting from either parasitic mechanism.

In summary, these results demonstrate that by utilizing our packaging and experimental strategies to minimize the parasitic reactions in interconnect dead volume and by non-specific binding on microchannel walls, we improve the signal-to-background ratio of sequential enzymatic reactions from 0.72 to 2.43.



## 5.6 Discussion

Estimation of enzyme specific activity was reported previously in Section 4.3.4. The enzyme specific activity for the Pfs-chitosan conjugate assembled on the electrode in this chapter ( $0.35 \mu\text{mol SAH/ min/ mg Pfs}$ ) is lower than what we estimated in the previous chapter ( $3.7 \mu\text{mol SAH/ min/ mg Pfs}$ ). The difference might be due to several reasons. First, the enzyme solution used here was from a different batch prepared at different time, which might have different specific activity. Second, the bioMEMS device used here has a different configuration, which might result in different activity after enzyme assembly. The device design in Figure 5-3 consists of two counter electrodes besides the working electrode for enzyme assembly. During electrodeposition, this configuration might generate higher pH gradient at the working electrode surface, thereby deactivating the enzyme activity. Nonetheless, the estimated specific activity is within the range of reported Pfs specific activities in the literature which vary over 3 orders of magnitude (Duerre 1962, Ferro, et al. 1976, Ragione, et al. 1985). Importantly, given the enzyme specific activity and flow rate conditions, the purpose of suppressing parasitic reactions has been demonstrated by the decreasing background signal and increasing S/B ratio, as shown in Fig.6 and Fig.7, while the site-specific conversions remained at the same level.

The use of chitosan as an intermediary interface allows for the programmable assembly of enzymes in a microfluidic network, making this bioMEMS platform both versatile and functional (Fernandes et al. 2004, Wu, et al. 2003). By improving the ability to specify the site of the individual enzymatic reactions, these modifications

allow for the construction of the complex networks needed to simulate biologically relevant pathways. In these networks, each enzymatic step would be catalyzing a specific reaction with known conversion efficiency. The conversion rate of each step could be measured independently, and the conversion action would be attributable only to the specifically bound enzyme, with minimal side-reactions.

Advanced methods for reducing parasitic reactions can be further developed. Homogenous parasitic reactions could be addressed by the use of zero dead-volume interconnect designs to interface the microfluidic channel with the external pumping and fluid delivery. By incorporating in-line valves for flow control, it is possible to envision purging flows which would flush the channel areas of any non-specifically bound enzyme. Additionally, through stronger and longer chemical pretreatment of the microchannel walls than the BSA solution used here, it might be possible to further repel enzyme binding and thereby eliminate heterogeneous parasitic reactions.

## 5.7 Conclusions

In summary, this work demonstrates a novel packaging technique to minimize the homogeneous parasitic reactions in the dead volume of packaging interconnects and an experimental strategy to minimize heterogeneous parasitic reactions due to non-specific binding on microchannel walls. Our experiment and simulation results prove that the combined strategies of fabricating packaging aligners to avoid the interconnect reservoirs and separating flow directions for enzyme immobilization and the subsequent enzymatic reactions are efficient in minimizing

the background noise up to 70%. These strategies increase the signal-to-background ratio from 0.72 to 2.43 for the given device design and enzyme activity. These techniques can be easily applied to versatile microfluidic devices to minimize cross-contamination in sequential biochemical reactions.

## Chapter 6. Conclusions and Future Work

### 6.1 Conclusions

The overall goal of this research is to demonstrate the programmable assembly and the biological activity of biomolecules in prepackaged bioMEMS devices.

Chitosan-mediated, signal-guided biofunctionalization approach was implemented throughout this research for programmable assembly and activity of biomolecules in bioMEMS devices. Our approach is based on electro-deposition of the aminopolysaccharide chitosan scaffold as a stable thin film onto patterned conductive surfaces of bioMEMS devices followed by covalent assembly of biomolecules onto the surface of the electrodeposited chitosan scaffold.

Our approach for biomolecule assembly in bioMEMS devices offers several unique capabilities. First, the electric signal-guided nature of the chitosan assembly allows simple *in situ* assembly of biological molecules when and where it is needed, even long after the device is fully manufactured. Second, biomolecules are assembled from the aqueous environment, thus preserving their biological activities through the assembly procedure. Third and finally, our technique offers generic, flexible strategies for different target biomolecules since a wide variety of conjugation schemes can be utilized for different biomolecules. Combined, these advantages make our assembly approach appealing for a wide variety of bioMEMS and biosensing applications that require device biofunctionalization.

I have demonstrated the chitosan-mediated *in situ* biomolecule assembly as a simple approach to direct the assembly of biological components into prefabricated

bioMEMS devices. In the first demonstration, GFP was *in situ* assembled onto chitosan scaffold in a bioMEMS device by chemically activating the amine groups of chitosan with glutaraldehyde. Next, GFP was *in situ* assembled onto chitosan scaffold in a bioMEMS device by enzymatic activation of the genetically fused pentatyrosine pro-tag at the protein's C-terminus. Finally, DNA hybridization was demonstrated on chitosan scaffold by glutaraldehyde activation of the amine groups of chitosan for assembly of probe DNA. Importantly, the biomolecules in all cases were assembled onto patterned electrodes in prepackaged microchannels with spatial and temporal programmability. Because the assembly of biological elements is signal-guided through the electrodeposition process, the active biology can be introduced into prefabrication bioMEMS devices upon demand.

Particularly, the programmable assembly and activity of a metabolic pathway enzyme have been demonstrated as an important step to reconstruct the AI-2 synthesis pathway in bioMEMS environment. The enzyme Pfs is genetically fused with a pentatyrosine "pro-tag" at its C-terminus. Signal responsive assembly is based on covalent conjugation of Pfs to the aminopolysaccharide, chitosan, upon biochemical activation of the pro-tag, followed by electrodeposition of the enzyme-chitosan conjugate onto readily addressable sites in microfluidic channels. The work demonstrated that the assembled enzymes are catalytically active, robust, and stable with time, and that our strategy is reproducible, allowing for multiple uses of bioMEMS devices. Compared to traditional physical entrapment and surface immobilization approaches in microfluidic environments, our signal-guided

electrochemical assembly is unique in that the enzymes are assembled under mild aqueous conditions with spatial and temporal programmability and orientational control. We report here for the first time the signal-guided assembly of catalytically active enzymes at localized sites which can be programmed both spatially and temporally within a prepackaged bioMEMS. The demonstration of their catalytic activity represents a key step in progress toward a bioMEMS technology to support metabolic engineering research and development, where multi-step biochemical reactions are common and separation of these steps is highly desirable for understanding reaction details and modifying pathways and kinetics for various applications (e.g. drug discovery).

Additionally, this research has investigated the design optimization of bioMEMS devices and experimental strategy for studies of metabolic pathway enzyme. A novel packaging technique is demonstrated to minimize the homogeneous parasitic reactions in the dead volume of packaging interconnects and an experimental strategy to minimize heterogeneous parasitic reactions due to non-specific binding on microchannel walls. The previous investigations of enzyme assembly in bioMEMS have revealed some unintended (or parasitic) effects including products generated by the enzyme either (1) in the homogeneous phase (in the liquid), or (2) nonspecifically bound to microchannel surfaces. To reduce homogeneous reactions, a new packaging and assembly strategy has been developed to eliminate fluid reservoirs that are commonly used for fluidic interconnect with external tubing. To suppress reactions by nonspecifically bound enzyme on

microchannel walls, a cross-flow microfluidic network design has been implemented so that enzyme flow for assembly and substrate/product for reaction share only the region where the enzyme is immobilized at the intended reaction site. Our experiment and simulation results show that the signal-to-background ratio of sequential enzymatic reactions increases from 0.72 to 1.28 by eliminating the packaging reservoirs, and increases to 2.43 by separating the flow direction of enzymatic reaction from that of enzyme assembly step. These techniques can be easily applied to versatile microfluidic devices to minimize parasitic reactions in sequential biochemical reactions.

In summary, this work demonstrated the facile assembly and the biological activity of biomolecules in prepackaged bioMEMS devices with spatial and temporal programmability. Importantly, the biofunctionalization of bioMEMS device provides a novel approach for assembly of nano-bio-components in the microfluidic environment while retaining the biological activities of the assembled species. The advancement of the device design can be readily applied to benefit sequential biochemical reactions in bioMEMS devices. More importantly, the demonstration of a bacterial pathway enzyme assembly and the catalytic activity represents a key step toward reconstructing and investigating a quorum sensing pathway in the microfluidic environment, which provides a versatile platform to screen for antimicrobial drug candidates that promises to overcome the antibiotic resistance of bacteria.

## 6.2 Future work

This research is part of our entire research project of creating an *in vitro* AI-2 biosynthesis pathway in microsystem to screen inhibitors of AI-2 synthases Pfs and LuxS as antimicrobial drug candidates. The future work after this research has been envisioned as shown to the right side of Figure 6-1.

The biofunctionalization strategy demonstrated in this research for programmable biomolecule assembly in bioMEMS provides a versatile template for reconstructing the quorum sensing pathway. The demonstrated enzymatic reaction of converting SAH into SRH and adenine represents the first of the two-step AI-2 synthesis pathway in bioMEMS. The next crucial goal of this research is to complete constructing the AI-2 synthesis pathway in our bioMEMS, which is to assemble both enzymes Pfs and LuxS separately in microfluidic channel.

Inhibition or knock-down of enzymes in this pathway represents opportunities for new antimicrobial drugs that expected to either intercept or rewire the QS communication network. Several Pfs inhibitors have been reported recently

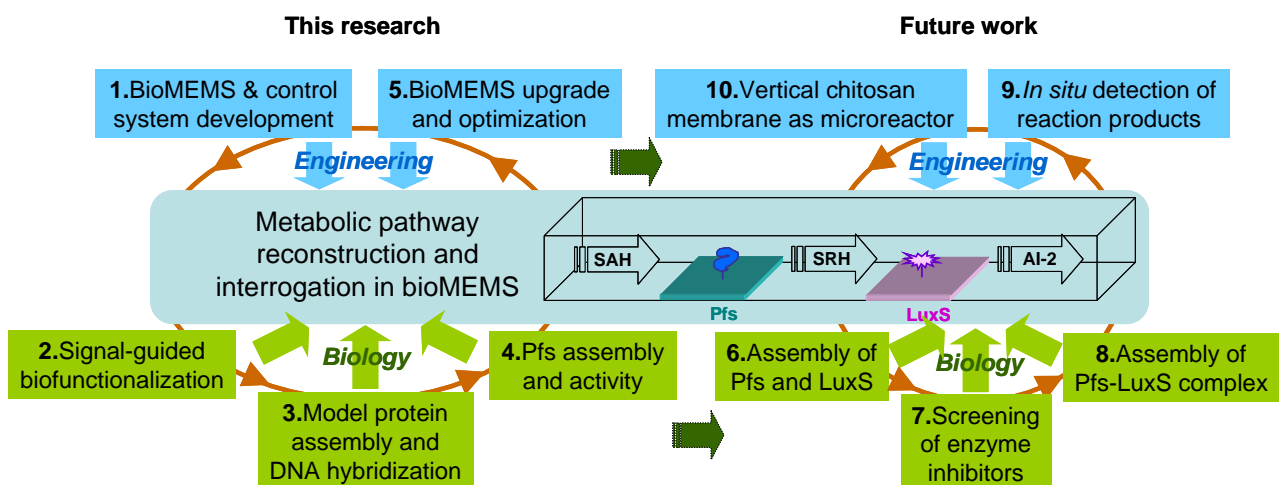


Figure 6-1: Roadmap of this research and future work.



(Cornell et al. 1996, Lee et al. 2003, Shim, et al. 2003, Singh et al. 2005, Singh et al. 2006). Therefore, the subsequent important goal is to use the demonstrated template to screen for inhibitors of the AI-2 biosynthesis enzymes, of which Pfs turn out to be more stable and can be initiated as a first try.

While assembly of the AI-2 synthases at separate localized assembly sites in bioMEMS provides the platform to study the individual enzymes Pfs and LuxS in a well-controlled manner, coupling the Pfs and LuxS as a nanofactory and the assembly of the so-formed complex onto chitosan scaffold in bioMEMS stabilizes the more fragile enzyme LuxS. Therefore, another parallel research is being investigated to assemble the AI-2 synthesis nanofactory and study biofilm formation in the bioMEMS environment.

Currently, the enzymatic reaction products are collected and analyzed with HPLC to measure the enzymatic conversion. A very desirable alternative detection cf. *ex situ* HPLC analysis is to build an *in situ* sensor to quantify the enzymatic conversion in real time. Research is underway to develop a reactive substrate downstream of the enzymatic reaction site to measure the enzymatic conversion products by *in situ* surface enhanced Raman spectrometry (SERS).

Finally, because of the intrinsic laminar flow in microfluidics, the enzymatic conversion efficiency is limited by the slow diffusion of substrate to and products off the assembled enzymes on the assembly site on the microchannel floor parallel to the flow stream. To improve the conversion efficiency, we are currently exploring the assembly of enzyme onto vertical, permeable chitosan membrane structure such

that each of substrate molecules in the perpendicular flow stream might interact with the assembled enzymes on the membrane.

# Appendices

## Appendix I Estimation of enzyme specific activity

This appendix presents supplementary information to Section 4.3.4 regarding the estimation of enzyme specific activity.

### Materials

Mouse anti-polyhistidine and goat anti-mouse IgG conjugated to alkaline phosphatase were purchased from Sigma (St. Louis, MO). Glacial acetic acid, Tris base, acrylamide, Bis-acrylamide, methanol, and  $MgCl_2 \cdot 6H_2O$  were purchased from Fisher Chemical (Fair Lawn, NJ). Sodium dodecyl sulfate (SDS), glycine, non-fat dry milk, and Tween 20 were purchased from BioRad (Hercules, CA).

### Chip fabrication

The microfabrication process for the chips was reported previously (Yi, et al. 2004). Briefly, 4" diameter silicon wafers were coated with 1  $\mu m$  silicon nitride film, followed by deposition of 50 Å chromium film, and finally, deposition of 2000 Å gold film. The patterns were created by photolithography, and the photoresist removed using acetone. The chips contain two upper gold rectangular patterns (6 mm long  $\times$  3 mm wide). The left upper pattern was where the alligator clip was attached. The upper patterns are each linked by gold lines to two lower gold rectangular patterns. The left lower gold pattern was where assembly took place, and two patterned areas were investigated: 8 mm long  $\times$  0.5 mm wide ( $4 \text{ mm}^2$ ), and 8 mm long  $\times$  4 mm wide ( $32 \text{ mm}^2$ ).

### **Pfs-chitosan conjugation, chip assembly, and disassembly**

First, the chip was incubated in 1 % (w/v) BSA – PBS for 2 h, rinsed with de-ionized water, and set aside. The conjugate was prepared as described previously (see Materials and Methods section), and deposited onto the left gold electrode pattern by dipping the chip into the conjugate until the pattern was submerged and applying negative bias to the pattern (4 min at 3 A/m<sup>2</sup>). This was done by connecting the cathode and anode (nickel chromium wire) using alligator clips to a DC power supply (Keithley 2400 SourceMeter). After deposition, the chip was rinsed with de-ionized water, and washed with gentle shaking 3 × 5 min in 5 mL each of PBS buffer. The deposited conjugate was then resolubilized by washing the chip in 2 % (v/v) acetic acid. Next, the resolubilized conjugate samples were analyzed via Western blot.

### **SDS-PAGE and Western blot analysis**

Sample buffer (0.0625 M Tris-HCl, pH 6.8, 10% (v/v) glycerol, 2% (w/v) SDS, 5% (v/v) β-mercaptoethanol, 0.025% (w/v) bromophenol blue) was mixed with the resolubilized conjugate samples 1:1 (v:v), and these mixtures were then heated at 92 – 95 °C for 10 minutes. Proteins were separated by SDS polyacrylamide gel electrophoresis using 12.5% acrylamide gels at 180 V for 1 hour using the BioRad Mini Protean 3 system, and blotted onto BioRad nitrocellulose membranes using a BioRad Trans-Blot semi-dry transfer cell and Bjerrum-Schafer-Nielsen transfer buffer (48 mM Tris, 39 mM glycine, 20% (v/v) methanol, 0.0375% (w/v) SDS) for 30 minutes at 15 V. Unbound membrane sites were blocked using 5% (w/v)

non-fat dry milk in 20 mM Tris-HCl, pH 7.5, 500 mM NaCl. The membrane was first incubated for 2 hours at room temperature in mouse monoclonal anti-polyhistidine at 1:4,000 dilution. The membrane was then incubated at room temperature for 1 hour in goat anti-mouse IgG conjugated to alkaline phosphatase at 1:4,000 dilution. Both antibodies were diluted in 20 mM Tris-HCl, pH 7.5, 500 mM NaCl, 1% (w/v) non-fat dry milk, 0.05% (v/v) Tween 20. Membranes were developed colorimetrically using Roche NBT/BCIP stock diluted 1:50 (v:v) in 0.1 M Tris-HCl, pH 9.5, 0.1 M NaCl, 0.05 M MgCl<sub>2</sub>.

#### **Estimations of Pfs specific activity**

Pfs-chitosan conjugate was prepared and electrodeposited onto different electrode areas of microfabricated chips. Each deposited conjugate was resolubilized with dilute acid, and finally analyzed via Western blot. By comparing the Western blot band intensities of the resolubilized conjugate samples with that of a known quantity of purified Pfs standard, the mg Pfs in each sample (i.e. mg Pfs attached on each chip) was estimated. The mg Pfs attached was plotted against assembly area to generate a linear fit, which was extrapolated to 0.5 mm<sup>2</sup>, the assembly (electrode) area inside the microchannel, to estimate the mg Pfs attached to the electrode inside the microchannel. The  $\mu\text{mol SAH}$  converted per minute was calculated from the % SAH conversion at 3  $\mu\text{L}/\text{min}$  averaged over all reaction samples (3  $\mu\text{L}/\text{min} \times 3 \text{ min}$  collection time = 9  $\mu\text{L}$  reaction sample volume).

## Appendix II Calculation of the missing enzymatic conversion of intersection-channels

This appendix presents supplementary information to Section 5.5.2 with the effort to calculate the missing enzymatic conversion of intersection-channels.

In the original design of Figure 5-3, the working electrode's exposed area ( $0.75 \text{ mm}^2$ ) in the  $500\mu\text{m}$  cross-channel design was designed to match the exposed area in the  $500\mu\text{m}$  single-channel design, as shown in Figure S-1. The actual catalysis area for enzymatic conversion in the cross-channel design is affected by two factors. First, the vertical channel in Figure S-2(a) was filled with Pfs-chitosan conjugate solution before assembly of Pfs enzyme. During the 4-min electrodeposition time, the Pfs-chitosan conjugate had diffused only slightly into the horizontal side channels. Therefore, only the Pfs enzyme within the diffusion distance was available for electrodeposition in the horizontal direction as in Figure S-2(a). Second, during continuous pumping of SAH into the horizontal channel as in Figure S-2(b), SAH diffused out of the flow stream to encounter assembled enzyme in the

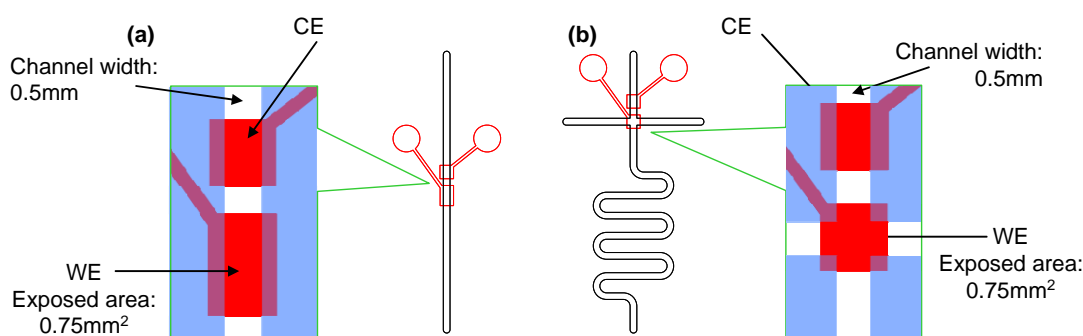


Figure S-1: Working electrodes (WE) were fabricated to match the exposed surface area in both (a) single-channel and (b) cross-channel.

vertical side channels. The reaction products (SRH + adenine) then diffused back to the flow stream in the horizontal channel. Therefore, the enzymatic reaction in the vertical side channel is not as efficient as that in the flow stream in the horizontal channel. As a result, the missing enzymatic conversion of intersection-channels needs to be calculated to compare with the conversion in the single-channel.

The normalization was performed first by estimating the diffusion of Pfs-chitosan conjugate to the Pfs\_diff area as in Figure S-2(c) during electrodeposition. Next, the diffusion of enzymatic substrate to the SAH\_diff area during continuous reaction was simulated to determine the conversion efficiency in the SAH\_diff area. The sum of these lateral areas, and the central electrode area, gives the nominal active catalytic area in the cross-channel design. Finally, a curve-fitting relationship between the conversion and active catalytic area was

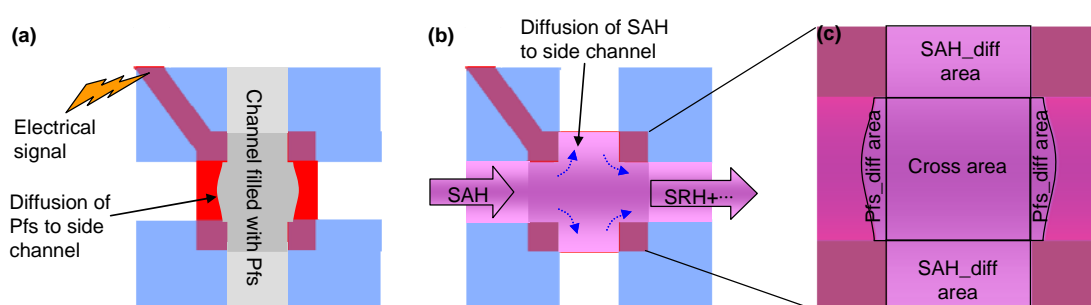


Figure S-2: Factors that affect the enzymatic conversion in the cross-channel. (a) Enzyme is only available within the diffusion distance for electrodeposition in the horizontal side channel due to the low diffusivity of Pfs-chitosan conjugate. (b) The enzymatic reaction in the vertical side channel, which mainly depends on the diffusion of reaction substrate and products back and forth to the flow stream in the horizontal channel, is not as efficient as that in the central cross area. (c) Enlargement of the nominal active area including Pfs\_diff area, SAH\_diff area and the central cross area.

obtained to yield the conversion on the  $0.75\text{mm}^2$  active catalytic area in cross-channel.

### **Estimation of diffusion of Pfs-chitosan conjugate during electrodeposition**

Diffusivity generally scales inversely with molecular weight (MW). Although the diffusivity of the Pfs-chitosan is not available, we can easily make an approximate estimation. It is reported that the diffusivity of chitosan with MW of 223 kDa is  $4.3 \times 10^{-8} \text{ cm}^2/\text{s}$  at pH 4.3 (Tsaih and Chen 1999). The diffusivity of proteins varies between  $10^{-6}$  and  $10^{-8} \text{ cm}^2/\text{s}$  for lysozyme (MW: 14 kDa) and  $4.4 \times 10^{-8} \text{ cm}^2/\text{s}$  for TMV virus (MW: 50,000 kDa) (Malkiel 1952), (Brune and Kim 1993). It is reasonable to assume Pfs (MW: 45 kDa (Bose and Momany 2001)) has diffusivity in the range of  $10^{-7} \text{ cm}^2/\text{s}$ . In the Pfs-chitosan conjugate solution, the weight ratio of Pfs to chitosan is 0.04% (see Materials and Methods section). Therefore, the diffusivity of chitosan dominates the diffusivity of Pfs-chitosan conjugate, thus yielding an approximate diffusivity of  $4 \times 10^{-8} \text{ cm}^2/\text{s}$ .

The diffusion distance of Pfs-chitosan conjugate in 10 minutes (3 min to introduce conjugate solution, 4 min for electrodeposition, then 3 min to drain) is calculated to be  $48 \mu\text{m}$  on each side. Therefore, the ratio of the two Pfs\_diff areas to cross-area is  $2 \times 48 \times 500 \mu\text{m}^2 / 500 \times 500 \mu\text{m}^2 = 0.192$ .

### **Simulation of SAH diffusion during the continuous enzymatic reaction**

As shown in Figure S-3, Pfs enzyme covers the entire exposed surface area of the working electrode in the vertical channel. Using the Wilke-Chang correlation, the diffusivities of SAH and adenine were calculated to be  $3.42 \times 10^{-6} \text{ cm}^2/\text{s}$  and



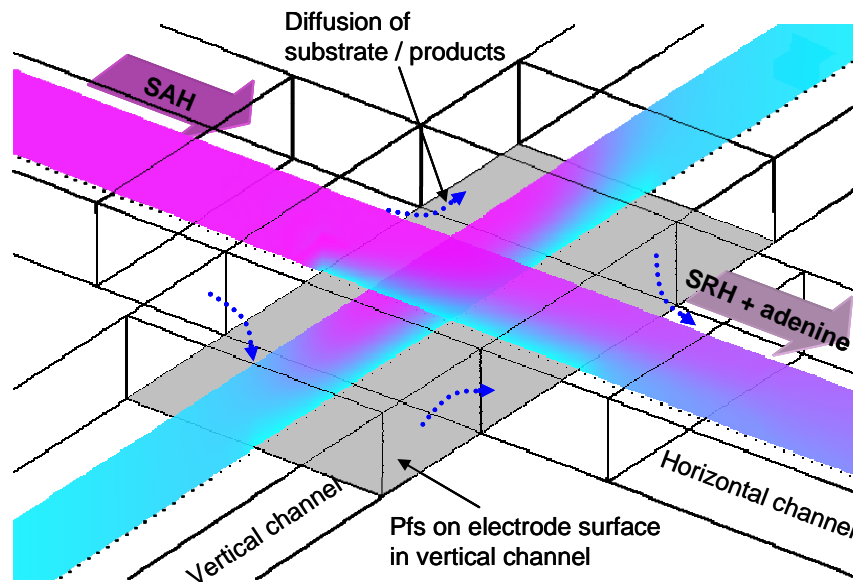


Figure S-3: Simulation of SAH diffusion during enzymatic reaction. The vertical channel is filled with buffer (turquoise blue). SAH (purple) in the horizontal channel diffuses out of the flow stream into the vertical side channels and is converted by assembled Pfs in side channels. Reaction products SRH and adenine diffuse back to flow stream into the horizontal channel. Simulation result shows that conversion in vertical side channels equals to 45% of conversion in horizontal flow stream.

$4.13 \times 10^{-6} \text{ cm}^2/\text{s}$ , respectively. Finite element simulation using COMSOL Multi-Physics (COMSOL) was performed to investigate the diffusion of reaction substrate SAH molecules from the horizontal flow stream into the vertical side channel during the enzymatic reaction.

The surface reaction is diffusion transport limited (Gervais and Jensen 2006) for Damköhler number  $Da \gg 1$  and  $k_{on} = 9.149 \times 10^6 \text{ 1/Ms}$ , so we assume all substrate reaching the active enzyme surface is converted into products. During the enzymatic reaction, the two ends of vertical channel were sealed leak-tight with parafilm to stagnate the lateral flow. Simulation results show that the flux through

the two SAH\_diff areas ( $2 \times 0.125 \text{ mm}^2$ ) is 44.6% of the flux through the central cross-area ( $0.25 \text{ mm}^2$ ). Therefore, the ratio of the two SAH\_diff areas to the central cross area is 0.446.

The ratio of 0.192 due to enzyme diffusion during enzyme assembly and the ratio of 0.446 due to substrate diffusion during enzymatic reaction are from processes on orthogonal axes. Therefore, the total nominal active area is  $0.25 \text{ mm}^2 \times (1 + 0.192 + 0.446) = 0.411 \text{ mm}^2$ .

### Normalization of conversion in cross-channel

Based on the nominal active catalysis area in the cross-channel, estimated to be  $0.411 \text{ mm}^2$ , the normalization of conversion was performed as follows. *Step 1*, in the case of diffusion limited, we assume all reaction substrate reaching the enzyme is instantly converted into products. The relationship between the conversion and catalysis area was established with simulation in COMSOL software (blue

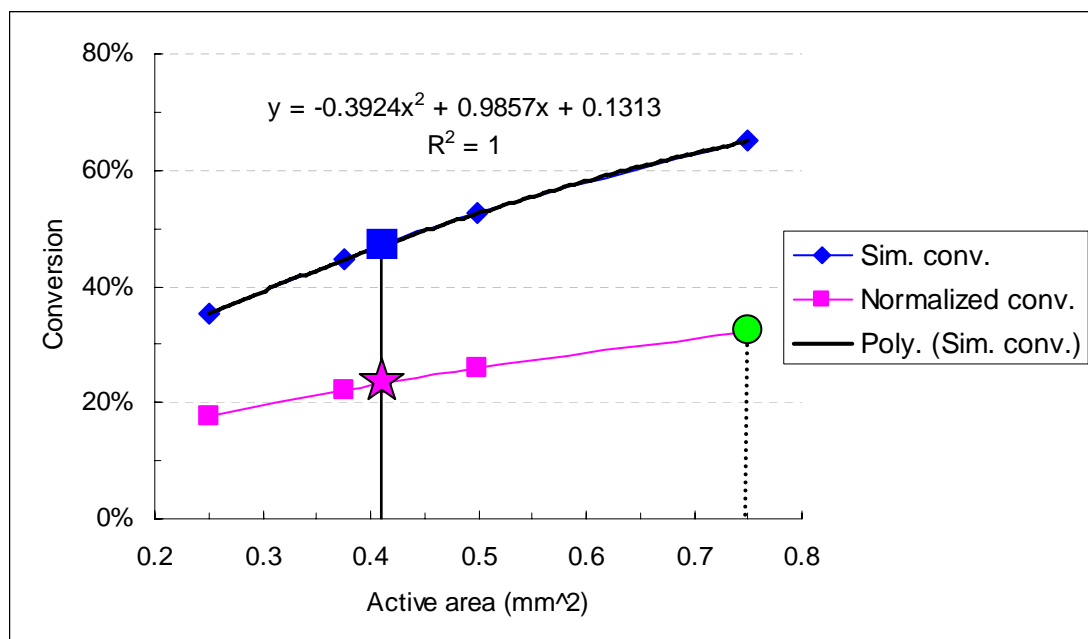


Figure S-4: Normalization of enzymatic conversion. See the text for details.

line/diamonds, Figure S-4). *Step 2*, polynomial curve fitting of this relationship was obtained (black line), and the conversion of  $0.411 \text{ mm}^2$  active catalysis area was calculated to be 47.0% (blue squares). *Step 3*, the ratio of actual conversion from experiment (23.4%, purple star) to the afore-calculated conversion (47.0%) was determined to be 0.497 by this  $0.411 \text{ mm}^2$  active area. *Step 4*, the entire fitted curve was scaled by the ratio of 0.497 (purple line/squares) to compensate factors that slow down the conversion but were not considered in the simulation of the conversion-catalysis area relationship. *Step 5*, the normalized conversion on a  $0.75 \text{ mm}^2$  active area in a cross-channel was obtained from the purple curve to be 32.3% (green circle).

## References

- Andersson H, van den Berg A. Microfluidic devices for cellomics: a review. *Sensors and Actuators B-Chemical* **92**:315-325 (2003)
- Andersson H, van den Berg A. Where are the biologists? A series of mini-reviews covering new trends in fundamental and applied research, and potential applications of miniaturised technologies. *Lab on a Chip* **6**:467-470 (2006)
- Atencia J, Beebe DJ. Controlled microfluidic interfaces. *Nature* **437**:648-655 (2005)
- Auroux PA, Iossifidis D, Reyes DR, Manz A. Micro total analysis systems. 2. Analytical standard operations and applications. *Analytical Chemistry* **74**:2637-2652 (2002)
- Balestrino D, Haagensen JAJ, Rich C, Forestier C. Characterization of type 2 quorum sensing in *Klebsiella pneumoniae* and relationship with biofilm formation. *Journal of Bacteriology* **187**:2870-2880 (2005)
- Barrios AFG, Zuo RJ, Hashimoto Y, Yang L, Bentley WE, Wood TK. Autoinducer 2 controls biofilm formation in *Escherichia coli* through a novel motility quorum-sensing regulator (MqsR, B3022). *Journal of Bacteriology* **188**:305-316 (2006)
- Beebe DJ, Mensing GA, Walker GM. Physics and applications of microfluidics in biology. *Annual Review of Biomedical Engineering* **4**:261-286 (2002)
- Bhagat AAS, Jothimuthu P, Pais A, Papautsky I. Re-usable quick-release interconnect for characterization of microfluidic systems. *Journal of Micromechanics and Microengineering* **17**:42-49 (2007)
- Bilitewski U, Genrich M, Kadow S, Mersal G. Biochemical analysis with microfluidic systems. *Analytical and Bioanalytical Chemistry* **377**:556-569 (2003)
- Bose N, Momany C. Crystallization and preliminary X-ray crystallographic studies of recombinant human betaine-homocysteine S-methyltransferase. *Acta Crystallographica Section D-Biological Crystallography* **57**:431-433 (2001)
- Brune D, Kim S. Predicting Protein Diffusion-Coefficients. *Proceedings of the National Academy of Sciences of the United States of America* **90**:3835-3839 (1993)
- Can Wang ROFOJLPTDJH. Integration of immobilized trypsin bead beds for protein digestion within a microfluidic chip incorporating capillary electrophoresis separations and an electrospray mass spectrometry interface. *Rapid Communications in Mass Spectrometry* **14**:1377-1383 (2000)
- Cao LQ. Immobilised enzymes: science or art? *Current Opinion in Chemical Biology* **9**:217-226 (2005)
- Caruso F, Schuler C. Enzyme multilayers on colloid particles: Assembly, stability, and enzymatic activity. *Langmuir* **16**:9595-9603 (2000)
- Chaki NK, Vijayamohan K. Self-assembled monolayers as a tunable platform for biosensor applications. *Biosensors & Bioelectronics* **17**:1-12 (2002)

- Chang WJ, Akin D, Sedlak M, Ladisch MR, Bashir R. Poly(dimethylsiloxane) (PDMS) and silicon hybrid biochip for bacterial culture. *Biomedical Microdevices* **5**:281-290 (2003)
- Christensen AM, Chang-Yen DA, Gale BK. Characterization of interconnects used in PDMS microfluidic systems. *Journal of Micromechanics and Microengineering* **15**:928-934 (2005)
- Cornell KA, Swarts WE, Barry RD, Riscoe MK. Characterization of recombinant *Escherichia coli* 5'-methylthioadenosine/S-adenosylhomocysteine nucleosidase: Analysis of enzymatic activity and substrate specificity. *Biochemical and Biophysical Research Communications* **228**:724-732 (1996)
- Deng JL, Guo CX, Lu WS, Liu T, Jiang L. Polydiacetylene vesicle - A device based on molecular assembly for biological molecular recognition. *Progress in Chemistry* **18**:1397-1408 (2006)
- Dittrich PS, Tachikawa K, Manz A. Micro Total Analysis Systems. Latest Advancements and Trends. *Anal Chem* **78**:3887-3908 (2006)
- Dittrich PS, Tachikawa K, Manz A. Micro total analysis systems. Latest advancements and trends. *Analytical Chemistry* **78**:3887-3907 (2006)
- Duerre JA. Hydrolytic Nucleosidase Acting on S-Adenosylhomocysteine and on 5'-Methylthioadenosine. *Journal of Biological Chemistry* **237**:3737-3741 (1962)
- Duffy DC, McDonald JC, Schueller OJA, Whitesides GM. Rapid prototyping of microfluidic systems in poly(dimethylsiloxane). *Analytical Chemistry* **70**:4974-4984 (1998)
- Federle MJ, Bassler BL. Interspecies communication in bacteria. *Journal of Clinical Investigation* **112**:1291-1299 (2003)
- Fernandes R, Tsao CY, Hashimoto Y, Wang L, Wood TK, Payne GF, Bentley WE. Magnetic nanofactories: Localized synthesis and delivery of quorum-sensing signaling molecule autoinducer-2 to bacterial cell surfaces. *Metabolic Engineering* **9**:228-239 (2007)
- Fernandes R, Yi HM, Wu LQ, Rubloff GW, Ghodssi R, Bentley WE, Payne GF. Thermo-biolithography: A technique for patterning nucleic acids and proteins. *Langmuir* **20**:906-913 (2004)
- Ferro AJ, Barrett A, Shapiro SK. Kinetic-Properties and Effect of Substrate Analogs on 5'-Methylthioadenosine Nucleosidase from *Escherichia-Coli*. *Biochimica Et Biophysica Acta* **438**:487-494 (1976)
- Fredrickson CK, Fan ZH. Macro-to-micro interfaces for microfluidic devices. *Lab on a Chip* **4**:526-533 (2004)
- Gervais T, Jensen KF. Mass transport and surface reactions in microfluidic systems. *Chemical Engineering Science* **61**:1102-1121 (2006)
- Gray BL, Collins SD, Smith RL. Interlocking mechanical and fluidic interconnections for microfluidic circuit boards. *Sensors and Actuators a-Physical* **112**:18-24 (2004)
- Haber C. Microfluidics in commercial applications; an industry perspective. *Lab on a Chip* **6**:1118-1121 (2006)

- Haerberle S, Zengerle R. Microfluidic platforms for lab-on-a-chip applications. *Lab on a Chip* **7**:1094-1110 (2007)
- Han A, Graff M, Wang O, Frazier AB. An approach to multilayer microfluidic systems with integrated electrical, optical, and mechanical functionality. *Ieee Sensors Journal* **5**:82-89 (2005)
- Hickey AM, Marle L, McCreedy T, Watts P, Greenway GM, Littlechild JA. Immobilization of thermophilic enzymes in miniaturized flow reactors. *Biochem Soc Trans* **35**:1621-1623 (2007)
- Holden MA, Jung SY, Cremer PS. Patterning enzymes inside microfluidic channels via photoattachment chemistry. *Analytical Chemistry* **76**:1838-1843 (2004)
- Honda T, Miyazaki M, Nakamura H, Maeda H. Facile preparation of an enzyme-immobilized microreactor using a cross-linking enzyme membrane on a microchannel surface. *Adv Synth Catal* **348**:2163-2171 (2006)
- Hong JW, Chen Y, Anderson WF, Quake SR. Molecular biology on a microfluidic chip. *Journal of Physics-Condensed Matter* **18**:S691-S701 (2006)
- Janasek D, Franzke J, Manz A. Scaling and the design of miniaturized chemical-analysis systems. *Nature* **442**:374-380 (2006)
- Jo BH, Van Lerberghe LM, Motsegood KM, Beebe DJ. Three-dimensional micro-channel fabrication in polydimethylsiloxane (PDMS) elastomer. *Journal of Microelectromechanical Systems* **9**:76-81 (2000)
- Jung GY, Stephanopoulos G. A functional protein chip for pathway optimization and in vitro metabolic engineering. *Science* **304**:428-431 (2004)
- Kim S, Huang B, Zare RN. Microfluidic separation and capture of analytes for single-molecule spectroscopy. *Lab on a Chip* **7**:1663-1665 (2007)
- Kisailus D, Truong Q, Amemiya Y, Weaver JC, Morse DE. Self-assembled bifunctional surface mimics an enzymatic and templating protein for the synthesis of a metal oxide semiconductor. *Proceedings of the National Academy of Sciences of the United States of America* **103**:5652-5657 (2006)
- Ku BS, Cha JH, Srinivasan A, Kwon SJ, Jeong JC, Sherman DH, Dordick JS. Chip-based polyketide biosynthesis and functionalization. *Biotechnology Progress* **22**:1102-1107 (2006)
- Kumar A, Schweizer HP. Bacterial resistance to antibiotics: Active efflux and reduced uptake. *Advanced Drug Delivery Reviews* **57**:1486-1513 (2005)
- L'Hostis E, Michel PE, Fiaccabrino GC, Strike DJ, de Rooij NF, Koudelka-Hep M. Microreactor and electrochemical detectors fabricated using Si and EPON SU-8. *Sensors and Actuators B-Chemical* **64**:156-162 (2000)
- Lee JE, Cornell KA, Riscoe MK, Howell PL. Structure of Escherichia coli 5'-methylthioadenosine/S-adenosylhomocysteine nucleosidase inhibitor complexes provide insight into the conformational changes required for substrate binding and catalysis. *Journal of Biological Chemistry* **278**:8761-8770 (2003)
- Lee SW, Lee SS. Shrinkage ratio of PDMS and its alignment method for the wafer level process. *Microsystem Technologies-Micro-and Nanosystems-Information Storage and Processing Systems* **14**:205-208 (2008)

- Leeb M. Antibiotics: A shot in the arm. *Nature* **431**:892-893 (2004)
- Lewandowski AT, Small DA, Chen TH, Payne GF, Bentley WE. Tyrosine-based "activatable pro-tag": Enzyme-catalyzed protein capture and release. *Biotechnology and Bioengineering* **93**:1207-1215 (2006)
- Lewandowski AT, Yi HM, Luo XL, Payne GF, Ghodssi R, Rubloff GW, Bentley WE. Protein Assembly onto Patterned Microfabricated Devices through Enzymatic Activation of Fusion Pro-tag. *Biotechnology and Bioengineering* **99**:499-507 (2008)
- Li YG, Zhou YX, Feng JL, Jiang ZH, Ma LR. Immobilization of enzyme on screen-printed electrode by exposure to glutaraldehyde vapour for the construction of amperometric acetylcholinesterase electrodes. *Analytica Chimica Acta* **382**:277-282 (1999)
- Liu Y, Lu HJ, Zhong W, Song PY, Kong JL, Yang PY, Girault HH, Liu BH. Multi layer-assembled microchip for enzyme immobilization as reactor toward low-level protein identification. *Anal Chem* **78**:801-808 (2006)
- Logan TC, Clark DS, Stachowiak TB, Svec F, Frechet JMJ. Photopatterning enzymes on polymer monoliths in microfluidic devices for steady-state kinetic analysis and spatially separated multi-enzyme reactions. *Anal Chem* **79**:6592-6598 (2007)
- Long Z, Shen Z, Wu D, Qin J, Lin B. Integrated multilayer microfluidic device with a nanoporous membrane interconnect for online coupling of solid-phase extraction to microchip electrophoresis. *Lab on a Chip* **7**:1819-1824 (2007)
- Luckarift HR, Ku BS, Dordick JS, Spain JC. Silica-immobilized enzymes for multi-step synthesis in microfluidic devices. *Biotechnol Bioeng* **98**:701-705 (2007)
- Luo X, Lewandowski AT, Yi H, Payne GF, Ghodssi R, Bentley WE, Rubloff GW. Programmable assembly of a metabolic pathway enzyme in a pre-packaged reusable bioMEMS device. *Lab on a Chip* **8**:420-430 (2008)
- Ma J, Zhang L, Liang Z, Zhang W, Zhang Y. Monolith-based immobilized enzyme reactors: Recent developments and applications for proteome analysis. *J Sep Sci* **30**:3050-3059 (2007)
- Malkiel S. Immunochemical Studies on Tobacco Mosaic Virus .8. The Specificity of Chemically-Altered Virus. *Journal of Immunology* **69**:533-538 (1952)
- Malpass CA, Millsap KW, Sidhu H, Gower LB. Immobilization of an oxalate-degrading enzyme on silicone elastomer. *Journal of Biomedical Materials Research* **63**:822-829 (2002)
- Mao HB, Yang TL, Cremer PS. Design and characterization of immobilized enzymes in microfluidic systems. *Analytical Chemistry* **74**:379-385 (2002)
- March JC, Bentley WE. Quorum sensing and bacterial cross-talk in biotechnology. *Current Opinion in Biotechnology* **15**:495-502 (2004)
- McDonald JC, Duffy DC, Anderson JR, Chiu DT, Wu HK, Schueller OJA, Whitesides GM. Fabrication of microfluidic systems in poly(dimethylsiloxane). *Electrophoresis* **21**:27-40 (2000)
- McDonald JC, Whitesides GM. Poly(dimethylsiloxane) as a Material for Fabricating

- Microfluidic Devices. *Acc Chem Res* **35**:491-499 (2002)
- Niemeyer CM, Wacker R, Adler M. Combination of DNA-directed immobilization and immuno-PCR: very sensitive antigen detection by means of self-assembled DNA-protein conjugates. *Nucleic Acids Research* **31** (2003)
- Park JJ, Luo XL, Yi HM, Valentine TM, Payne GF, Bentley WE, Ghodssi R, Rubloff GW. Chitosan-mediated in situ biomolecule assembly in completely packaged microfluidic devices. *Lab on a Chip* **6**:1315-1321 (2006)
- Payne GF, Raghavan SR. Chitosan: a soft interconnect for hierarchical assembly of nano-scale components. *Soft Matter* **3**:521-527 (2007)
- Peterson DS, Rohr T, Svec F, Frechet JMJ. Enzymatic microreactor-on-a-chip: Protein mapping using trypsin immobilized on porous polymer monoliths molded in channels of microfluidic devices. *Anal Chem* **74**:4081-4088 (2002)
- Projan SJ, Youngman PJ. Antimicrobials: new solutions badly needed. *Current Opinion in Microbiology* **5**:463-465 (2002)
- Psaltis D, Quake SR, Yang CH. Developing optofluidic technology through the fusion of microfluidics and optics. *Nature* **442**:381-386 (2006)
- Qu H, Wang H, Huang Y, Zhong W, Lu H, Kong J, Yang P, Liu B. Stable Microstructured Network for Protein Patterning on a Plastic Microfluidic Channel: Strategy and Characterization of On-Chip Enzyme Microreactors. *Anal Chem* **76**:6426-6433 (2004)
- Quake SR, Scherer A. From micro- to nanofabrication with soft materials. *Science* **290**:1536-1540 (2000)
- Quist AP, Pavlovic E, Oscarsson S. Recent advances in microcontact printing. *Analytical and Bioanalytical Chemistry* **381**:591-600 (2005)
- Ragione ED, Porcelli M, Cartenifarina M, Zappia V. Escherichia-Coli S-Adenosylhomocysteine/5'-Methylthioadenosine Nucleosidase - Purification, Substrate-Specificity and Mechanism of Action. *Biochemical Journal* **232**:335-341 (1985)
- Randall GC, Doyle PS. Permeation-driven flow in poly(dimethylsiloxane) microfluidic devices. *Proceedings of the National Academy of Sciences of the United States of America* **102**:10813-10818 (2005)
- Rasmussen TB, Bjarnsholt T, Skindersoe ME, Hentzer M, Kristoffersen P, Kote M, Nielsen J, Eberl L, Givskov M. Screening for quorum-sensing inhibitors (QSI) by use of a novel genetic system, the QSI selector. *Journal of Bacteriology* **187**:1799-1814 (2005)
- Rasmussen TB, Skindersoe ME, Bjarnsholt T, Phipps RK, Christensen KB, Jensen PO, Andersen JB, Koch B, Larsen TO, Hentzer M, Eberl L, Hoiby N, Givskov M. Identity and effects of quorum-sensing inhibitors produced by Penicillium species. *Microbiology-Sgm* **151**:1325-1340 (2005)
- Ren DC, Sims JJ, Wood TK. Inhibition of biofilm formation and swarming of Escherichia coli by (5Z)-4-bromo-5-(bromomethylene)-3-butyl-2(5H)-furanone. *Environmental Microbiology* **3**:731-736 (2001)
- Reyes DR, Iossifidis D, Auroux PA, Manz A. Micro total analysis systems. 1.



- Introduction, theory, and technology. *Analytical Chemistry* **74**:2623-2636 (2002)
- Shim J, Bersano-Begey TF, Zhu XY, Tkaczyk AH, Linderman JJ, Takayama S. Micro- and nanotechnologies for studying cellular function. *Current Topics in Medicinal Chemistry* **3**:687-703 (2003)
- Singh V, Evans GB, Lenz DH, Mason JM, Clinch K, Mee S, Painter GF, Tyler PC, Furneaux RH, Lee JE, Howell PL, Schramm VL. Femtomolar transition state analogue inhibitors of 5'-methylthioadenosine/S-adenosylhomocysteine nucleosidase from *Escherichia coli*. *Journal of Biological Chemistry* **280**:18265-18273 (2005)
- Singh V, Shi WX, Almo SC, Evans GB, Furneaux RH, Tyler PC, Painter GF, Lenz DH, Mee S, Zheng RJ, Schramm VL. Structure and inhibition of a quorum sensing target from *Streptococcus pneumoniae*. *Biochemistry* **45**:12929-12941 (2006)
- Sperandio V, Torres AG, Giron JA, Kaper JB. Quorum sensing is a global regulatory mechanism in enterohemorrhagic *Escherichia coli* O157 : H7. *Journal of Bacteriology* **183**:5187-5197 (2001)
- Sperandio V, Torres AG, Kaper JB. Quorum sensing *Escherichia coli* regulators B and C (QseBC): a novel two-component regulatory system involved in the regulation of flagella and motility by quorum sensing in *E. coli*. *Molecular Microbiology* **43**:809-821 (2002)
- Swift S, Throup JP, Williams P, Salmond GPC, Stewart G. Quorum sensing: A population-density component in the determination of bacterial phenotype. *Trends in Biochemical Sciences* **21**:214-219 (1996)
- Tan YC, Cristini V, Lee AP. Monodispersed microfluidic droplet generation by shear focusing microfluidic device. *Sensors and Actuators B-Chemical* **114**:350-356 (2006)
- Thorsen T, Maerkl SJ, Quake SR. Microfluidic large-scale integration. *Science* **298**:580-584 (2002)
- Tsaih ML, Chen RH. Effects of ionic strength and pH on the diffusion coefficients and conformation of chitosan molecule in solution. *Journal of Applied Polymer Science* **73**:2041-2050 (1999)
- Unger MA, Chou HP, Thorsen T, Scherer A, Quake SR. Monolithic microfabricated valves and pumps by multilayer soft lithography. *Science* **288**:113-116 (2000)
- Urban PL, Goodall DM, Bruce NC. Enzymatic microreactors in chemical analysis and kinetic studies. *Biotechnology Advances* **24**:42-57 (2006)
- Vilkner T, Janasek D, Manz A. Micro total analysis systems. Recent developments. *Analytical Chemistry* **76**:3373-3385 (2004)
- Walsh C. Molecular mechanisms that confer antibacterial drug resistance. *Nature* **406**:775-781 (2000)
- Wu LQ, Gadre AP, Yi HM, Kastantin MJ, Rubloff GW, Bentley WE, Payne GF, Ghodssi R. Voltage-dependent assembly of the polysaccharide chitosan onto an electrode surface. *Langmuir* **18**:8620-8625 (2002)
- Wu LQ, Yi HM, Li S, Rubloff GW, Bentley WE, Ghodssi R, Payne GF. Spatially selective deposition of a reactive polysaccharide layer onto a patterned

- template. *Langmuir* **19**:519-524 (2003)
- Xavier KB, Bassler BL. LuxS quorum sensing: more than just a numbers game. *Current Opinion in Microbiology* **6**:191-197 (2003)
- Yakovleva J, Davidsson R, Lobanova A, Bengtsson M, Eremin S, Laurell T, Emneus J. Microfluidic enzyme immunoassay using silicon microchip with immobilized antibodies and chemiluminescence detection. *Anal Chem* **74**:2994-3004 (2002)
- Yi HM, Nisar S, Lee SY, Powers MA, Bentley WE, Payne GF, Ghodssi R, Rubloff GW, Harris MT, Culver JN. Patterned assembly of genetically modified viral nanotemplates via nucleic acid hybridization. *Nano Letters* **5**:1931-1936 (2005)
- Yi HM, Wu LQ, Bentley WE, Ghodssi R, Rubloff GW, Culver JN, Payne GF. Biofabrication with chitosan. *Biomacromolecules* **6**:2881-2894 (2005)
- Yi HM, Wu LQ, Ghodssi R, Rubloff GW, Payne GF, Bentley WE. A robust technique for assembly of nucleic acid hybridization chips based on electrochemically templated chitosan. *Analytical Chemistry* **76**:365-372 (2004)
- Yi HM, Wu LQ, Ghodssi R, Rubloff GW, Payne GF, Bentley WE. Signal-directed sequential assembly of biomolecules on patterned surfaces. *Langmuir* **21**:2104-2107 (2005)
- Zhu J, Miller MB, Vance RE, Dziejman M, Bassler BL, Mekalanos JJ. Quorum-sensing regulators control virulence gene expression in *Vibrio cholerae*. *Proceedings of the National Academy of Sciences of the United States of America* **99**:3129-3134 (2002)